UNIVERSITEIT VAN PRETORIA
UNIVERSITY OF PRETORIA
YUNIBESITHI YA PRETORIA

PHOTOCATALYTIC DEGRADATION OF 2,4 - DICHLOROPHENOL USING SILVER HALIDE CATALYSTS

MAHLAKO MARY MOJA

© University of Pretoria

PHOTOCATALYTIC DEGRADATION OF 2, 4 - DICHLOROPHENOL USING SILVER HALIDE CATALYSTS

MAHLAKO MARY MOJA

A dissertation submitted in partial fulfilment of the requirements for the degree of

MASTER OF ENGINEERING (WATER UTILISATION ENGINEERING)

In the

FACULTY OF ENGINEERING

UNIVERSITY OF PRETORIA

2022

© University of Pretoria

PHOTOCATALYTIC DEGRADATION OF 2, 4 - DICHLOROPHENOL USING SILVER HALIDE CATALYSTS

Author: Mahlako Mary Moja

Supervisor: Prof. Shepherd M. Tichapondwa

Co-Supervisor: Prof. Evans M.N. Chirwa

Department: Chemical Engineering

University: University of Pretoria

Degree: Master of Engineering (Water Utilisation Engineering)

ABSTRACT

Chlorophenols are classified as the most widespread and largest group of phenols. The presence of chlorophenols in the environment is related to the use and degradation of organic compounds including pesticides, phenoxyherbicides as well as phenolic biocides. The most popular chlorophenols such as 2,4-dichlorophenoxyacetic acid (2,4-D), 4-chloro-2-methylphenoxyacetic acid (MCPA) and 2,4,5-trichloro-phenoxyacetic acid (2,4,5-T) tend to produce phenol, 2-chlorophenol (2-CP) and 2,4-dichlorophebol (2,4-DCP) as byproducts. 2,4-DCP has been listed as a priority pollutant by the US Environmental Protection Agency (USEPA) due to its high toxicity, carcinogenicity, bioaccumulation and mutagenicity to living organisms.

Conventional and advanced treatment strategies have been employed in preventing the spread of 2,4-DCP in the natural environment. However, conventional treatment methods generate large amounts of secondary pollutants, where as, advanced treatments tend to bear a very high

© University of Pretoria

operational and energy cost. There is therefore an urgent need for the scientific community to develop cost effective and environmentally friendly treatment processes for water and wastewater contaminated with 2,4-DCP and other aromatic organic co-pollutants. In one of the fastest growing technologies, photocatalysis is an advanced oxidation process that has the potential of degrading recalcitrant organic contaminants in water. This treatment process uses a semiconductor material as a catalyst which is irradiated using a light source (UV or visible light) to produce highly reactive $^{\bullet}OH$ or $O_2^{\bullet}$ free radicals. The most commonly used experimental photocatalyst is titanium dioxide (TiO_2) due to its semiconductor properties, chemical stability, non-toxic and low cost. The biggest limitation of TiO_2 is its limited response to low output sources such solar light. Titanium dioxide is most effectively activated under ultraviolet (UV) light. The high energy consumption makes this process impracticable. Solar radiation is an integral part of renewable energy resources and a cheaper alternative energy source. On the other hand, processes that utilise the visible light range of solar radiation are desirable due the fact that solar radiation is abundant and cheap. In this study, a visible-light wavelength driven photocatalyst is developed based on the knowledge that inclusion of silver-halide complexes AgX (X=Cl, Br, I) can reduce the band-gap energy required to excite electrons and move them to hypothetical conduction band.

Highly efficient silver halide (Ag/AgX where X= Cl, Br, I), photocatalysts were successfully synthesized through a hydrothermal method. The prepared samples were characterized using a range of techniques such as X-ray diffraction (XRD), X-ray fluorescence (XRF), scanning electron microscopy (SEM) and Brunauer-Emmett-Teller (BET). All compounds were confirmed to be pure with the associated planes being identified. XRD patterns of Ag/AgBr photocatalyst presented cubic phase AgBr. The presented diffraction peaks are sharp and intense, indicating the high degree of crystallinity of the Ag/AgX species. SEM presented agglomerated and non-uniformly distributed particles of the prepared catalysts, as a result of

© University of Pretoria

surfactant-free precipitation reactions in aqueous media. X-ray photoelectron spectroscopy (XPS) confirmed the presence element Ag on the surface of AgX (X = Cl, Br, I).

The photocatalytic activity of these photocatalysts were evaluated through the degradation of 2,4-dichlorophenol (2,4-DCP) under UV and visible light irradiation. Variant photocatalytic efficiency was exhibited dependent on the material used. The Ag/AgBr photocatalysts exhibited the best efficiency among all three catalysts, resulting in an 83.37 % and 89.39 % photodegradation under UV and visible light after 5 h, respectively, at a catalyst loading of 0.5 g L^{-1}. Factors such as initial catalysts loading, pH effects and the initial organic contaminants concentration were also investigated. The reusability of the Ag/AgBr was evaluated and displayed a reduced stability after 5 cycles of irradiation. The photocatalytic capacity of Ag/AgBr decreased by 50 % after 5 cycles The 2,4-DCP degradation kinetics were determined to fit the pseudo-first order Langmuir-Hinshelwood model.

The results from this study indicate the feasibility of utilizing Ag/AgX under visible light irradiation for the removal and mineralization of organic compounds for water.

Keywords: Advanced Oxidation Processes, Photocatalysis, Semiconductor, Degradation, Visible light, Wastewater Treatment

© University of Pretoria

DECLARATION

I, **Mahlako Mary Moja, student No. 12035166,** do hereby declare that this research is my original work and that to the best of my knowledge and belief, it has not been previously in its entirety or in part been submitted and is not currently being submitted either in whole or in part at any university for a degree or diploma, and that all references are acknowledged.

SIGNED on the of 2022.

_____

Mahlako Mary Moja

© University of Pretoria

DEDICATION

This dissertation is dedicated to my parents, Mr. David Mashishi Moja and Mrs. Jane Katlego Moja, and my lovely siblings Tlou Nathaniel Moja and Khutso Anna Moja.Thank you for your abundant inspiration and patience.

(Mount Zion)

"Peace be unto you"

© University of Pretoria

ACKNOWLEDGEMENTS

I would like to thank the following people and organisations who have supported and assisted me in their own special and various ways:

Prof Shepherd M. Tichapondwa for his immense support, encouragement, constructive scientific critique, countless suggestion towards solving my research challenges, and giving me the opportunity to take a leading role;

Prof EMN Chirwa,for his support and guidance and for creating a learning environment;

Mrs Alette Devenga for her laboratory assistance and Mrs Elmarie Otto for her administrative assistance throughout the course of my studies;

Dr. Fisseha Bezza, Nathaniel Tlou Moja, and Pabi Mputle for the editing and formatting of edition documents for the dissertation;

Geology Department; Wiebke Groete (XRD), Jeanette Dykstra (XRF), Charity Maepa and Erna Van Wilpe (SEM), Gugu Khathide (PL) and from Chemical engineering; Noble Zonga (BET) Dorcas Adenuga (HPLC), Shane Tabana (GC-MS) and from NMISA; Werner Jordaan (XPS) for their technical assistance.

Shane Tabana, Mpumelelo Matsena, Oscar Kubheka, Kevin Mathebula and other fellow colleagues for their time, support and making my stay at South Campus memorable

GIBB Engineering and NRF for the financial support;

The Moja family, to whom I cannot sufficiently express my gratitude; and Manane ‘Malebala wa Tibane’ Nathaniel, Anna Manthibu and Ramathabatha Gloria ‘Hunadi’ Chuene;

The Almighty of Mount Zion for giving me the strength, courage, and knowledge to see this through, as well as blessing me with His amazing grace that guided, protected, and preserved me throughout this journey.

© University of Pretoria

TABLE OF CONTENTS

© University of Pretoria

© University of Pretoria

© University of Pretoria

© University of Pretoria

NOMENCLATURE

AOP	Advanced Oxidation Processes
BET	Brunauer-Emmett-Teller
BJH	Barrett-Joyner-Halenda
BQ	Benzoquinone
CB	Conduction Band
GC-MS	Gas Chromatography – Mass Spectrometry
HPLC	High Performance Liquid Chromatography
ICSD	Inorganic Crystal Structure Database
LOI	Loss of Ignition
PL	Photoluminescence Spectroscopy
PSD	Pore size distribution
ROS	Reactive Oxygen Species
SEM	Scanning Electron Microscopy
SEM/EDS	SEM/Energy Dispersive X-Ray Spectroscopy
SPE	Solid Phase Extraction
SPR	Surface plasmon resonance
TC	Triclosan
TiO_2	Titanium dioxide
TOC	Total Organic Carbon
USEPA	United States Environmental Protection Agency
UV	Ultraviolet
UV-Vis	Ultraviolet-Visible Spectroscopy
VB	Valence Band
WHO	World Health Organisation

© University of Pretoria

XPS	X-ray Photoelectron Spectroscopy
XRD	X-Ray Diffraction
XRF	X-Ray Fluorescence
2,4-DCP	2,4-Dichlorophenol
e^-	Conduction band electron
h^+	Valence band hole
eV	Electron volt
mg/L	Milligrams per litre
nm	Nanometer

© University of Pretoria

LIST OF FIGURES

© University of Pretoria

© University of Pretoria

© University of Pretoria

LIST OF TABLES

© University of Pretoria

LIST OF SCHEMES

© University of Pretoria

RESEARCH OUTPUTS

Journal Articles

1. Moja M.M., Chirwa E.M.N., Tichapondwa S.M. (2021). Visible Light Activated Photocatalytic Degradation of 2,4-dichlorophenol Using Silver Halide Photocatalysts. *Chemical Engineering Transactions*, 86, 1411-1416. https://doi.org/10.3303/CET2186236
2. Moja M.M., Chirwa E.M.N., Tichapondwa S.M. Photodegradation of 2,4-dicholophenol over Ag/AgX (X = Cl, Br, I) with detailed mechanism and proposed reaction pathway. [Target Journal] *Journal of Industrial and Engineering Chemistry* [Under preparation]
3. Moja M.M., Chirwa E.M.N., Tichapondwa S.M. Visible light induced photocatalytic degradation of phenolic compounds using silver halide photocatalysts. *WISA 2022 Biennail Conference and Exhibition* [Under preparation]

Conference Presentation

4. Visible Light Activated Photocatalytic Degradation of 2,4-dichlorophenol Using Silver Halide Photocatalysts. Proceedings of the 15th International Conference on Chemical and Process Engineering (ICheaP15). 23rd-26th May 2021, Naples, Italy. (Oral presentation).
5. Photocatalytic degradation of phenolic compounds using silver halide photocatalysts. WISA 2022 Biennail Conference and Exhibition. 28th-30th September 2022, Sandton, South Africa. (Oral presentation)

© University of Pretoria

CHAPTER 1

1 INTRODUCTION

1.1 Background

Water pollution is a major globally issue, which presents a major risk to the long-term sustainability of the environment and its ability to support human life (Schwarzenbach et al., 2010, Kurniawan et al., 2012). The rapid increase in the human population has resulted into a corresponding increase in the production industry to produce new technologies and chemicals to satisfy daily and energy needs. As a consequence, water bodies across the world are receiving higher and higher volumes of waste containing a range of emerging pollutants most of which are constituted from aromatic organic compounds and their halogenated congeners (Ullah et al., 2013, Hanchang, 2009). Suffice to say, industrial effluents are frequently contaminated by organic substances, such as aromatic intermediates and phenolic compounds, as well as other halogenated or volatile organic substances, metals (mainly, Cu, Sb, Pu, Cd, Zn, Cr, Ni, Hg) and other chemical species, such as benzene, cyanide (CN^-) and chloroform (Fechete et al., 2012, Reddy et al., 2016, Zhang et al., 2020, Ramírez-García et al., 2019, Brandão et al., 2017). The presence of these compounds in wastewater and drinking water is a major problem, due to their intrusiveness to biological processes. The unintended effects of these compounds to the ecosystems are disruptions in metabolic processes (Giulivo et al., 2016), disruption of endocrine systems in mammals (Marty et al., 2018),and carcinogenicity and mutagenicity to almost all life forms (Choi et al., 2004).

Phenolic compounds are harmful to human health, as they can cause digestive problems, and liver and kidney damage (Verma and Dwivedi, 2013, Anku et al., 2017). The presence of phenolic compounds and their derivatives in drinking water at concentrations as low as 1 mg

© University of Pretoria

L^{-1} may cause serious public health issues and the death of aquatic life (Prado et al., 2002). At concentrations greater than 1 mg L^{-1}, phenolics causes disruptions in ecosystems resulting in loss of biodiversity (Jones et al., 2003, Strade and Kalnina, 2019, Rahman et al., 2020).

1.2 Problem Statement

Pollution of water sources by chlorinated organic compounds is reported to be one of the major environmental threats lately (Zhang et al., 2019, Gupta and Saleh, 2013). Herbicides and pesticides containing chlorophenols are the major source of these compounds (Igbinosa et al., 2013, Adeola, 2018). Other sources are biocides and wood preservatives. These compounds often have chemical structures and tend to photodegrade into several by-products, some of which with toxicity higher than the parent compounds. The chlorinated organic compound 2,4-dichlorophenol (2,4-DCP) is the photodegradation by-product of triclosan (TC), a common antimicrobial agent as well as 2,4-dichlorophenoxyacetic acid (2,4-D) herbicide (Melián et al., 2013). The toxicity of phenolic compounds in various water bodies such as surface water, groundwater and wastewater, at environmental levels of over 1 mg L^{-1}, greatly affect the organoleptic properties of water (Rodriguez-Proteau and Grant, 2005, Chindo et al., 2013). Table 1-1. presents exposure and regulatory limits of phenol and some phenolic compounds.

2,4-Dichlorophenol has been listed as a priority pollutant by the United States Environmental Protection Agency (USEPA) (Melián et al., 2013, Gaya et al., 2010), as it poses a serious threat to both marine and human health due to its profuse toxicity, mutagenic, carcinogenic and obstinately refractory properties (Liu et al., 2019, Bel Hadjltaief et al., 2018). The concentration of chlorophenols in drinking water has been set to a limit of less than 1.0 mg/L. The development of effective methods for the degradation of 2,4-DCP is imperative. Biological treatment has been considered as a viable method for the decomposition of 2,4-DCP as 2,4-DCP could be mineralized by microorganisms under aerobic or anaerobic conditions (Dixit et al., 2011, Hassan et al., 2018).

© University of Pretoria

Table 1-1. Regulatory limits and exposure of phenol and phenolic compounds (Michalowicz and Duda, 2007, Chowdhury et al., 2017).

Compounds (min contaminant levels)	**Use/exposure**	**Health effects**
Phenol: Phenol (4 mg L^{-1})	(i) Utilised in the production of phenolic resins, aniline alkylphenols, dyes, pesticides, disinfectant, and antiseptic, synthetic fiber; (ii) detected in industrial effluent from various industries such as food processing, pulp and paper, textile, coal gasification, pharmaceuticals, and petroleum refining	Skin irritation, headache, liver damage, kidney damage
Chlorophenols: 2-Chlorophenol (0.03 mg L^{-1}), 3-methyl-4-chlorophenol (0.5 mg L^{-1}), 2,4- Dichlorophenol (0.01 mg L^{-1}), pentachlorophenol (0.03 µg L^{-1}), 2,4,6-Trichlorophenol (1.5 µg L^{-1})	(i) Utilised in pesticide and antiseptics production, (ii) produced in chlorine-bleaching process during paper production, (iii) formed through the chlorination of humic matter during the chlorination of drinking water, and (iv) also made in textile, pharmaceutical and chemical industry	Burning pain in the mouth, headache, lung damage, affects the digestive tract and immune system
Nitrophenols: 2,4-Dinitrophenol (0.01 mg L^{-1})	(i) Produced through the reaction of nitrite ions and phenol in water under light (UV or solar), (ii) also formed during both the production and degradation of pesticides, (iii) produced from metallurgic and electronic industry, and (iv) used in solvents, dyes, and plastic production	Weakness, muscles pain, anorexia, kidney damage

However, aerobic 2,4-DCP degradation in bioreactor was limited, this could be influenced by the toxicity or inhibition of 2,4-DCP to microorganisms (Quan et al., 2004, Wang et al., 2020a). Wang et al. (2007) developed an aerobic granule for the biological degradation of 2,4-DCP in

© University of Pretoria

a sequencing batch reactor and was able to remove 94 % of 2,4-DCP after 39 days of exposure. This treatment method would not be commercially viable due to its lengthy reaction time.

In order to reduce the risk of 2,4-dichlorophenol in the environment, remediation through the development of suitable alternative removal techniques is essential. Several technologies have been investigated for the removal of 2,4-DCP in aqueous solutions, namely adsorption (Melián et al., 2013), ozonation (Aziz et al., 2018) and electrochemical treatment (Liu et al., 2019). Most of these technologies have disadvantages such as high operational cost, low efficiency, and the production of excessive by-products.

As such, further development of effective methods for the degradation of 2,4-DCP is required. Recently, photocatalysis has been identified as an economically feasible and environmentally friendly advanced oxidation process (AOP) that is capable of mineralizing a wide range of organic compounds including recalcitrant phenolics (Adenuga et al., 2019). The most widely investigated photocatalysts are TiO_2-based nanoparticles as they are inexpensive, non-toxic and structurally stable (An et al., 2016, Kaneco et al., 2006, Xiao et al., 2015). However, the large band gap of TiO_2 (3.2 eV (Cui et al., 2015, Meng and Zhang, 2016, Bhatt and Patel, 2019)), has limited its application. TiO_2 can be directly excited by ultraviolet (UV) irradiation which accounts for only 4% of the solar spectrum. Consequently, efforts have been made to develop photocatalysts that can absorb visible light which accounts for approximately 43% of the solar spectrum (Ma et al., 2012), yielding a green energy source, economical and an eco-friendly strategy of environmental remediation. This makes it imperative to develop visible light responsive photocatalytic materials.

Plasmonic photocatalyst typically consists of noble metals namely Au, Ag, Pt, Cu, which display high adsorption coefficients in the UV-Visible-near infrared spectral range. The high adsorption coefficients are due to their strong surface plasmon resonance (SPR) (Cui et al., 2015). The SPR is the resonant photon-induced collective oscillation of valence electrons

© University of Pretoria

which occurs when the frequency of the exciting light is equivalent to the natural frequency of the surface electrons (Ye et al., 2012). Silver nanoparticles exhibit efficient plasmon resonance in the visible region. Silver halides are highly photosensitive and can be utilised as metallic silver precursors. AgX can absorb light photons under visible light to generate electron-hole pairs, thus AgX may be utilised as a possible visible photocatalyst for the degradation of organic pollutants (Rehan et al., 2018).

1.3 Aims and objectives of study

This study aims to investigate the efficacy of AgX photocatalysts on the degradation of 2,4-DCP. To evaluate the feasibility of visible light driven photocatalysis taking advantage of plasmonic silver nanoparticles. The main objectives of this study were to:

- Synthesise the Ag/AgX (X =Cl, Br, I) photocatalysts;
- Investigate the chemical and physical properties of the synthesised materials through various characterisation techniques;
- Compare the photocatalytic performance of the synthesised materials under both UV and visible light irradiation;
- Study the kinetics under optimum conditions of photodegradation of 2,4-DCP under visible light irradiation;
- Study the photostability of the of the most efficient photocatalyst.

Scheme 1-1. Illustrates the experimental design and analysis conducted in this study.

© University of Pretoria

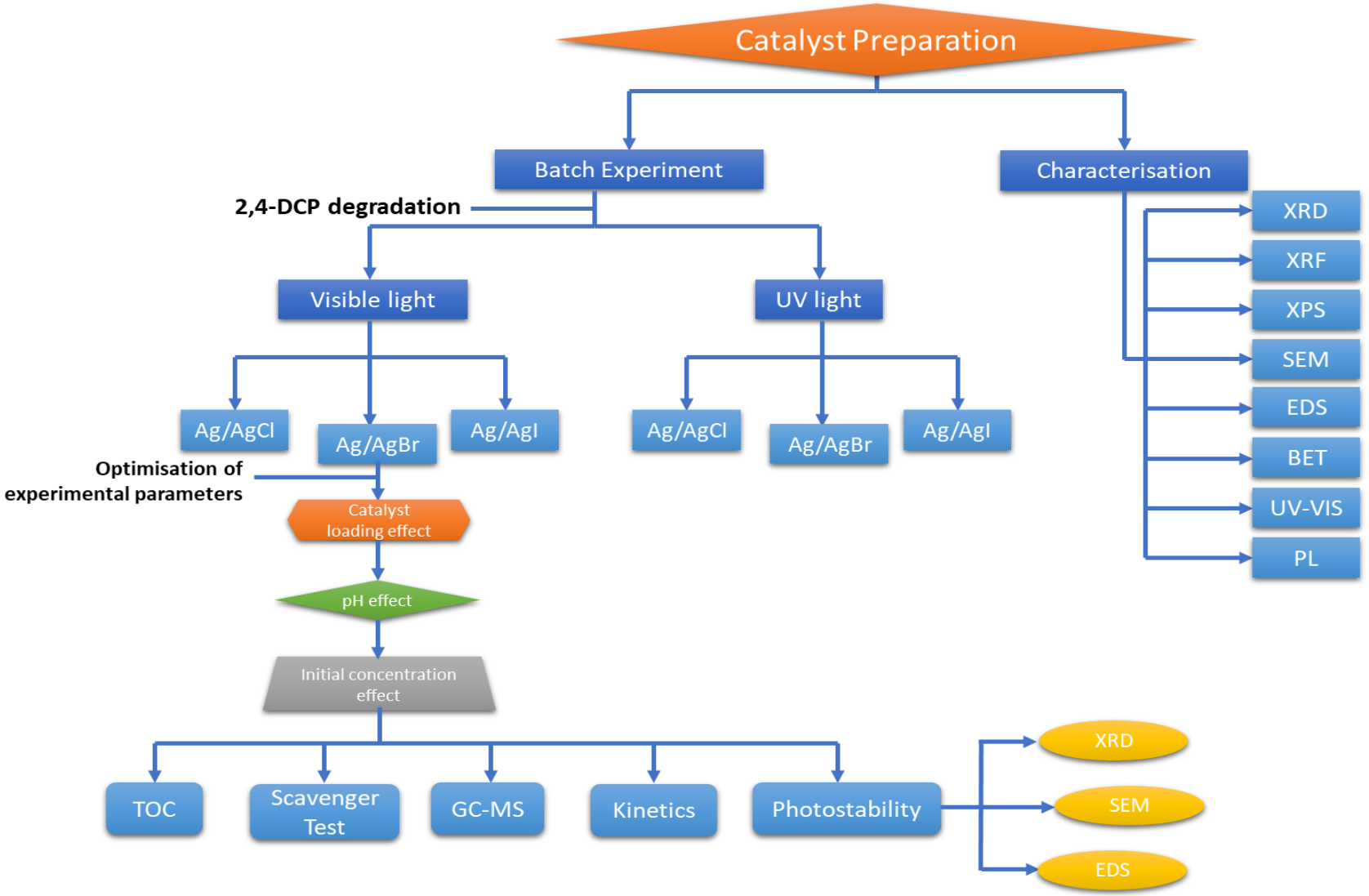

Scheme 1-1. Schematic illustration of the experimental design and analysis conducted in this study.

© University of Pretoria

1.4 Outline of dissertation

Chapter 1

This chapter provides a background on water pollution by chlorophenols specifically 2,4-DCP. It further provides a brief overview of the available strategies on the removal of organic contaminants from wastewater and the advantages of photocatalysis as a treatment method over other methods. Plasmonic photocatalysts, silver halides as well as the overall aims and objectives of the study are defined.

Chapter 2

This chapter presents the literature review of this study. It is divided into four sections, namely, water pollution, treatment processes, synthesis methods of silver halides and the application of silver halide photocatalysts.

Chapter 3

This chapter presents the materials, experimental procedures, characterisation techniques as well as analytical techniques used in this study.

Chapter 4

This chapter outlines the characterisation results of the synthesised silver halide photocatalysts. These were conducted in order to elucidate the crystallinity, and phase identification, chemical states, and composition, morphologies, BET surface area, and pore distribution, and the optical and photoelectrochemical properties of the prepared catalyst.

Chapter 5

This chapter provides the photodegradation results of 2,4-DCP as divided into three sections which are presented as follows:

© University of Pretoria

1. The photocatalytic performance of Ag/AgX (X = Cl, Br, I), under both UV and visible light irradiation;
2. Effect of various process parameters such as the effect of initial pH, catalyst loading, initial concentration and kinetics of 2,4-DCP degradation;
3. Determining the extent of mineralisation, formation of photocatalytic intermediates, photostability and degradation mechanism of Ag/AgBr.

Chapter 6

This chapter presents the conclusions deduced from results attained in Chapters 4 and 5 and stipulates recommendations for further studies.

© University of Pretoria

CHAPTER 2

2 LITERATURE REVIEW

2.1 Water Pollution

Researchers and industries find treating water and wastewater problematic due to the complex inorganic and organic pollutants present. This is because of the rapid growth of population and industrial developments. The wide usage of toxic chemicals in the industries also increases the deterioration of marine life (Webb et al., 2013). Due to the disposal practices, toxic substances are introduced into the marine environment. For example, pollution of water by the effluent wastewater having constituents such as pesticides, heavy metals and dyes (Saravanan et al., 2021).These pollutants may harm the ecosystem and living organism as well as human health through bioaccumulation resulting in carcinogenic disorders, respiratory and reproductive illnesses.

Most water pollution associated with agricultural chemicals are generally organochlorine compounds (Jayaraj et al., 2016). These chemicals may be toxic when exposed to humans (Rani et al., 2021). According to the South African Environmental Health and Safety, exposure to chloro-phenols complexes may cause kidney and liver damage, skin burn, tremor, convulsion and twitching. Symptoms of exposure include weight loss, exhaustion, weakness and muscle ache WHO (2021). The most common way chlorophenols compounds can be exposed to humans is through consumption of water containing the pollutant; hence, it important to quantify and treat the polluted water before any consumption can take place. Typical organo-chlorinated compounds are 2,4-dichlorophenol and 2,4,5-trichlorophenoxypropionic acid; which are mainly used as solvents or as insecticide/pesticide agents whist the most common phenols such as Bisphenols and phenyl phenols are applied in hospitals and households as a disinfectant leather, and textile and paper industry (Solá-Gutiérrez et al., 2019, Adeola, 2018).

© University of Pretoria

Due to the highly solubility of the abovementioned compounds, they tend to leak into the ground water thus polluting the ecosystem (Srinivasan and Fogler, 1990, Postigo and Barceló, 2015).

2.2 2, 4-Dichlorophenol

Polyphenolic composites belong to organic complexes and extensively spread in the environment through wastewater and natural underground waters (Leontopoulos et al., 2020). Due to their bioaccumulation, toxic effect and tendency to persist in environment, phenolic compounds are among the chemicals of major concern. According to the World Health organisation (WHO) and United States Environmental Protection Agencies (US-EPA) the permissible limit of phenol in consumable water is 2 mg/L and water standard of less than 1 ppb for 2,4 dichlorophenol in surface water (Ma et al., 2017). The toxic stages are between 9-25 mg/L for marine environment. However, an amount exceeding the threshold would results in severe damages to the human health (Ustaoğlu and Tepe, 2019).

There are various ways in which 2,4-dichlorophenol compound can be introduced to the environment. Manufacturing industries such as paper manufacturing, agriculture, pharmaceuticals, petrochemical industry, coal processing or as municipal wastes are the main sources of the pollutant. Although the international regulatory bodies have, set strict discharge limits for phenols for sustainable environment; there are still discharges of the pollutant into the water mainstreams (Parida et al., 2021). Figure 2-1. Illustrates the molecular structure of 2,4-DCP.

© University of Pretoria

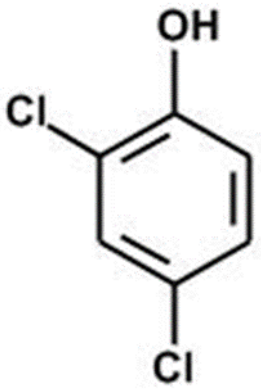

Figure 2-1. Molecular structure of 2,4-dichlorophenol (Rasdi et al., 2016).

2.3 Advanced Oxidation Processes as a Treatment Method

There are various industrial processes for the degradation of phenols (Chowdhury et al., 2017). Extractive membrane bioreactor, hollow fibre membrane, and reverse osmosis are the most commonly used method (Stephenson et al., 2000). However, advanced oxidation processes (AOP's) are regarded as a viable method for degradation of 2,4 dichlorophenol and other organophenols complexes. This is due to its ability to convert/mineralise complex organic mixtures to a more stable inorganic compounds such as water, carbon dioxide, and salts with little to no sludge formation, which eliminates the requirement for an additional pre-treatment step. Most AOPs are costly processes due to their high energy demand, high chemical dosage and long reaction time (Chaplin, 2018). Therefore, minimizing total cost effects during treatment of processes.

AOP are characterised by a common chemical feature which is the capability of exploiting the hydroxyl radicals in oxidation processes (Andreozzi et al., 1999). Hydroxyl radicals are extremely unstable and reactive because of their high reactivity (Lelieveld et al., 2004). Generally, most AOPs present pseudo-first order degradation kinetics (Butt et al., 2021). However, there are various AOPs which identified pseudo-second order kinetic reaction such as Youssef et al. (2016) in the degradation of methyl orange. Presented in Figure 2-2. are the

© University of Pretoria

various AOPs processes Fenton, ozonation, photolysis and photocatalysis which posses different oxidation mechanism.

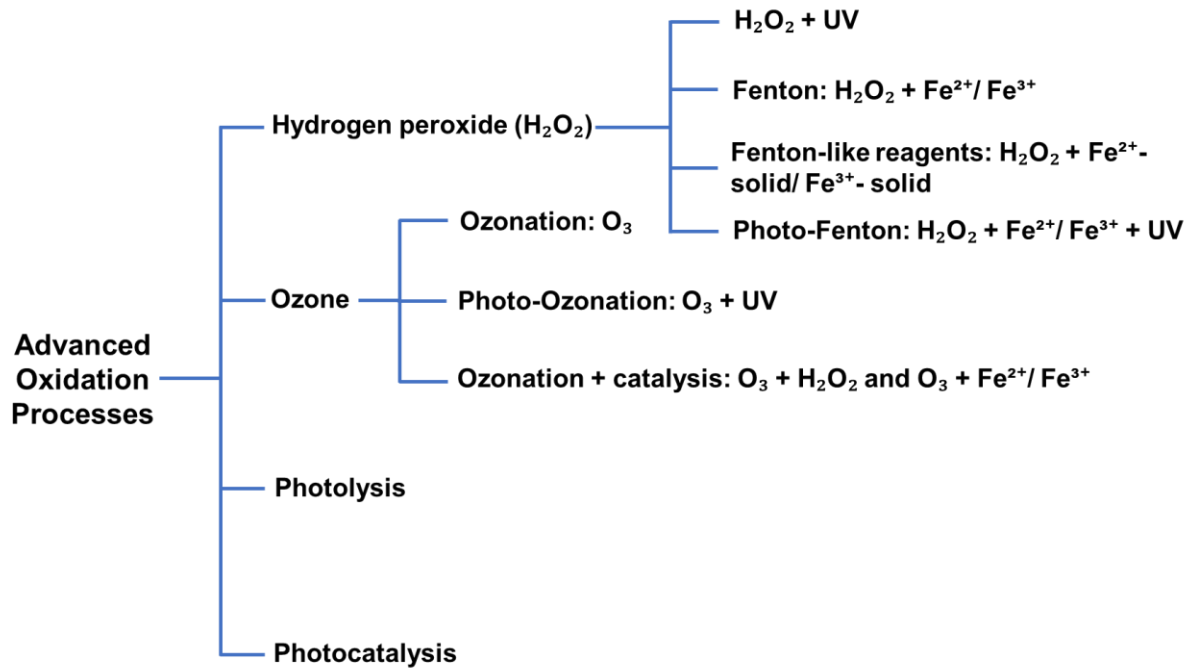

Figure 2-2. Illustration of various AOP processes.

For Fenton reagent, the system incorporate the generation of hydroxyl radicals through the reaction between iron(II) salts and hydrogen peroxide (Benitez et al., 2001, Bissey et al., 2006). The global reaction for the production of OH·in acidic pH conditions. The mechanism for the ferric ion catalysed decomposition of hydrogen peroxide in acid solution has been widely described by Walling and Goosen (Walling and Goosen, 1973, Esplugas et al., 2002).

Mechanistic studies have demonstrated the Fenton process through the formation of hydroxyl radical. Equation (2-1) demonstrates the Fenton reaction that can be applied to degrade various organic pollutants:

$$Fe^{2+} + H_2O \rightarrow Fe^{3+} + OH^{\bullet} + OH^{-} \quad (2\text{-}1)$$

As the Fenton reaction occur in acidic medium, it can be expressed as:

$$Fe^{2+} + H_2O + H^{+} \rightarrow Fe^{3+} + H_2O + OH^{\bullet} \quad (2\text{-}2)$$

© University of Pretoria

Only a small catalytic amount of Fe^{2+} is required as this ion is regenerated from the Fenton-like reaction (2-3) between Fe^{3+} and H_2O_2.

$$Fe^{3+} + H_2O_2 \rightarrow Fe^{2+} + HO_2^{\bullet} + H^+ \quad (2\text{-}3)$$

Fenton-like reaction (2-3) was reported to have a slower reaction than Fenton's reaction (2-1). Fe^{2+} can be rapidly regenerated by the reduction of Fe^{3+} with $HO_2^{\bullet}$ from reaction (2-4), with an organic radical $R^{\bullet}$ in reaction (2-6) and/or with superoxide ion ($O_2^{\bullet-}$) from reaction (2-6):

$$Fe^{3+} + HO_2^{\bullet} \rightarrow Fe^{2+} + O_2 + H^+ \quad (2\text{-}4)$$

$$Fe^{3+} + R \rightarrow Fe^{2+} + R^+ \quad (2\text{-}5)$$

$$Fe^{3+} + O_2^{\bullet-} \rightarrow Fe^{2+} + O_2 \quad (2\text{-}6)$$

The ozonation (O_3) procedure has two possible oxidizing processes: firstly, the direct procedure, which is caused by the reaction between the ozone and the dissolved compounds, and the radical procedure caused by the reactions between the generated radicals produced in the ozone decomposition (hydroxyl radicals) and the dissolved compounds (Mena et al., 2012, Benitez et al., 2004). Kinetic models for the reaction of ozone with various organic and inorganic compounds have been established by Hoigné and Bader (1994). Figure 2-3. displays the mechanism of organic pollutants mineralisation by ozonation.

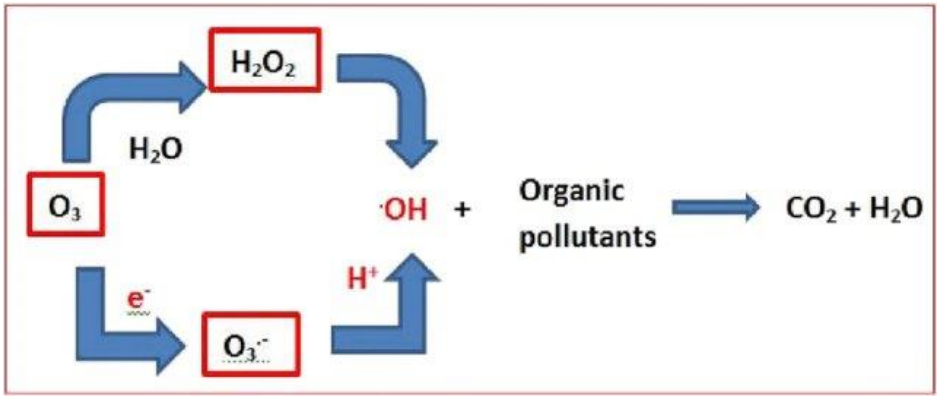

Figure 2-3. The mechanism of organic pollutants mineralization by ozonation (Litter, 2005, M'arimi et al., 2020).

© University of Pretoria

The UV photolysis method is based on supplying energy to the chemical compounds as radiation, which is absorbed by reactant molecules that can pass to excited states and have sufficient time to promote reactions (Esplugas et al., 2002, Chen et al., 2010). The mechanism for the direct photolysis of phenol has been presented in equation (2-7) to (2-16).

$$C_6H_5OH \rightarrow C_6H_5O^{\bullet} + H^+ + e_{aq}^- \quad (2\text{-}7)$$

$$e_{aq}^- + O_2 \rightarrow O_2^{\bullet -} \quad (2\text{-}8)$$

$$e_{aq}^- + H_2O \rightarrow H^{\bullet} + OH^- \quad (2\text{-}9)$$

$$H^{\bullet} + H_2O \rightarrow H_2 + OH^{\bullet} \quad (2\text{-}10)$$

$$H^{\bullet} + O_2 \rightarrow H_2 + HO_2^{\bullet} \quad (2\text{-}11)$$

$$H^{\bullet} + O_2^{\bullet -} \rightarrow HO_2^{\bullet -} \quad (2\text{-}12)$$

$$H^+ + HO_2^{\bullet -} \rightarrow H_2O_2 \quad (2\text{-}13)$$

$$H^{\bullet} + HO_2^{\bullet} \rightarrow H_2O_2 \quad (2\text{-}14)$$

$$H^{\bullet} + HO_2^{\bullet} \rightarrow H_2O_2 \quad (2\text{-}15)$$

$$H_2O_2 \rightarrow 2OH^{\bullet} \quad (2\text{-}16)$$

In the case photocatalysis: the interaction between a semiconductor and the UV or visible light radiation forms electron-hole pairs on the semiconductors surface. The charged points react with both organic compounds and water. The redox reactions are responsible for the destruction of the organic compound, whereas the latter hydroxyl radicals are generated and these radicals react with the organic compound (Grebel et al., 2010, Esplugas et al., 2002). The most common semiconductor used in photocatalysis is TiO_2 (anatase).

© University of Pretoria

2.4 Photocatalytic Mechanism

Photocatalysis is classified as a direct conversion technique between solar and chemical energy in the presence of catalyst which accelerates the photoreaction (Linic et al., 2011, Xia et al., 2021, Fan et al., 2018). The photocatalytic reaction primarily depends on the light energy and catalyst. Generally, semiconducing materials are utilised as catalysts, were they function as sensitisers for the light stimulated redox process (Khan et al., 2017, Saravanan et al., 2017, Reddy et al., 2020). Figure 2-4. displays the general mechanism of a photocatalytic reaction. The photocatalysis process consists of three main components namely semiconductor photocatalyst, light energy, and electron donor or hole acceptor (Zhong et al., 2018). When a semiconductor photocatalyst is illuminated with light energy greater than the band gap of the photocatalyst, electron-hole pairs are produced which result in the generation of hydroxyl and superoxide radicals in the system (Sun et al., 2015, Chowdhury et al., 2017).

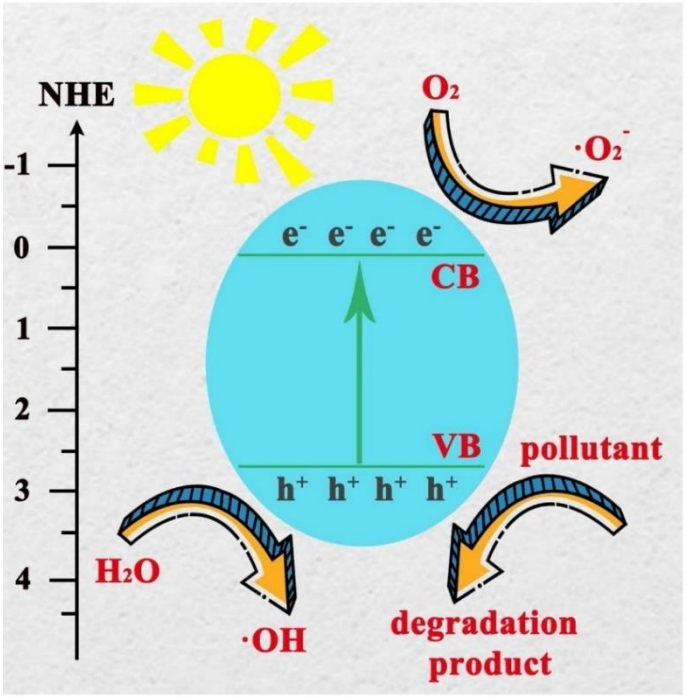

Figure 2-4. Mechanism for the photocatalytic reduction of organic pollutant (Cheng et al., 2021).

© University of Pretoria

2.4.1 Principles of plasmonic Ag/AgX photocatalysts

Synthesis of photocatalyst with extened visible light absorption and plasmonic properties have gained great reseach interest as they are efficient in harvesting light energy for chemical processes. Noble metals such as silver (Ag) and gold (Au) possess higher absorption coefficient in the wide UV-visible-near infraed range (NIR) (Thakur et al., 2020). Ag nanopartilces (NPs) are generally selected due to their low cost relative to Au NPs and display efficient surface plasmon resonance (SPR) in solar light. When a metal particle is exposed to light, the oscillation electromagnetic field of the light generates a collective oscillation of free electrons of the metal (Xu et al., 2011). The electron oscillation around the particle surface creates a charge separation with regard to the ionic lattice, thus generating a dipole oscillation in the direction of the electric field as depicted in Figure 2-5a (Wang et al., 2013d). The amplitude of the oscillation reaches maximum at a specfic frequency, identified as the surface plasmon resonance (SPR).

The photocatalytic performance of a semiconductor photocatalyst can be efficiently improved by metallic SPR effect through the transfer of energy to the semiconductor and increasing the steady-state concentration of “chemically useful” energetic charge carriers in the semiconductor (Loka and Lee, 2021, Grabowska et al., 2013, Tian and Zhang, 2012, Hong, 2020, Chen et al., 2014).

There are approximately three energy-tranfer mechanisms in which SPR can improve the concentration of charge carriers, namely, Near-field electromagnetic, SPR-mediated charge injection from metal to semiconductor and scattering mechanisms (Feng et al., 2016, Zhang et al., 2017, Fan and Leung, 2016).

In the case of Ag/AgX plasmonic photocatalysts, the Ag NPs are generated in situ through chemical or light reduction and are in direct contact with its AgX matix, permitting a rapid

© University of Pretoria

transfer of charge carriers from Ag NPs to AgX semiconductor. Thus, the improvement of visible light photocatalytic performance is likely achieved through SPR-mediated charge injection from Ag to AgX. Figure 2-5b., illustates the indirect band gap of AgBr and AgI as 2.30 eV and 2.73 eV, repectively. Based on the indirect band-gaps, Ag/AgBr and Ag/AgI can absorb visible light (400 - 750 nm) by both Ag NPs and their own intrinsic absorption. AgCl possess an indirect band gap of 3.25 eV and a direct band gap of 5.6 eV nevertheless AgCl nanoparticles are photosenstive due to their intrinsic point defects and electron traps (Wang et al., 2008, Kumar and Chakarvarti, 2012).

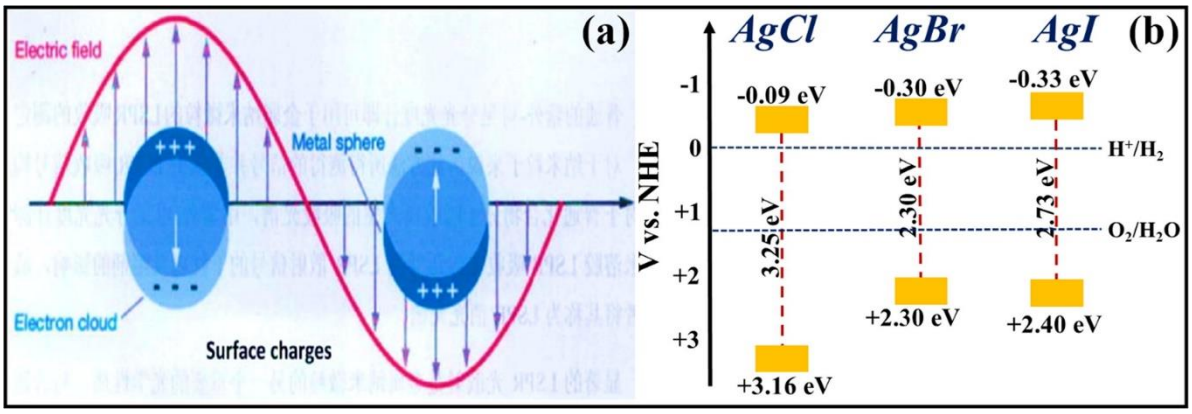

Figure 2-5. Schematic illustration of (a) Surface Plasmon Resonance (SPR) phenomenon (Thakur et al., 2020) and (b) the indirect band gap of AgCl, AgBr and AgI with their respective VB and CB potentials (Ye et al., 2014, Yao et al., 2016, Islam et al., 2016, Thakur et al., 2020).

2.4.2 Reaction mechanism of Ag/AgX photocatalysts

Photocatalytic reaction mechansims have been investigated through numerous experimental methods such as electron spin resonance (ESR) (Huang et al., 2019), cyclic voltammetry (CV) analyses, trapping tests of active species and surface photovoltage spectroscopy (SPV) (Xu et al., 2019, An et al., 2016). Figure 2-6., illstrates the degradation process of organic contaminates over Ag/AgX plasmonic photocatalysts. When Ag/AgX is irradiated with visible-light, Ag nanoparticles produce photogenerated electrons (e^-) and holes (h^+), which can be separated by the SPR-induced local electromagnetic field (Xiao et al., 2015, Chen et al., 2013,

© University of Pretoria

Wang et al., 2012d, Li et al., 2018). Generally, AgX is prepared in X-rich conditions, then the surface of AgX is terminated by X^- ions, and thus negatively charged (Tian and Zhang, 2012). Because of the polarisation effect of the negatively charged AgX surface, the e^- are transferred to the surface of Ag nanoparticles away from the Ag/AgX interface (Assis et al., 2020, Murali et al., 2020, Zhang et al., 2014, Li et al., 2018), whereas the h^+ are transferred to the surface of AgX. Subsequently, the e^- will be trapped by electronic acceptors such as dissolved O_2 to generate superoxide anion radicals ($O_2^{\bullet -}$). On the other hand, h^+ would oxidise X^- to X^0 atoms (highly oxidative halogen X• radicals) which can directly oxidise organic pollutant molecules. Thus, the overall photocatalytic reaction can be regarded as the oxidation of organic molecules assisted by the O_2 and SPR accelerated visible-light absorption (Chen et al., 2008, Ji et al., 2010).

© University of Pretoria

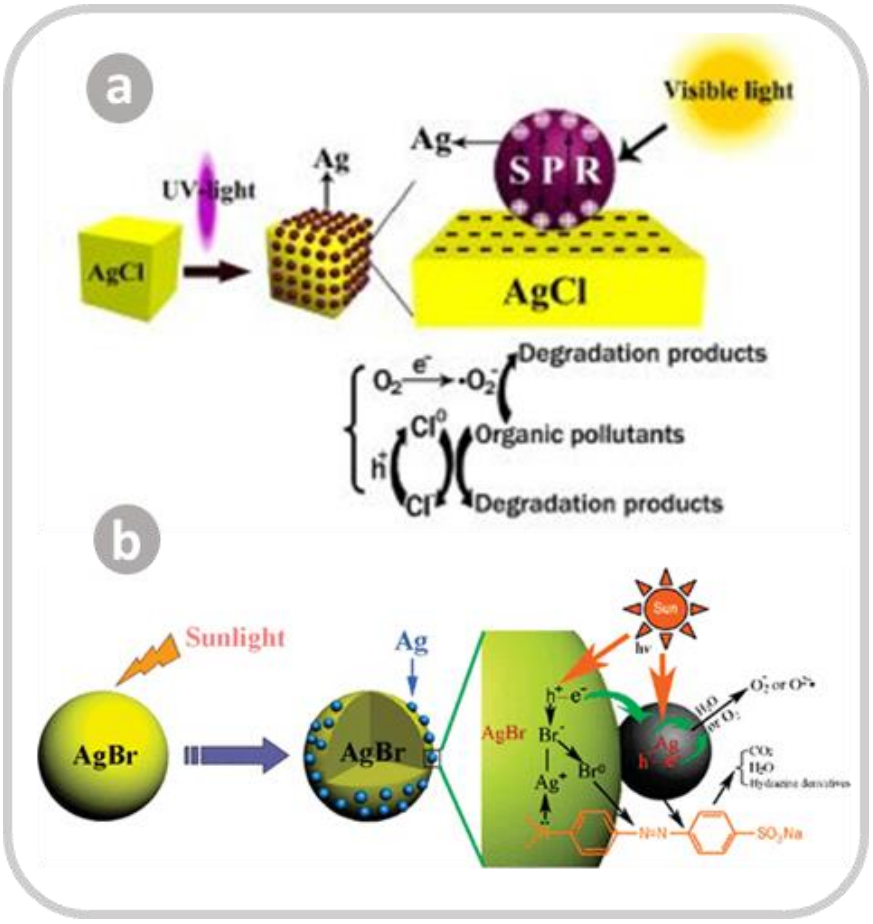

Figure 2-6. Schematic diagram illustrating the producton of Ag NPs on AgX as well as the proposed degradation mechanism of organic pollutants over Ag/AgX plasmonic photocatalyst (Dong et al., 2013, Kuai et al., 2010).

2.5 Synthesis Methods of Ag/AgX photocatalysts

Synthesis methods can affect the morphology, size and surface area of the photocatalyst, thus affecting the adsorption properties as well as photocatalytic activities of photocatalysts. Economically friendly and "green" methods are also essential for industrialization. Table 2-1. displays a summary of typical synthesis methods and the resulting morphologies of the Ag/AgX produced. The silver source is generally $AgNO_3$ (Clark et al., 2021, Adenuga et al., 2021, Moja et al., 2021) while KX, NaX, HX, CTAX (X = Cl, Br or I) and ionic liquids with halogen elements are usually used as the halogen source (Sridharan et al., 2021, Jin et al., 2017, Ye et al., 2014). The main synthesis methods for Ag/AgX include hydrothermal, solvothermal,

© University of Pretoria

precipitation, ionic liquid, and in-situ ion exchange processes. Hydrothermal and solvothermal synthesis methods are performed in a sealed Teflon autoclave under high temperature and pressure. The photocatalysts produced have high crystallinity and narrow size distribution (Fan and Leung, 2016, Xu et al., 2018). For Ag/AgX, this promotes strong interaction between Ag and AgX due to the in situ growth process which benefits the charge transfer. Moreover, the reaction temperature, reaction time and pH value influence the morphology and size of Ag/AgX (Kumar et al., 2022, Ismael, 2021).

Table 2-1. shows an array of morphologies such as sphere, cubic, polygonal plates, tube, concave, cashew and frame prepared through various synthesis methods. Ag/AgCl nanoparticles prepared by a hydrothermal method were reported by Xu et al. (2011). The hydrothermal temperature influences the crystallinity and particle size of Ag nanoparticles covering the surface of AgCl. When the temperature was 80 °C the estimated diameter of Ag nanoparticles was in the range of 40-80 nm while at 160ºC, the diameter enlarged to 300-700 nm.

© University of Pretoria

Table 2-1. Summary of typical synthesis methods and morphologies of Ag/AgX (X = Cl, Br, I) photocatalysts (Fan et al., 2018).

Photocatalyst	Synthesis method	Shape	Illustration	Reference
AgCl; AgBr	Template-assisted in-situ synthetic route; Oxidation reaction	Sphere	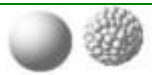	(Lou et al., 2015, Ma et al., 2013)
AgCl	Ionic liquids-assisted hydrothermal	Near-spherical		(Lou et al., 2011b)
AgCl; Ag_3PO_4/AgBr	Surfactant-assisted method; hydrothermal method; In-situ ion exchange	Cube and truncated cube		(Wang et al., 2013c, An et al., 2010, Zhu et al., 2011b, Han et al., 2011)
AgBr; AgI	Polyvinylpyrrolidone-assisted precipitation	Polygonal plates and disc		(An et al., 2012a, Wang et al., 2012a, Kuang et al., 2014, Wang et al., 2013b)
AgCl	Template-directed growth; Ionicliquids etching	Tube and rod		(Xu et al., 2013, Li et al., 2014)
AgCl	One-pot solvothermal method	Polyhedra		(Zhang et al., 2015)

© University of Pretoria

Table 2-1. Continued…\

Photocatalyst	Synthesis method	Shape	Illustration	Reference
AgCl; AgI	One-pot solvothermal method; Etching	Concave		(Zhang et al., 2015, An et al., 2014a)
AgCl	Polyvinylpyrrolidone-assisted precipitation	Cube-tetrapod		(Cai et al., 2014)
Ag@AgBr/AgCl	Anion-exchange reaction	Cashew		(An et al., 2012b)
AgCl	Site-selected growth	Frame		(Han et al., 2014)
AgCl	Water-soluble sacrificial salt-crystal-template process	Cage		(Li et al., 2015, Tang et al., 2013)

© University of Pretoria

2.6 Engineering silver halide for photocatalysis application

2.6.1 AgX decorated with Ag nanoparticles

AgX NPs are classified as an optically sensitive material in photographic films, which are generally unstable during prolonged light irradiation. Under light irradiation, the AgX components generate electron-hole pair, thereafter the photogenerated electron combines with interstitial Ag^{+} ions to form metallic Ag^{0} atoms and finally Ag NPs. The generated Ag NPs lead to an SPR effect which results in strong optical absorption of Ag NPs. In situ partial reduction of AgX is a facile approach to prepare efficient Ag/AgX composite photocatalyst (Wang et al., 2012e). This method is achieved through a precipitation reaction of Ag^{+} and X^{-} ions followed by photo- or chemical reduction in the presences of reducing agents such as $NaBH_4$, polyol (ethylene glycol (EG) or glycerol) (Dong et al., 2018, An et al., 2016, Duan et al., 2018), poly (vinyl pyrrolidone) (PVP) and poly(vinyl alcohol) (PVA) (Song et al., 2014, Guo et al., 2021, Long and Cai, 2014). Compared with pristine AgX NPs, Ag/AgX exhibit strengthened absorption in both UV and visible regions due to the SPR effect of the Ag components (Han et al., 2014).

2.6.2 Composite nano-photocatalysts of AgX with photoactive semiconductors

The modification of the crystal structure and shape of AgX introduce additional stability. The introduction of co-catalysts, loading noble metals, transition-metals including nonmetal-oxides has proved valid for additional stability (Li et al., 2019b, Hoang and Gao, 2016, Prieto et al., 2016, Radha et al., 2019). AgX and Ag/AgX can be used to adjust semiconductors with suitable energy-band structures. This method assists in acquiring efficiently coupled photocatalysts as the obtained composites generally display higher activity and stability compared to their constituents. AgX and Ag/AgX are usually utilised as sensitizers, in composite photocatalysts, to engineer wide band gap semiconductors response to visible light (An et al., 2016, Tian et

© University of Pretoria

al., 2022). Combination of AgX with narrow-gap semiconductors can alter the transfer pathway of photogenerated charge carriers and suppress the recombination probability consequently, improving their photocatalytic efficiency (Liu et al., 2021, Zhang et al., 2021a, Jia et al., 2019, Gu et al., 2016).

The photostability and activity of AgX NPs can be improved through the anchoring of other supporting composites, namely, bismuth oxyhalide (BiOX, X = Cl, Br, I) (Liu et al., 2012, Cheng et al., 2011, Xiong et al., 2011, Adenuga et al., 2020, Adenuga et al., 2021), graphene oxide (GO) (Zhu et al., 2011a, Wang et al., 2013d, Gao et al., 2016, Fan et al., 2015) and titanate, which display various abilities of facilitating separation and transportation of the photogenerated electron-hole pairs.

© University of Pretoria

Table 2-2. Examples of the fabrication and application of AgX photocatalysts.

Photocatalyst	Synthesis method	Application	Reference
AgCl concave cubes	Wet chemical oxidization method	O_2 evolution	(Lou et al., 2012b)
Ag@AgCl	Deposition-photoreduction	Photocatalytic degradation of MB, RB; inactivation of cancer cells	(Wang et al., 2013a)
Ag@AgCl	Simple ion-exchange and light induced chemical reduction	Photodegradation of Methyl Orange (MO) dye	(Wang et al., 2010a)
Ag@AgCl	Polyol precipitation and photoreduction	Photodegradation of MO, RhB, MB, CV and alAR	(Wang et al., 2012c)
Ag/AgCl	Hydrothermal reaction	Photocatalytic degradation of MO	(Xu et al., 2011)
Ag@AgX (X=Cl, Br)	Facile and glycerol-mediated solution route	CO_2 reduction	(An et al., 2012a)
Ag@AgX (X=Cl, Br)	Double-jet precipitation method	Photodegradation of MO dye and 2,4-dichlorophenol	(Li et al., 2018)
Ag/AgX (X=Cl, Br, I)	Facile and template-free direct-precipitation method	Photocatalytic degradation of MO and Congo red (CR)	(Cui et al., 2015)
Ag/AgX (X=Cl, Br, I)	Hydrothermal method	Photodegradation of 2,4-DCP	(Moja et al., 2021)
AgBr	Ionic liquids-assisted hydrothermal method	Photodegradation of RhB	(Lou et al., 2011a)
AgBr nanowires	Replacement process	Degradation of MO	(Bi and Ye, 2010)

© University of Pretoria

Table 2-2. Continued…\

Photocatalyst	Synthesis method	Application	Reference
AgBr	Precipitation	Degradation of MO	(Wang et al., 2012a)
Ag/AgBr	Ion-exchange	Photocatalytic degradation of MO	(Duan et al., 2021)
Ag/AgBr	Hydrothermal and sunlight-induced routed	Degradation of MO	(Kuai et al., 2010)
Ag/AgBr	Double jet method	Degradation of MO	(Wang et al., 2011)
Ag/AgBr	One-pot solvothermal reaction	Photodegradation of MO, phenol and 2-chlorophenol	(Yan et al., 2013)
Ag/AgBr	Ion-exchange	Decomposition of isopropyl alcohol (IPA) and MO	(Wang et al., 2009)
Ag@AgBr	Facile wet chemical precipitation	Degradation of RhB and MO	(Li et al., 2013a)
Ag@AgBr polyhedral	Ion-exchange process with PVP as capping agent	Degradation of MO	(Wang et al., 2012b)
Ag@Ag(Br, I)	Ion-exchange	Reduction of $Cr^{(VI)}$ and degradation MO	(Wang et al., 2010b)
AgI	Anion-exchange route	MO and phenol photocatalytic decomposition	(Yu et al., 2012)
AgI concaves	Controlled precipitation	Degradation of RhB	(An et al., 2014a)
β-AgI	PVP-assisted-aqueous solution method	Degradation of RhB	(Jiang et al., 2014)
Ag@AgI	Ion-exchange	Degradation of RhB, hydrogen production	(An et al., 2014b)

© University of Pretoria

Transitional metal oxides are inexpensive, structural stable and possess a suitable band-gap, however UV-excitation is often required to perform photoreactions. Additionally, most metal oxides form a class of listed environmental pollutants due to their toxicity and the ability to affect organisms at the molecular level. However, under the applicable concentration levels, these toxic impacts are expected to be minimal compared to the energy reduction and low cost operational benefit. Thus, visible light responsive composite photocatalyst of AgX or Ag/AgX coupled with transitional metal oxides such as TiO_2 (Geng et al., 2017, Yu et al., 2015, Tian et al., 2014), ZnO (Kumar et al., 2020, Phongarthit et al., 2020, Lu et al., 2014) and WO_3 (Cao et al., 2011, Senthil et al., 2019) have been investigated. These composites photocatalysts have presented excellent stability and visible-light response. Furthermore, bismuth (Bi) coupled with AgX has gained considerable attention. Nanocomposites of Ag/AgBr/BiOBr displayed higher visible-light photocatalytic activity for the degradation of toluene and ethylbenzene than Ag/AgBr and BiOBr (Deng et al., 2021). A visible light responsive Ag/γ-AgI/Bi/$Bi_2O_2CO_3$ was prepared through a hydrothermal and precipation method and exhibited higher than $Bi_2O_2CO_3$ (Yan et al., 2021). Carbon-based semiconductors coupled photocatalyst have also attracted great interest due to their electronic properties as well as high surface area. The coupling of Ag/AgX NPs with carbon nanotubes (CNTs) or GO nanosheets display strong absorbance in the visible light region as a result of the SPR adsorption of Ag NPs (Gangu et al., 2019). Moreover, the hybrid present increased absorptive capacity of organic molecules through π-π interactions, which is favourable for the photodegradation process. Typical examples for synthesis and application of AgX and AgX-composites are summarised in Table 2-2 and Table 2-3.

© University of Pretoria

Table 2-3. Examples of heterogenous photocatalysts by AgX and other semiconductors.

Heterogeneous photocatalyst	Synthesis method	Application	Reference
$AgCl/Al_2O_3$	Precipitation	NO_x conversion	(Yamashita et al., 1999)
$AgCl/Bi_{24}O_{34}Cl_{10}$	Hydrothermal and deposited precipitation	Degradation of 2,4-dichlorophenoxy acetic acid (2,4-D) and tetracycline (TC)	(Adenuga et al., 2021)
Ag/AgX-CNTs (X=Cl, Br, I)	Facile ultrasonic-assistant deposition-precipitation	Degradation of 2,4,6-tribromophenol (TBP)	(Shi et al., 2013)
Ag/AgCl/BiOCl	In-situ precipitation	Photodegradation of phenol	(Adenuga et al., 2020)
Ag/AgX (X=Cl, Br) @Graphene	Deposition	Degradation of acridine orange (AO) dye	(Wang et al., 2013d)
$Ag/AgCl/W_{18}O_{49}$	Photochemical method	Sterilisation of *Vibrio natriegens*	(Chang et al., 2012)
Ag@AgCl-CA/SF	In-situ deposition	Bacterial inactivation of *E.coli* and *S.aureus*	(Wang et al., 2020b)
Ag@AgCl-KTO	Precipitation-photoreduction	Degradation of RhB	(Pan et al., 2016)
Ag@AgCl/ZnO	One-step radiation-assisted	Antimicrobial activity against *E.coli*, *P.aeruginosa*, *S.salivarius*, *S.aureus*, *C.albicans*	(Svoboda et al., 2020)

© University of Pretoria

Table 2-3. Continued…/

Heterogeneous photocatalyst	Synthesis method	Application	Reference
AgBr/CdS	Hydrothermal method	H_2 evolution using triethanolamine (TEOA)	(Ren et al., 2021)
AgBr/SiO_2	Schumann emulsion method	H_2 evolution from methanol in distilled water	(Kakuta et al., 1999)
Ag/AgBr/AgO_2/SPS	In-situ ion-exchange and photoreduction	Degradation of RhB	(Song et al., 2017)
Ag/AgBr/ mesoporous γ-Al_2O_3	Deposition-precipitation	Degradation of 2-chlorophenol (2-CP), 2,4-dichlorophenol (2,4-DCP) and trichlorophenol (TCP)	(Zhou et al., 2010)
Ag/AgBr/BiOBr	Photoreduction-precipitation	Photodegradation of MO, toluene and ethylbenzene	(Deng et al., 2021)
Ag/AgBr/$Cs_2Nb_4O_{11}$	Photoreduction-precipitation	Degradation of RhB	(Venkataswamy et al., 2019)
Ag/AgBr/rGO	Facile solution-mixing method	Degradation of RhB	(Meng et al., 2013)
Ag/AgBr/$NiFe_2O_4$	Coupled hydrothermal and solvothermal	Degradation of RhB	(Ge et al., 2017)
Ag/AgBr/ZnO	Two steps of deposition-precipitation	Degradation of RhB	(Shi et al., 2014)
AgI/WO_3 HHNFs	In-situ deposition-precipitation	Degradation of Eosin B and tetracycline chloride	(Zhi et al., 2020)

© University of Pretoria

Table 2-3. Continued…/

Heterogeneous photocatalyst	Synthesis method	Application	Reference
AgI/Bi_3O_4Cl	Solvothermal-calcination and in-situ deposition process	Photodegradation of RhB and tetracycline	(Chen et al., 2020)
AgI/$Bi_{24}O_{31}Br_{10}$	Solvothermal and coprecipitation	RhB degradation	(Ding et al., 2020)
AgI/$Bi_4O_5I_2$/NGCN	Microwave-assisted precipitation	Photodegradation of MB, MO, CR, RhB	(Habibi-Yangjeh et al., 2020)
AgI/BiOI	In-situ mechanical mixing	Degradation Eriochrome black T (EBT) dye	(Pourshirband et al., 2020)
AgI/g-C_3N_4	In-situ decomposition-thermal polymerization	N_2 photo-fixation	(Hu et al., 2020)
AgI/SnS_2	Hydrothermal - precipitation	Photocatalytic degradation of RhB	(Li et al., 2020)
AgI/MnO_2	In-situ deposition-precipitation	Sterilisation of *E.coli* and *S.aureus*	(Zhang et al., 2021b)
AgI/ZnO	Hydrothermal – chemical deposition	Degradation of RhB	(Liu et al., 2021)
Ag-AgI/Ag2O3	Deposition-precipitation	Degradation of 2-chlorophenol (2-CP), 2,4-dichlorophenol (2,4-DCP) and trichlorophenol (TCP)	(Hu et al., 2010)
Ag/AgI/TiO_2	Deposition-precipitation	Sterilisation of *E.coli*	(Yang and Zhou, 2011)

© University of Pretoria

Table 2-3. Continued…\

Heterogeneous photocatalyst	Synthesis method	Application	Reference
Ag/γ-AgI/Bi/$Bi_2O_2CO_3$	Hydrothermal – precipitation	Degradation of tetracycline	(Yan et al., 2021)
Ag@AgI/WO_3/PSCN	One-pot precipitation	Degradation of malachite green dye	(Hasija et al., 2020)

© University of Pretoria

2.7 Application of silver halide photocatalyst

2.7.1 Photocatalytic oxygen evolution

Photocatalytic water splitting into the H_2 and O_2 gaseous components, represents a promising approach for addressing energy and environmental issues (Di et al., 2017, Bai et al., 2015). This could theoretically allow direct generation of energy carrier (H_2)that is easily stored and transformed into electric energy (Hou et al., 2012). During the catalytic or photocatalytic water splitting, O_2 evolution presents a more challenging evolution process, as it requires a sequence of multiple reaction steps transferring a net of four electrons per oxygen molecules generated (Hou et al., 2012). Oxygen evolution is an absolute hole-participating reaction, which requires the VB edge to be lower positioned (more positive) than the potential of oxidation half reaction (Bai et al., 2015). Photocatalytic oxygen evolution was achieved by using 3D AgCl hierarchical structures under visible light irradiation (300 W Xe arc lamp) with $AgNO_3$ as the electron sacrificial agent. 3D hierarchical superstructures are formed through the fast growth of cubic seeds along the <111> direction, from the lower surface energy of (111) facets (Lou et al., 2012a). 3D AgCl hierarchical superstructures possess more active sites compared to concave cubic AgCl and cubic AgCl, consequently, drastically improving the oxygen efficiency form water, with an oxygen production of 254 μmol g^{-1} (Lou et al., 2012a). In addition, graphene-supported Ag_3PO_4/Ag/AgBr was prepared for oxygen evolution photolysis under 300 W Xe lamp with a 400 nm edge filter, visible light source, with $AgNO_3$ as a sacrificial reagent. The composite presented double the O_2-production, then that of bare Ag_3PO_4. Likewise, the composite presented improved activity compared to unsupported Ag_3PO_4/Ag/AgBr, graphene supported bare Ag_3PO_4 powder and Ag/AgBr. This increase in O_2-production can be attributed to a combination of depletion of the conduction band of the as prepared n-doped Ag3PO4 material as well as, the downshift of the Ag_3PO_4 valence band due to the pinning of its

© University of Pretoria

conduction at the Silver Fermi level, a process that is assisted by charge transfer and distribution onto the graphene support (Hou et al., 2012).

2.7.2 Photocatalytic hydrogen evolution

Since Fujishima and Honda discovered the generation of hydrogen and oxygen through photoelectrochemical water splitting in TiO_2 electrodes, much research has been dedicated to the development of novel photocatalysts with desirable photocatalytic activities (Liu et al., 2017a). Recent results revealed Ag/AgX (X = Cl, Br, I)/g-C_3N_4 composites are photocatalytically active for hydrogen evolution in a triethanolamine (TEOA) system, under visible light irradiation (Bai et al., 2019). Ag/AgI/g-C_3N_4-4 possessed highest hydrogen evolution rate of 59.22 μmol g^{-1} h^{-1} and photostable under visible light irradiation as displayed in Figure 2-7. The enhanced photocatalytic activities of Ag/AgI/CN-4 was ascribed to the synergistic effect between g-C_3N_4, Ag/AgI nanoparticles and the localized surface plasmon resonance effect of metallic Ag (Bai et al., 2019).

© University of Pretoria

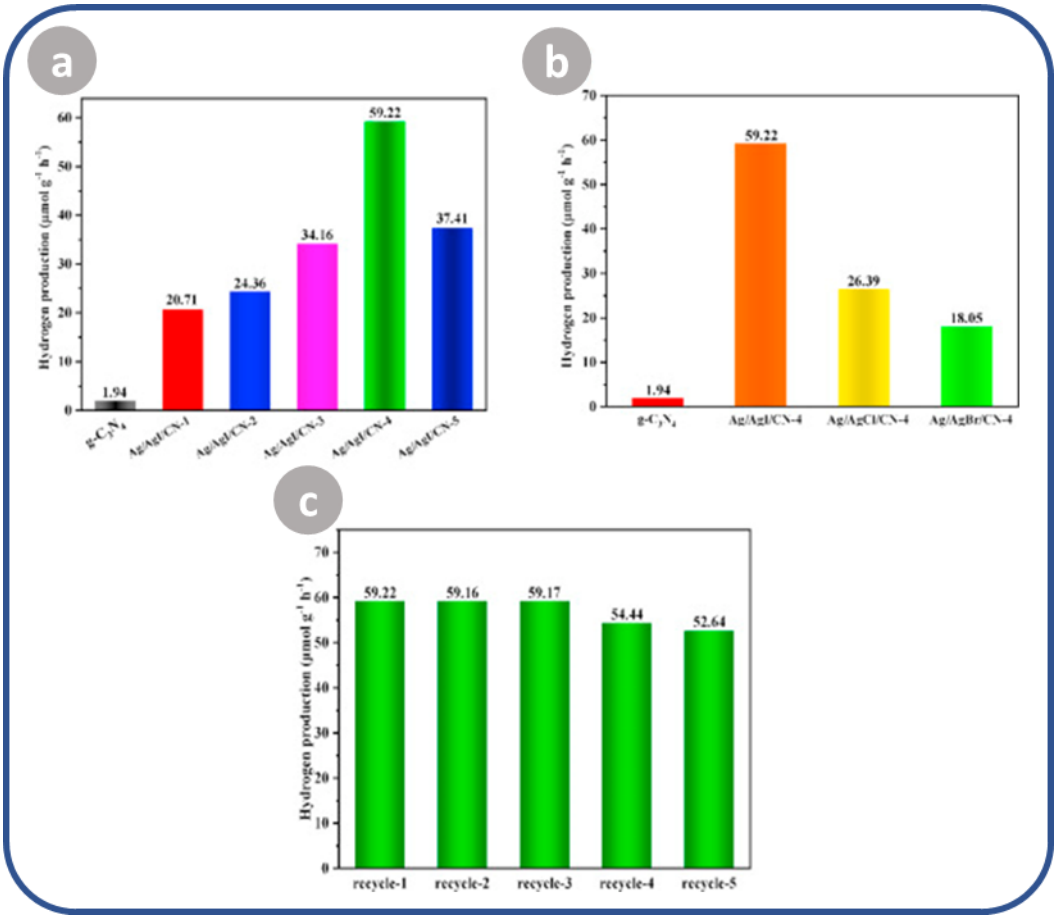

Figure 2-7. (a) Photocatalytic hydrogen evolution performance of pure g-C_3N_4 and Ag/AgI/CN heterjunction; (b) comparison of photocatalytic hydrogen evolution activities of pure g-C_3N_4 and Ag/AgX (X= Cl, Br, I)/CN-4 heterojunctions; (c) Recycle of photocatalytic hydrogen evolution over Ag/AgI/Cn-4 heterojunction under visible light irradiation (Bai et al., 2019).

In addition, g-C_3N_4-Ag/AgBr, prepared through solvothermal technology, promotes the hydrogen evolution capability of g-C_3N_4 with Ag/AgBr as the cocatalyst and triethanolamine (TEOA) as the sacrificial reagent (Li et al., 2019a). Tang et al. (2021), reported a novel efficient CDsAg-AgCl visible light photocatalyst, which exhibited a hydrogen evolution rate as high as 617.4 μmol g^{-1} h^{-1}. Photocatalytic hydrogen evolution of CDsAg-AgBr photocatalyst is reported to be 10.4 times higher than that of Ag/AgI/CN-4 composites (approx. 59.22 μmol g^{-1} h^{-1}) as reported by Bai et al. (2019).

© University of Pretoria

2.7.3 CO_2 photoreduction

In addition to photocatalytic oxygen and hydrogen evolution, CO_2 photoreduction into energy-bearing carbon fuels sources such as carbon monoxide, methane and ethanol, using semiconductor photocatalysts has been considered a sustainable and economical strategy for resolving the global energy crisis as well as decreasing the greenhouse effect (Di et al., 2017, Abou Asi et al., 2013, Torres et al., 2020). Binary AgX (Cl, Br) are promising photocatalysts in the conversion of CO_2 into liquid fuels as they possess more negative CB edges than $\phi^e(CO_2/CH_3OH)$ and $\phi^e(CO_2/C_2H_5OH)$ (-0.38 and -0.085 eV *vs*. NHE) (An et al., 2012a, An et al., 2012b, Cai et al., 2013). Recent research indicates that Ag/AgX photocatalysts are effective for photoreduction of CO_2. Cai et al. (2014) reported a red-coloured Ag/AgCl which performed better than normal Ag/AgCl photocatalysts (see Figure 2-8A.) for CO_2 photoreduction under 500 W Xenon arc lamp. The red-coloured Ag/AgCl photocatalyst was achieved through facile preparation using a versatile glycerol mediated method. The photocatalytic reduction products of CO_2 over red-coloured Ag/AgCl were methanol and ethanol with methanol as the major product. According to Cai et al. (2014), the enhanced optical adsorption of red Ag/AgCl can be attributed to both the synergy of Ag and AgCl as well as the Mie scattering effect due to the distinct morphology. In addition, AgCl, AgBr and $AgCl_XBr_{1-X}$ photocatalysts were synthesised and compared for their CO_2 conversion abilities(Cai et al., 2013). The element substitution promotes the photocatalytic activity in the photoreduction if CO_2 into methanol and ethanol for the ternary alloyed $AgCl_XBr_{1-X}$ photocatalysts. Figure 2-8B-c. compares the product yields for $AgCl_XBr_{1-X}$ NCs with various compositions, with $AgCl_{0.75}Br_{0.25}$ NCs exhibiting the highest conversion efficiency of methanol and ethanol yields at 181 and 362 μmol g^{-1}, respectively. Although there have been some advances in CO_2 photoreduction, the efficiency of existing photocatalytic materials is currently low (Di et al., 2017), thus more studies should be conducted in this field.

© University of Pretoria

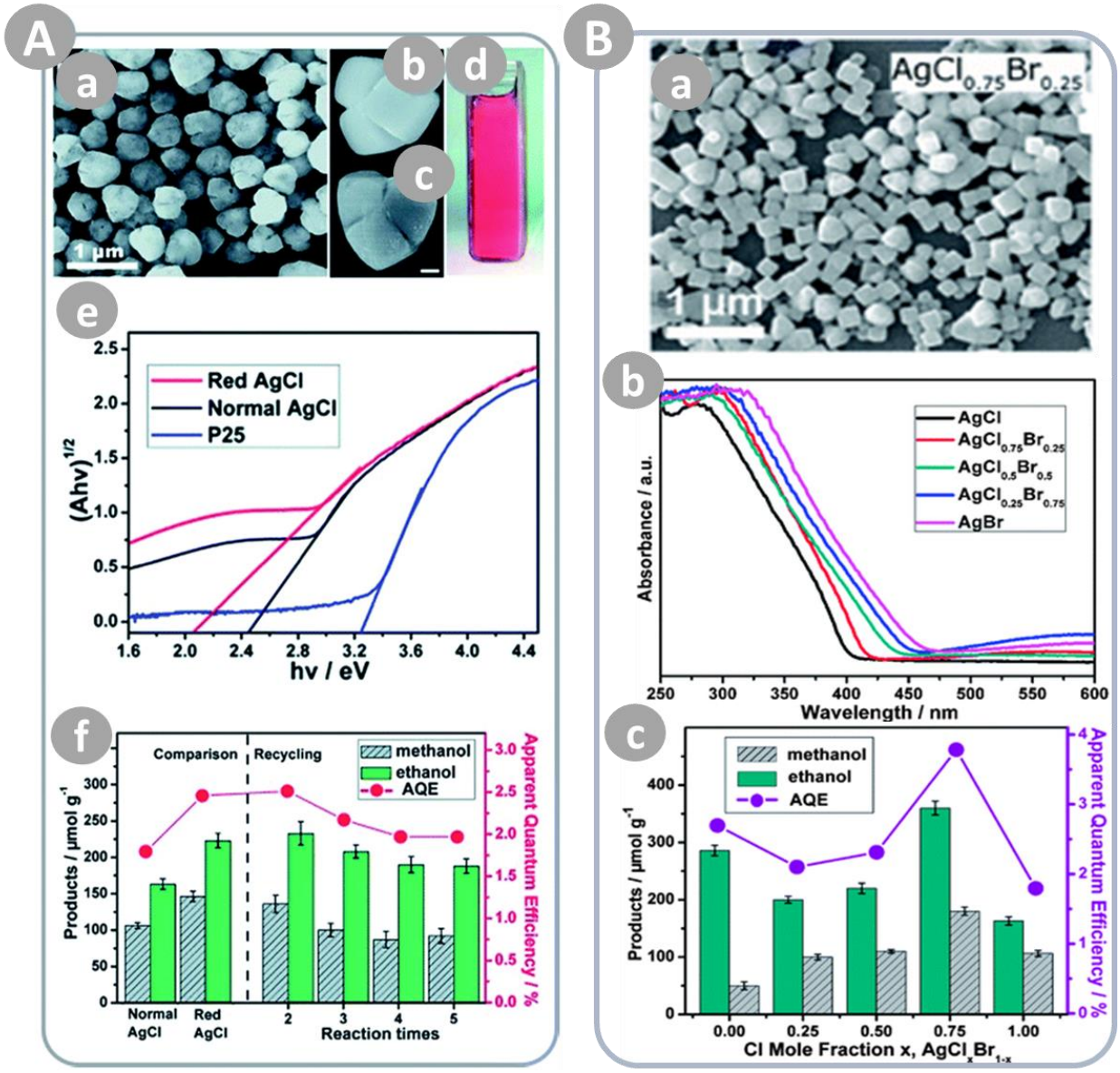

Figure 2-8. (A) Red Ag/AgCl photocatalyst: (a-c) SEM images, (d) photo image, (e) band-gap estimation using Kubelka-Munk theory and UV-Vis diffuse reflectance spectra, and (f) results of CO_2 conversion (Cai et al., 2014); (B) $AgCl_XBr_{1-X}$ NCs (a) SEM image of $AgCl_{0.75}Br_{0.25}$, (b) UV-Visible adsorption spectra, and (c) product yields of methanol and ethanol (Cai et al., 2013).

© University of Pretoria

2.7.4 Photocatalytic nitrogen

Nitrogen is the main component of building block structures such as amino acids and nucleotides (Vesali-Kermani et al., 2020, Liang et al., 2020). In natural environments enzyme nitrogenase reduce atmospheric N_2 into NH_3 (Hao et al., 2020, Xiao et al., 2018, Canfield et al., 2010, Ying et al., 2019, Shi et al., 2019). This process leads to the release of CO_2 gas into the atmosphere, which in one on the main greenhouse gases. Thus, studies have been conducted to develop cost-effective and low energy processes with mild conditions in the path of environmental protection of NH_3. To resolve this challenge, photocatalytic nitrogen fixation with catalysts possessing strong electron donors and abundant catalytic activation centres were utilised to enable interfacial charge transfer from the catalyst to N_2. Two-dimensional AgCl/δ-Bi_2O_3 nanosheets were synthesised through the hydrothermal method for efficient nitrogen fixation under visible light irradiation. The 3% AgCl/δ-Bi_2O_3 presented an excellent photocatalytic nitrogen fixation rate of 606 μmol h^{-1} g^{-1} under 3 h visible light irradiation, as the 2d nanosheets are able to chemically absorb and activate nitrogen as a result of oxygen vacancies (Gao et al., 2019). Following the aforementioned work, the Gao group further developed Ag/AgBr/δ-Bi_2O_3 nanosheets to fix N_2 to NH_4^+ under visible light irradiation. The 3% Ag/AgBr/δ-Bi_2O_3 exhibited a nitrogen fixation rate of 364.2 μmol h^{-1} g^{-1} which is 1.7 times lower than AgCl/δ-Bi_2O_3. The photocatalytic nitrogen fixation activity of 3% Ag/AgBr/δ-Bi_2O_3 could be attributed to the abundant surface active sites available on the 2D ultrathin nanosheets. Moreover, the obtained Ag/AgBr/δ-Bi_2O_3 exhibited excellent stability for visible light nitrogen fixation with no significant performance decrease after 5 cycles.

2.7.5 Photocatalytic disinfection

The conventional method of disinfecting drinking water is through the addition of chlorine. However, this method may produce potential mutagenic and carcinogenic disinfection

© University of Pretoria

by-products (DBP) during water chlorination, consequently alternative processes for disinfecting drinking water were developed. Alternative disinfection processes such as chemical oxidation (chlorine dioxide and ozonation), advanced filtration processes as well as germicidal ultraviolet (UV) radiation have been employed to disinfect drinking water. However, these alternative processes require expensive chemicals or costly equipment to generate the disinfectant onsite and by-products (Svoboda et al., 2020, Di et al., 2017). Among the alternative approach for disinfection, photocatalysis technology is becoming a viable option as a nontoxic, efficient, inexpensive and stable method. It has been illustrated that silver halide based photocatalysts can display antibacterial activity under visible light irradiation. Visible-light-driven photocatalytic inactivation of gram-negative *escherichia coli, pseudomonas aeruginosa* and gram-positive *streptococcus salivarius*, *staphylococcus aureus* bacteria strains and yeast *candida albicans* was accomplished in the presence of Ag@AgCl/ZnO (Svoboda et al., 2020). Under visible-light irradiation, AgCl and ZnO were excited to produce electron-hole pairs, and eletrons accumulated on the CB of ZnO thereafter trapped by O_2 to form $O_2^{\bullet -}$. The Ag-NPs show an SPR to form electron-hole pairs thus promoting the photocatalytic activity of bacterial destructions. The generated oxidative species (e.g., $O_2^{\bullet -}$., h^+) oxidized the cell membranes and then destroyed the cell.

2.7.6 Photocatalytic removal of pollutants

Due to their excellent photosensitivity and SPR; which can dramatically amplify visible-light absorption, Ag/AgX photocatalysts are widely used for the removal of pollutants such as toxic gases; poisonous ions (e.g· Cr (VI)) (Wang et al., 2012b); organic dyes (RhB, MB, MO) (Pan et al., 2016, Intaphong et al., 2021, Jiang et al., 2014, Wang et al., 2012c) and compounds such as ciprofloxacin (Abulizi et al., 2020), tetracycline (Huang et al., 2019), bisphenol A (Cheng et al., 2021), pentachlorophenol (Jiang et al., 2012), phenol (Tang et al., 2011), 4-chlorophenol (Xu et al., 2013), carbamazepine (Yentür and Dükkancı, 2020), 2-naphthol (Naya and Tada,

© University of Pretoria

2020), 2,4-dichlorophenol (Li et al., 2018), o-nitrophenol (Li et al., 2013b) and benzylic C(sp^3)-H bond (Hosseini-Sarvari and Dehghani, 2020). Generally, photogenerated holes and $O_2^{\bullet-}$ have been determined as the main active species under visible-light irradiation (Di et al., 2017).

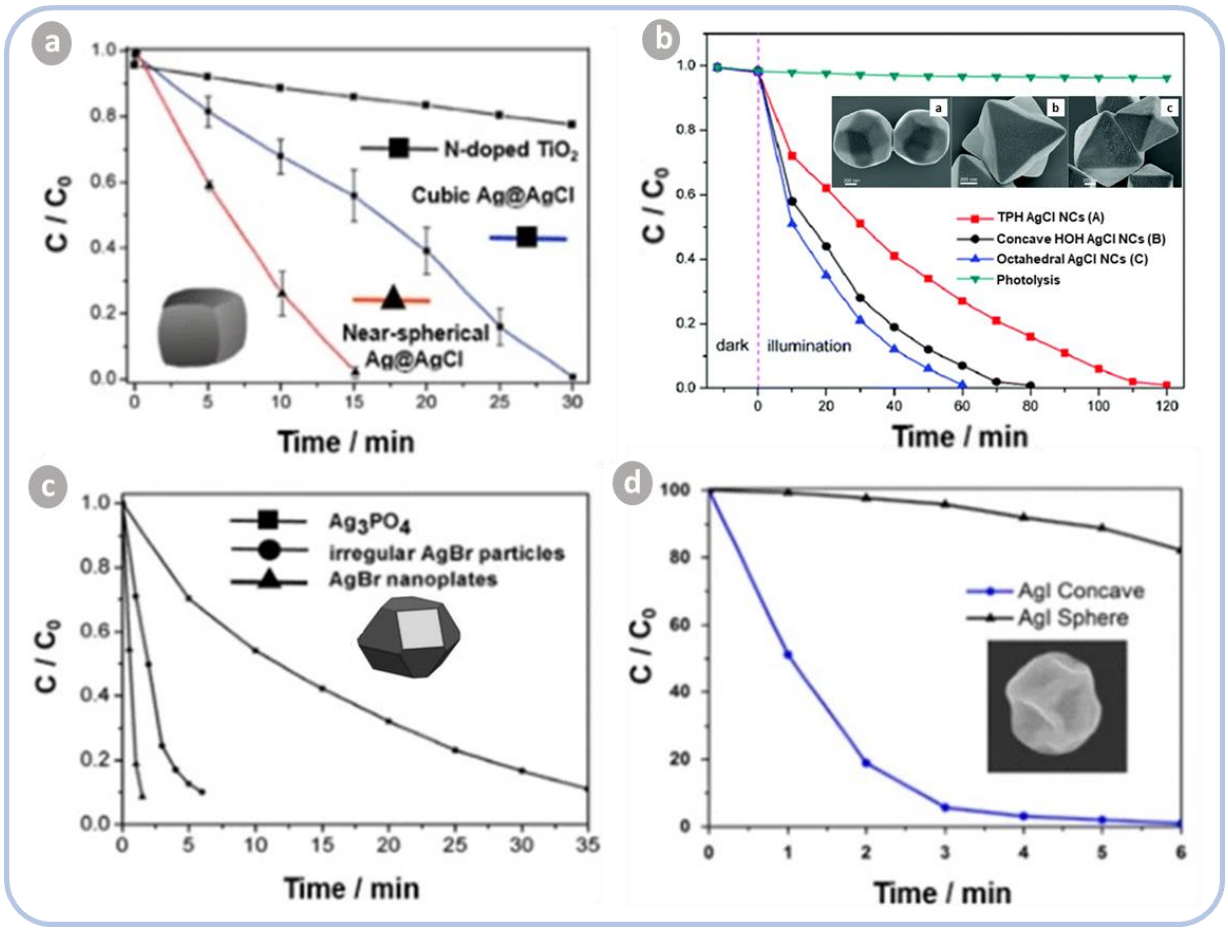

Figure 2-9. (a) Photodegradation of MO 20 mg L^{-1} dye solution over cubic Ag@AgCl, near-spherical Ag@AgCl and N-doped TiO_2 under visible light irradiation (Lou et al., 2011b, Fan et al., 2018), (b) Trapezohedral (TPH), concave hexoctahedral (HOH) and octahedral AgCl nanocrystals evaluated on MO dye under visible light irradiation (Zhang et al., 2015), (c) Photodecomposition of MO dyes over the irregular AgBr, AgBr nanoplates and Ag_3PO_4 (Wang et al., 2012a), (d) Concave and spherical AgI NPs with the concave NPs displaying superior performance to the spherical counterparts(An et al., 2014a).

AgCl semiconductor nanocrystals (NCs) with octahedral, trapezohedral (TPH) and concave hexoctahedral (HOH) morphologies were prepared through a direct one-pot solvothermal

© University of Pretoria

method (Zhang et al., 2015). They displayed enhanced photocatalytic activity for MO removal under visible-light irradiation, with the concave HOH AgCl NCs exhibiting the highest removal of 99 % of MO molecules in 60 min (Figure 2-9b.). Cubic Ag@AgCl removed 100 % of 2,4-dichlorophenol (100 mL, 40 mg L^{-1}) under visible-light irradiation after 60 min (Li et al., 2018). Furthermore, Ag@AgCl core-shell nanocomposites prepared using [Bmim]$FeCl_4$ IL (ionic liquid) etching Ag nanowires into Ag@AgCl decomposed over 81 %of 4-chlorophenol (100 mL, 10 mg L^{-1}) within 30 min (Xu et al., 2013). About 91.6 % of phenol was removed within 150 min using Ag/AgCl hollow microcubes with the ratio of Ag to AgCl (1:3) under visible light irradiation. The main active species of Ag/AgCl hollow microcubes was confirmed to be $^{\bullet}O_2^-$ and h^+ playing an important role in the process of photocatalysis (Tang et al., 2011, Lou et al., 2021). Ag/AgBr photocatalysts were synthesized using a simple one-pot synthesis method and further used to degrade Reactive Black 5 (RB5) as the model pollutant in investigating the effect of the concentration of excess silver ions on the SPR phenomenon (Bhatt and Patel, 2019). The synthesized AgBr exhibited 16.2 % degradation while Ag/AgBr exhibited an increased degradation of 86.5 % under visible irradiation. The presence of Ag^0 on AgBr improved the SPR effect thus improving the photocatalytic performance of Ag/AgBr. Furthermore, β-AgI nanoplates were fabricated using a facile polyvinylpyrrolidone (PVP)-assisted-aqueous -solution (PAAS) method under mild conditions (Jiang et al., 2014). The prepared AgI nanoplates exhibited excellent photocatalytic activity with enhanced durability in degrading RhB, under visible light irradiation relative to the bulk nanoparticles.

© University of Pretoria

CHAPTER 3

3 EXPERIMENTAL

3.1 Chemical and Materials

The following chemical reagents were used for the preparation of the photocatalysts. Silver nitrate ($AgNO_3$) was used as a source of metal ions while sodium chloride (NaCl), sodium bromide (NaBr) and potassium iodide (KI), were used as source of Cl, Br and I ions, respectively. All the aforementioned chemicals were attained from Glassworld (Johannesburg, South Africa). Ethanol (99.9 %, Illovo), was used to dissolve all impurities in the synthesized materials.

The simulation pollutants p-Benzoquinone (98 %) and isopropanol (99.5 %) were obtained from Sigma-Aldrich (St Louis, MO, USA) and applied as superoxide and hydroxyl radical scavenges, respectively. The electron and hole pair were scavenged with cupric nitrate (Associated Chemical Enterprises) and triethanolamine (Glassworld), respectively.

2,4-dichlorophenol ($C_6H_4Cl_2O$) was purchased from Sigma-Aldrich. HPLC mobile phase reagents acetonitrile (HPLC grade) and glacial acetic acid AR ($C_2H_4O_2$) were purchased from Merck and Glassworld, respectively.

The eluant reagents for the mobile phase in the HPLC, i.e., persulfate and phosphoric acid (Merck) was used as mobile phase in TOC analysis with potassium hydrogen phthalate (Merck) as the standard solution for calibration. Hydrochloric acid (HCl; 34 %) and sodium hydroxide (NaOH) obtained from Glassworld and Merck (South Africa), respectively, were applied for the variation of pH of sample solutions. Deionized water was used throughout this study, with

© University of Pretoria

ultrapure water only used in the study of TOC. All reagents were utilised without further purification.

3.2 Synthesis of Photocatalysts

The Ag/AgCl catalyst was produced using a hydrothermal method adapted and modified from Kuai et al. (2010). The preparation of AgCl followed a typical procedure of dissolving 105 mg of $AgNO_3$ in 30 mL of deionized water, thereafter 0.0016 mol of NaCl was added to the solution. After 10 min of vigorous stirring, the mixture was transferred into an autoclave and kept at 120 °C for 2 h. After cooling to room temperature, the product was collected and washed several times with deionized water and ethanol. Ag/AgCl was obtained through the dispersion of the obtained products in 10 mL of deionized water and irradiating under visible light for 3 h to convert some Ag^+ ions on the surface region of AgCl to Ag^0 species. Thereafter, the product was collected and dried at 60 °C for 12 h. The preparation of Ag/AgBr and Ag/AgI followed a similar procedure using NaBr and KI as halogen sources, respectively.

3.3 Characterisation

3.3.1 X-Ray Diffraction (XRD)

The crystal phases and composition of the Ag/AgX (X = Cl, Br, I) were evaluated using a PANalytical X'Pert Pro powder diffractometer in θ-θ configuration, equipped with an X'Celerator detector and variable divergence, as well as a fixed receiving slit with Fe filtered Co-Kα radiation (λ= 1.789 Å). Sample preparation was in accordance with the standardized Panlytical backloading system providing for near-random particle distribution. The data was collected in the angular range of 5° to 90° 2θ with a step size of 0.008° 2θ and 13 s scan step size. The mineralogy was evaluated through the selection of the best-fit pattern from the Inorganic Crystal Structure Database (ICSD) to the obtained diffraction pattern, through the X'Pert Highscore plus software.

© University of Pretoria

3.3.2 X-Ray Fluorescence (XRF)

The elemental percentage composition of the as prepared materials were investigated through the Thermo Fisher ARL Perform'X Sequential XRF instrument equipped with the Uniquant software. The software is able to analyse all periodic elements between sodium (Na) and Uranium (U), although only elements found above the detection limits were reported. A stable fused glass bead was prepared through mixing 1 g of sample with 6 g Lithiumteraborate flux and fused at 1050 °C. The samples were then roasted in alumina refractory crucible at 1000 °C to determine loss of ignition (LOI).

3.3.3 Scanning Electron Microscopy (SEM)/ SEM-Energy Dispersive X-ray spectroscopy (SEM/EDS)

The morphology and average particle size of the as-prepared particles were investigated using Scanning Electron Microscopy (SEM). The images were captured using a Zeiss Ultra Plus FEG scanning electron microscope, equipped with the Oxford instruments detector and Aztec 3.0 Software SP1. The elemental analysis was performed using SEM-EDS. For both analyses, the samples were prepared by distributing the as-prepared particles on a carbon tape stuck to a microscopy stub. Thereafter, the samples were stupor-coated with carbon under argon gas. The micrographs were performed at 3 kV.

3.3.4 X-Ray Photoelectron Spectroscopy (XPS)

XPS spectrometer (Thermo ESCAlab 250Xi) was utilised to quantitatively and qualitatively determine the surface composition of Ag/AgX (X = Cl, Br, I) as well as establishing whether elemental Ag was indeed formed on the surface of the AgX samples. The photoelectrons were excited by the monochromatic Al-kα (1486.7 eV) radiation as the excitation source and further detected with a hemispherical analyser. The analyser was operated with a pass energy of 100 eV for the survey spectra and the accumulation spectra of the core levels operated at 20 eV.

© University of Pretoria

Spot size of the XPS source on the samples was 200 µm with the pressure maintained below 10^{-8} mBar during data collection. The detection limit of XPS was approximately 0.1 atomic percentage.

3.3.5 Brunauer-Emmett-Teller (BET)

The surface properties, namely, specific surface area and pore size distribution were determined through nitrogen absorption-desorption and Brunauer-Emmett-Teller (BET) method by a surface area analyser (Micrometrics Tristar 3000 BET analyser). The samples were degassed at 150 °C for 24 h, for the removal of moisture or any other extraneous materials present. Degassing was performed under 10^{-5} Torr vacuum.

3.3.6 Ultraviolet-Visible Spectrophotometer (UV-Vis)

The optical properties of the as-prepared samples were investigated through Ultraviolet-visible spectroscopy using the UV-1600PC spectrophotometer with a grating 1200 line/mm silicon photo diode detector and a tungsten light source. Sample were analysed at room temperature at a range of 200-800 nm. The band gap energy (Eg) of the samples were estimated through the Tauc relation: $\alpha h\nu = A(h\nu - Eg)^{n/2}$ and attained through the determination of the straight line intercept of the plot of $(\alpha h\nu)^{1/2}$ or $(\alpha h\nu)^2$ against $h\nu$ for both indirect and direct conversions, respectively.

3.3.7 Photoluminescence Spectroscopy

The photoluminescence (PL) excitation and emission were measured on the Horiba Scientific Fluoro Max 4 Spectrofluorometer The measurements were conducted using a 150W CW Ozone free xenon arc lamp as an excitation source. Samples were excited at 360 nm and measured within wavelength range of 300 -800 nm.

© University of Pretoria

3.4 Degradation Studies

The photocatalytic degradation performance of the as-prepared Ag/AgX were evaluated with 2,4-dichlorophenol (2,4-DCP) under UV and visible light irradiation. The reactor set up comprised of 400 mL glass beaker placed on a magnetic stirrer, under a light source. The volume of the solution was maintained at 250 mL throughout the study. A 72 W LED lamp with a wavelength ranging from 380-800 nm was used as the visible light source and the UV light source was a 36 W LED (PHILIPS TUV 36 W/C36 T8) lamp. Before irradiation, 125 mg of photocatalyst was added into 250 mL of an aqueous 10 mg/L 2,4-DCP solution and stirred in the dark for 1 hour to reach the adsorption-desorption equilibrium. During photodegradation, 2 mL of aliquots were sampled at time intervals and collected for subsequent analysis after centrifugation and filtration for removal of catalysts.

Evaluation of the effects of catalyst loading

Based on the results from screening experiments under UV and visible light irradiation (as presented in Section 5.1), the best performing catalyst under visible light irradiation was further investigated to determine its optimum catalyst loading. The optimum catalyst loading was investigated through the evaluation of 0.25, 0.5, 0.75, 1.0, 1.5 and 2.0 mg/L loadings. This was executed by mixing 62.5, 125.0, 187.5, 250.0, 375, and 500 mg of catalyst in 250 mL of 10 mg/L of 2,4-DCP solution in a 400 mL reactor over 5 h.

Investigation of the effects of initial pH of 2,4-DCP solution

The effect of initial pH of the solution on photocatalytic degradation of the model pollutant *2,4-DCP* was evaluated through adjustment of solution pH to 3, 3.8, 5, 7, 9 and 11 from a pH of 5.8 using 0.1 M HCl and 0.1 NaOH, prior to conducting photocatalytic experiments. The photocatalytic degradation performance test of the photocatalysts was conducted with optimum catalyst loading.

© University of Pretoria

Evaluation of the effect of initial concentrations of 2,4-DCP on its photodegradation efficiency

The effect of pollutant concentration was investigated through the variation of initial 2,4-DCP concentrations as follows: 2.5, 5, 10, 20 and 40 mg/L. The photocatalytic test was conducted with optimum catalyst loading and optimum initial solution pH.

Modelling of 2,4-DCP photocatalytic kinetics

Upon determination of optimum conditions, the photocatalytic tests were performed under these conditions, with samples taken at 30 min intervals for 3 h, to investigate the kinetics.

Catalysts reusability studies

According to Zanjanchi et al. (2010) the stability of catalyst has a critical role in its reusability in environmental technology. Hence the effectiveness of catalysts reusability was examined for the photodegradation of 2,4-DCP during a five-cycle experiment. Each experiment was conducted under optimal conditions under visible light irradiation over 5 h. The suspensions were then centrifuged with a portion of the supernatant filtered through 0.22 µm Millipore filter prior to 2,4-DCP analysis with HPLC. Subsequent to each experiment, the solid residue from the photocatalytic degradation was washed and dried. The dried catalyst samples were used again for the degradation of 2,4-DCP employing similar conditions. After five cycles the residue was submitted for characterisation as presented in Section 3.3.1 and Section 3.3.3.

Study of the role of reactive oxidation species (ROS)

The experiments were performed using 1.5 g L^{-1} Ag/AgBr in 10 g L^{-1} solution at pH 5.0. The role of ROS: hydroxyl radicals, superoxide radicals, photo-generated hole and electron were evaluated using their respective scavenger: isopropanol (0.02 M), benzoquinone (0.001 M), triethanolamine (0.01 M) and cupric nitrate (5 mM).

© University of Pretoria

3.5 Analytical Methods

3.5.1 High Pressure Liquid Chromatography (HPLC)

The concentration of 2,4-DCP was determined using HPLC (Waters 2695 separation module with a 2489 UV/Visible detector). The HPLC was equipped with a Water PAH C18 (250 x 4.6 mm) and operated at 25 °C with the detector performing at 280 nm (Waters Instruments). The mobile phase was 60:40 (v/v) acetonitrile and deionized water and the flow rate at 1 $mLmin^{-1}$. The mobile phase solvents consisted of 0.1 % of acetic acid in both the acetonitrile and water. 2,4-DCP was identified through the comparison of the retention times with standard samples and thereafter, quantified with the calibration curve method. 2,4-DCP was identified at a retention time of 4.40 minutes. Empower software was used to collect the data.

Prior to HPLC analysis, the column was conditioned for 5 min, purged for 6.5 min thereafter equilibrated for 5 min to ensure that the column is primed and ready for analysis and has no contaminants.

3.5.2 Total Organic Carbon (TOC)

The degree of mineralisation was evaluated through the determination of TOC before and after the photodegradation of 2,4-DCP under optimal conditions. The rate of TOC removal was monitored with a Shimadzu TOC-V Analyser equipped with an autosampler. 35 mL of sample was taken before and after photodegradation, thereafter centrifuged and filtered with a 0.22 µm syringe filter (Millipore) prior to analysis. Ultra pure water was used as a blank to check for contaminants in the TOC injectors and tubes.

© University of Pretoria

CHAPTER 4

4 Characterisation of photocatalyst

4.1 Phase, Structure, and Morphology

XRD analysis was conducted to investigate the crystal structure of the as-prepared Ag/AgX (X=Cl, Br, I) photocatalysts. The obtained XRD spectra of the prepared photocatalysts are presented in Figure 4-1. The XRD pattern of Ag/AgCl displayed cubic phase of AgCl (Cui et al., 2015), with distinct diffraction peaks at a 2θ of 33°, 54° and 66° which can be assigned to (200), (311) and (400) planes, respectively. The XRD pattern of the Ag/AgBr catalyst showed cubic phase AgBr (Cui et al., 2015, Wang et al., 2011, Yan et al., 2013). AgBr peaks are located at a 2θ of 32.5, 52.5° and 65.5° correlating to (200), (311) and (400) plane, respectively. XRD patterns of Ag/AgI photocatalyst match the reported data by An et al. (2014b), of hexagonal phase β-AgI and cubic phase γ-AgI. The presented diffraction peaks are sharp and intense, indicating the high degree of crystallinity of the Ag/AgX species. The Ag^0 content could not be detected through XRD thus further characterization of the samples, such as XPS, was conducted to determine the presence of Ag^0 in the catalysts.

© University of Pretoria

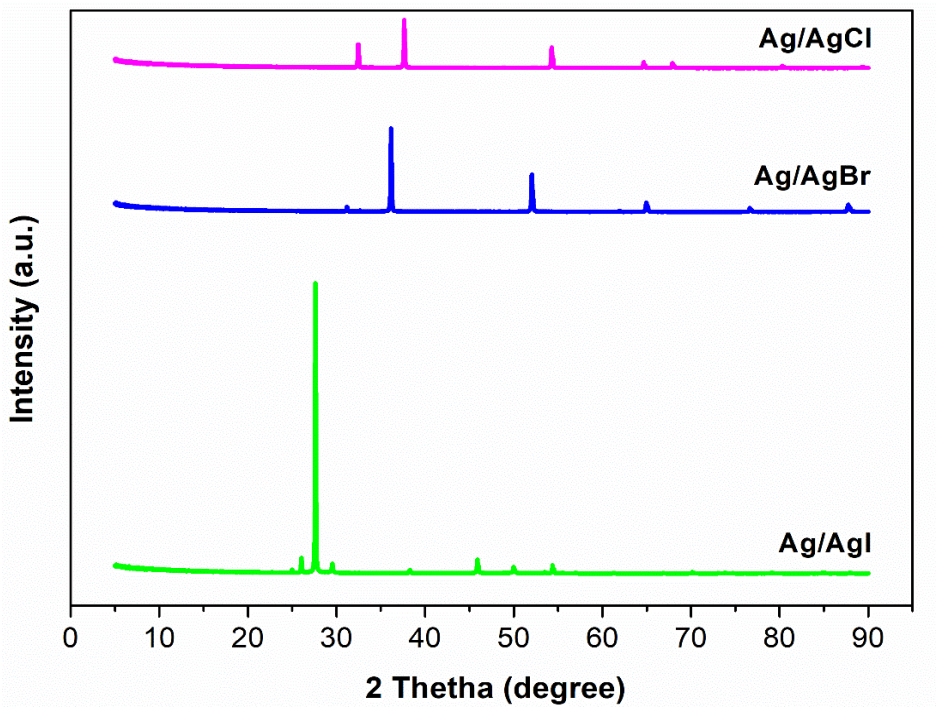

Figure 4-1. X-ray diffraction of the as-prepared Ag/AgCl, Ag/AgBr and Ag/AgI.

The morphology of the Ag/AgX particles has an effect on their photocatalytic properties as different morphologies lead to different surface areas and influence the rate of electron-hole recombination thus directly influencing their photocatalytic performance (Cui et al., 2015). The surface morphologies of the as-synthesized Ag/AgX were characterized by SEM and are presented in Figure 4-2 (a, c and e). Figure 4-2(a) presented an irregular and near-spherical morphology of Ag/AgCl while Ag/AgBr presented an irregular s shape (Figure 4-2(c)). Figure 4-2(e) show the polygonal plates of Ag/AgI. Based on the SEM results the as-prepared photocatalysts have particle size in the micron range. Kuai et al. (2010) and Wang et al. (2011) reported on the Ag/AgBr sphere-like morphology which presented enhanced photocatalytic activity of MO. Moreover, near-spherical Ag@AgCl crystals were synthesized by a hydrothermal method which presented enhanced performance compared to cubic Ag@AgCl due to its larger surface area. In addition, Kuang et al. (2014) investigated high-purity wurtzite-type β-AgI with hexagonal and triangular microplates in degrading organic pollutants. The as-prepared catalysts in the this study were agglomerated with a non-uniform distribution of

© University of Pretoria

particles, which is a characteristic of surfactant-free precipitation reactions in aqueous media (Reddy et al., 2015).

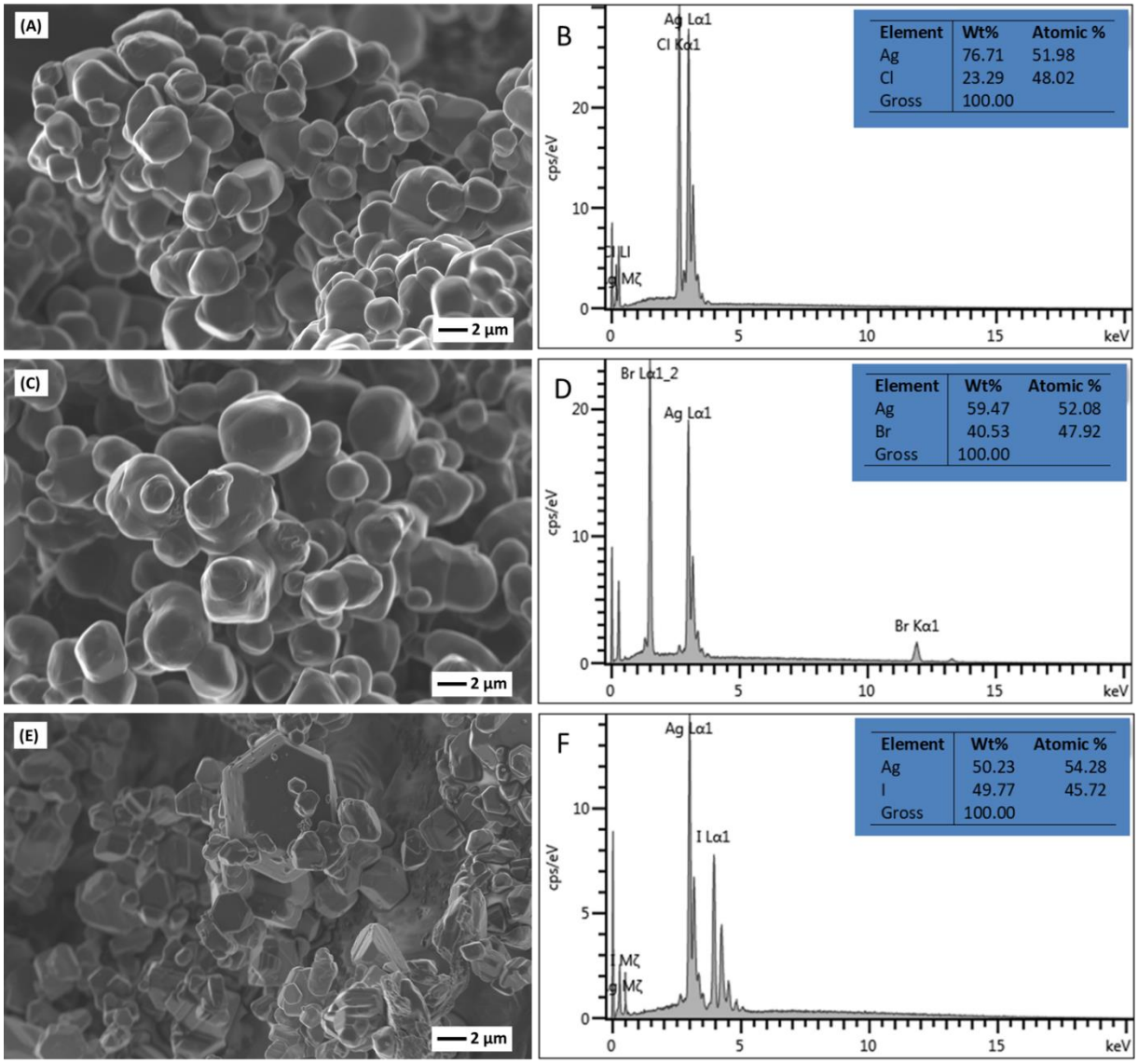

Figure 4-2. SEM images of (a) Ag/AgCl, (c) Ag/AgBr and (e) Ag/AgI as well as EDS spectrum of (b) Ag/AgCl, (d) Ag/AgBr and (f) Ag/AgI.

To further confirm the presence of silver and halide ions (-Cl, -Br, and -I) of the corresponding Ag/AgX catalysts an EDS analysis was performed. During the EDS measurement areas were focused and their corresponding peaks are presented in Figure 4-2 (b, d and f) for Ag/AgCl,

© University of Pretoria

Ag/AgBr and Ag/AgI respectively. The atomic weight percentage of Ag and halide ions for all the catalysts is relatively similar.

4.2 Chemical State and Composition

The surface composition and the chemical state of the as-prepared Ag/AgX nanoparticles were further verified through X-Ray Photoelectron Spectroscopy (XPS). As presented in Figure 4-3, the survey XPS spectra indicate that the samples of Ag/AgCl, Ag/AgBr and Ag/AgI all contain the peaks of Ag and C. The presence of carbon can be attributed to the hydrocarbon from the XPS instrument (Han et al., 2014, Jiang et al., 2014). Moreover, the peaks of Cl, Br and I were revealed in Ag/AgCl, Ag/AgBr and Ag/AgI, respectively.

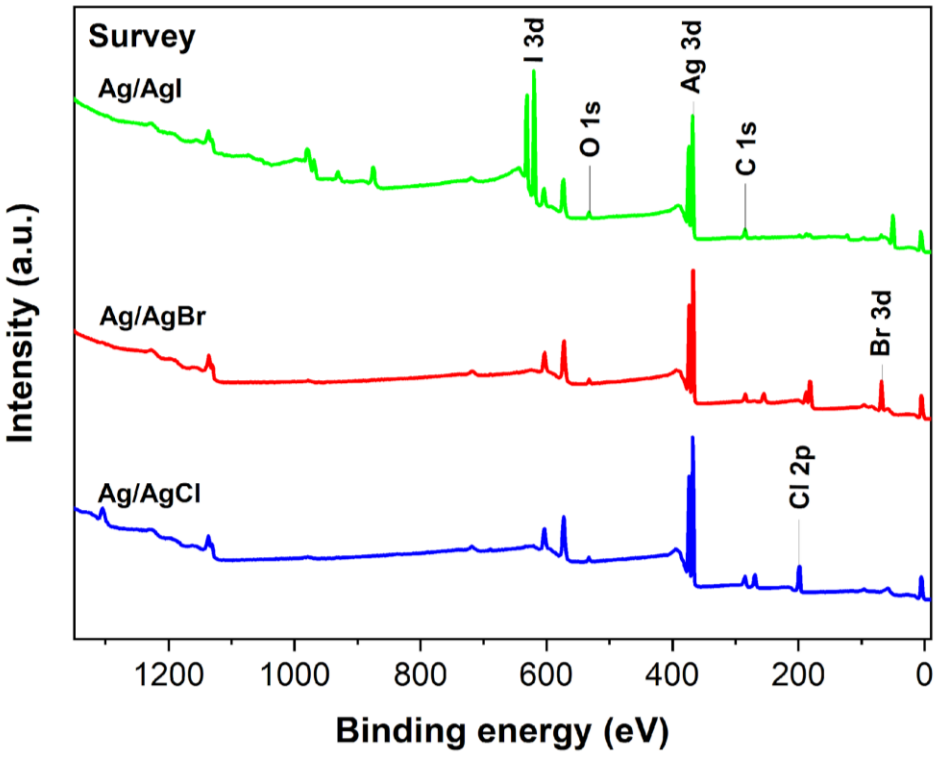

Figure 4-3. Overview XPS spectrum of the as-prepared Ag/AgCl, Ag/AgBr and Ag/AgI

As depicted in Figure 4-4a, c and e, Ag/AgX samples consist of two typical peaks of 3d located at ~367 and ~374 eV, which are ascribed to Ag $3d_{5/2}$ and Ag $3d_{3/2}$ binding energies (Mao et al., 2018, Liang et al., 2015, Liu et al., 2017b, Ai et al., 2013). The Ag $3d_{5/2}$ and Ag $3d_{3/2}$ peaks

© University of Pretoria

can be further deconvoluted into two peaks. In Figure 4-4a., the peaks at 367.7 and 373.7 eV are attributed to Ag^{+} of AgCl and those at 367.8 and 373.9 eV are attributed to metallic Ag^{0}. Shown in Figure 4-4c, are the peaks of 367.5 and 373.0 eV which are assigned to the binding energy of Ag^{+} of AgBr while the peaks at 367.8 and 373.9 eV are assigned to metallic Ag^{0}. Therefore, the results from XPS confirm the coexistence of Ag^{0} and AgX (X =Cl, Br and I). Moreover, Figure 4-4e., presents binding energies of Ag^{+} of AgI at 368.3 and 373.3 eV and those of metallic Ag^{0} at 368.4 and 374.4 eV. The high-resolution XPS spectra of Cl 2p, Br 3d and I 3d are presented in Figure 4-4b, d and f, respectively. Figure 4-4b., shows the spectrum of Cl 2p of AgCl with peaks at 198.0 and 199.6 eV attributed to Cl $2p_{1/2}$ and Cl $2p_{3/2}$ of metal Cl whereas the organic Cl are displayed at peak 200.2 (Cl $2p_{3/2}$) and 201.7 eV (Cl $2p_{1/2}$), respectively. The spectrum of Br 3d of AgBr in Figure 4-4d., presents the binding energies of Br $3d_{5/2}$ and Br $3d_{3/2}$ are 67.9 and 69.0 eV, respectively. In Figure 4-4f., the peaks at 619.8 and 631.3 eV are attributed to I $3d_{5/2}$ and I $3d_{3/2}$ of AgI, respectively.

© University of Pretoria

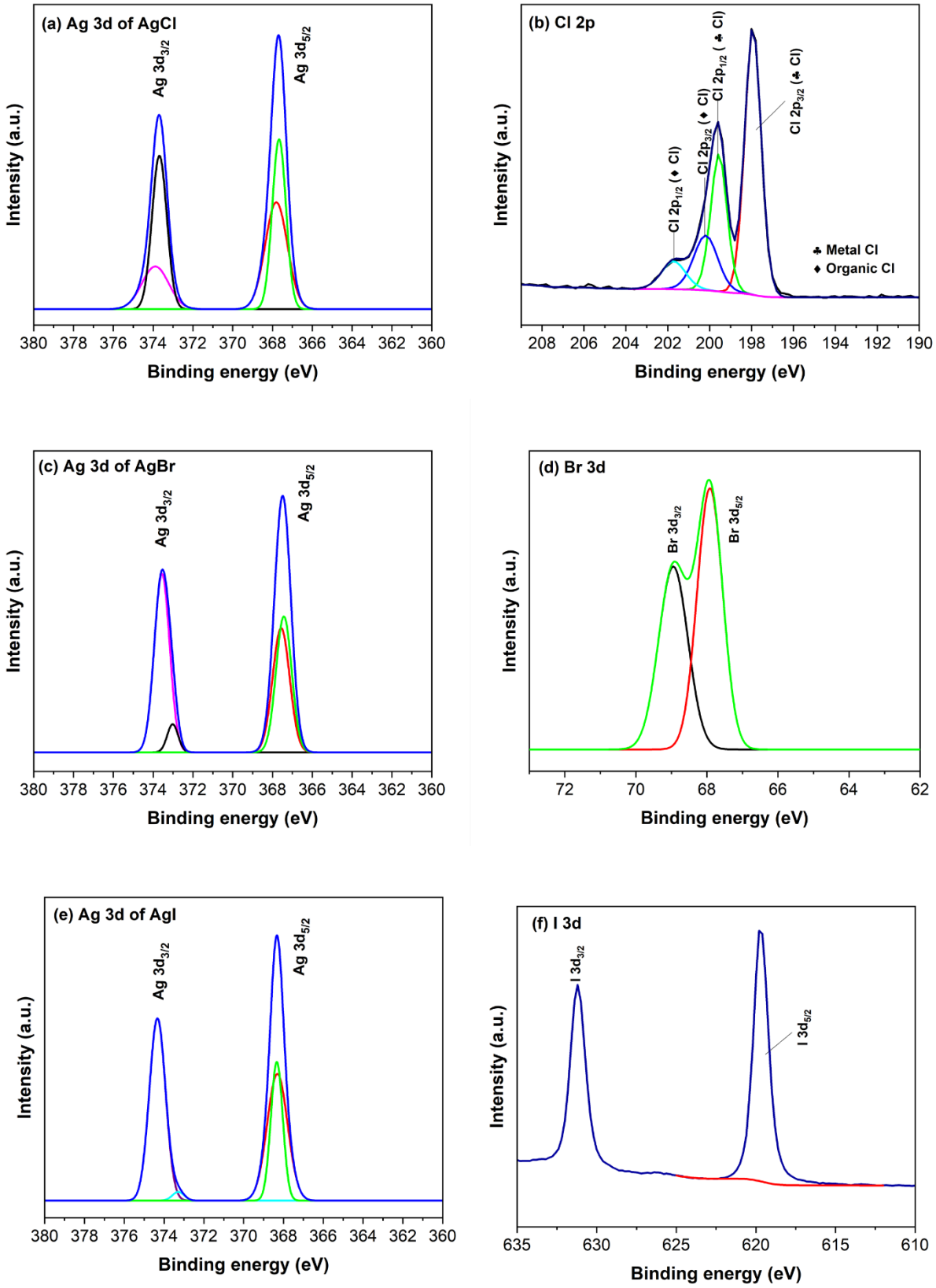

Figure 4-4. XPS narrow-scan spectra (a) Ag 3d and (b) Cl 2p of Ag/AgCl, (c) Ag 3d and (d) Br 3d of Ag/AgBr, (e) Ag 3d and (f) I 3d of Ag/AgI.

© University of Pretoria

4.3 Surface Areas and Pore Size Distribution

The pore size distribution and specific surface area of Ag/AgX were measured by the Brunauer-Emmett-Teller (BET) Nitrogen Adsorption-Desorption method. The adsorption-desorption isothermal curve of Ag/AgX samples is presented in Figure 4-5. According to the Brunaner-Deming-Deming-Teller (BDDT) classification all the samples presented type IV isotherms indicating the presence of mesopores with Ag/AgCl exhibiting an H3 hysteresis loop (Lv et al., 2018). The pore size distribution of the as-prepared samples was calculated using the Barrett-Joyner-Halenda (BJH) method from the desorption branch of the isotherms. As presented in inset Figure 4-5, the pore size distributions of Ag/AgCl, Ag/AgBr and Ag/AgI are relatively narrow with average pore size of 12.4, 6.8 and 5.8 nm, respectively. The calculated BET specific surface area of Ag/AgCl, Ag/AgBr and Ag/AgI is 0.09, 0.14 and 0.33 m^2/g, respectively. The BET surface area of the prepared photocatalyst are lower than those reported in literature. Lin et al. (2012) reported the BET surface area of 17.307 and 8.248 m^2/g for Ag/AgBr and Ag/AgI respectively. Moreover, Zai et al. (2017) reported a surface area of 1.40 m^2/g of AgCl, which is 15.5 times higher than the obtained surface area. The low surface area of the as-prepared Ag/AgX could be attributed the synthesis method which affected their morphology, which were different from those reported by Lin et al. (2012) and Zai et al. (2017). The photocatalyst surface area has a significant effect on the degradation of pollutants, the lower surface area has a low ability to absorb the pollutant from the solution, thus reducing the photocatalytic activity.

© University of Pretoria

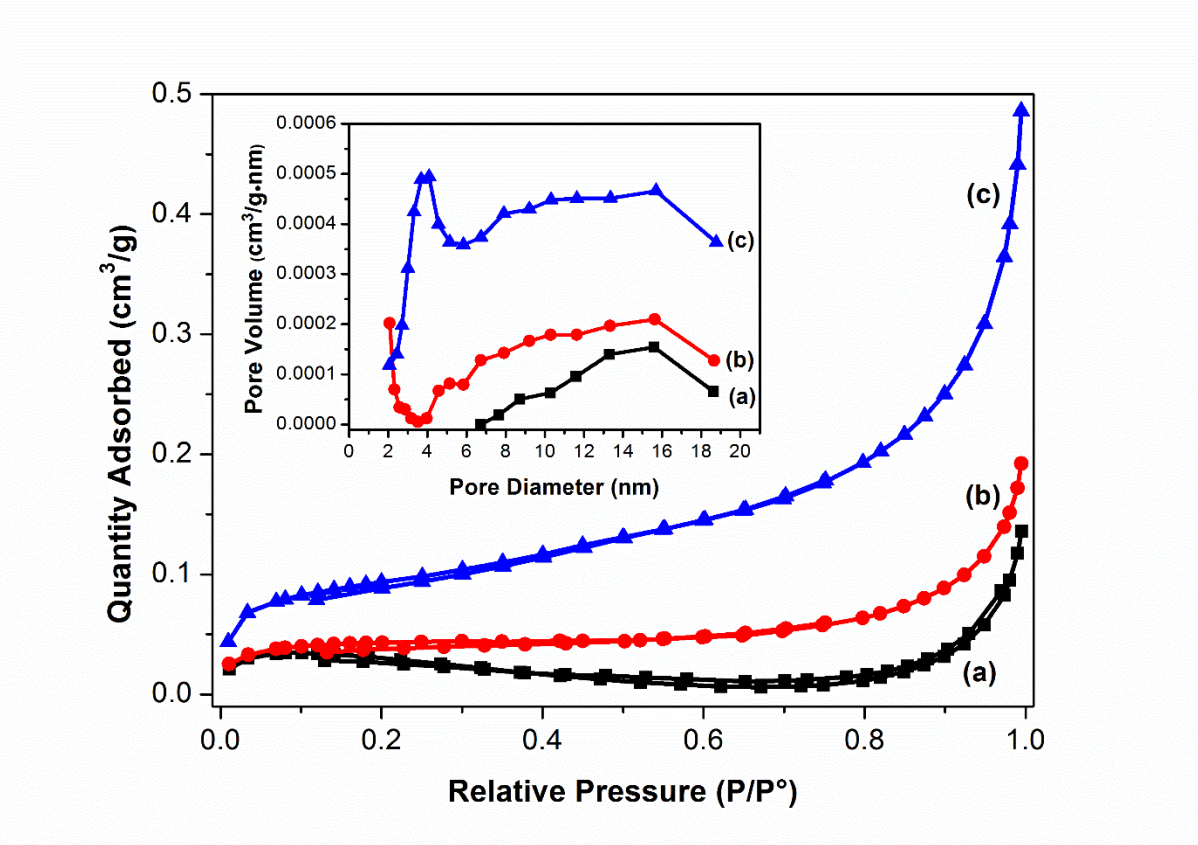

Figure 4-5. Nitrogen adsorption-desorption isotherms and inset corresponding pore size distribution curves of the as-prepared photocatalysts: (a) Ag/AgCl, (b) Ag/AgBr and (c) Ag/AgI.

© University of Pretoria

4.4 Optical and Photoelectrochemical Properties

The optical absorption properties of Ag/AgX nanoparticles were attained through UV-visible absorption spectroscopy in the spectral range of 200 – 800 nm. When AgCl, AgBr and AgI were irradiated by visible light, the photogenerated electrons combined with Ag^+ ions to form Ag^0 atoms, which further grow into Ag nanoparticles. Typically, the intensity of Ag SPR absorption is relative to the amount of Ag nanoparticles present in the sample (Li et al., 2018). In Figure 4-6a. the AgX (X =Cl, Br, I) samples exhibited distinct adsorption in the UV region but limited within the visible light region. The AgCl sample presents a peak which corresponds to the indirect exciton transition of 305 nm (An et al., 2010). The adsorption edge of AgBr was estimated to be at approximately 258 nm with an extended wavelength from 265 to 429 nm. The AgI nanoparticle presents a sharp absorption edge with an absorption maximum at approximately 428 nm, which was attributed to the characteristic band of AgI induced by the forbidden transition ($4d^{10}$ to $4d^9 5s^1$) permitted by the tetrahedral symmetry of the Ag^+ ion site (Reddy et al., 2015). The limitation and absence of absorption in the visible light region suggests the irradiated AgX (X = Cl, Br, I) produced trace amounts of metallic Ag.

The band gap energy of a semiconductor describes the energy needed to excite an electron from the valence band to the conduction band. The band-gap was determined from the DRS spectra, with the absorption coefficient (α) obtained through the Tauc equation ($(\alpha h\nu)^{1/n} = B\,(h\nu - E_g)$), where E_g is the band-gap energy, B is a constant that depends on the transition probability and n is the power index 2 for the direct band-gap (Reddy, 2016). The band-gap energies of the Ag/AgX nanoparticles were calculated by plotting the relation between the square of the Tauc function $(\alpha h\nu)^{1/2}$ and energy in electron volts as shown in Figure 4-6b, c. and d. From the Tauc plots, the optical direct band-gap of AgCl, AgBr and AgI were estimated as 4.95, 4.93 and 4.88 eV, respectively. Victora (1997) reported the direct band gap of AgCl, AgBr and β-AgI as 5.6 eV, 4.3 eV and 2.8 eV, respectively. The obtained band gap of AgCl was lower than the

© University of Pretoria

reported band gap, while the band gaps for AgBr and β-AgI were higher. Clearly the as-prepared photocatalysts cannot absorb visible light due to their wide band gaps.

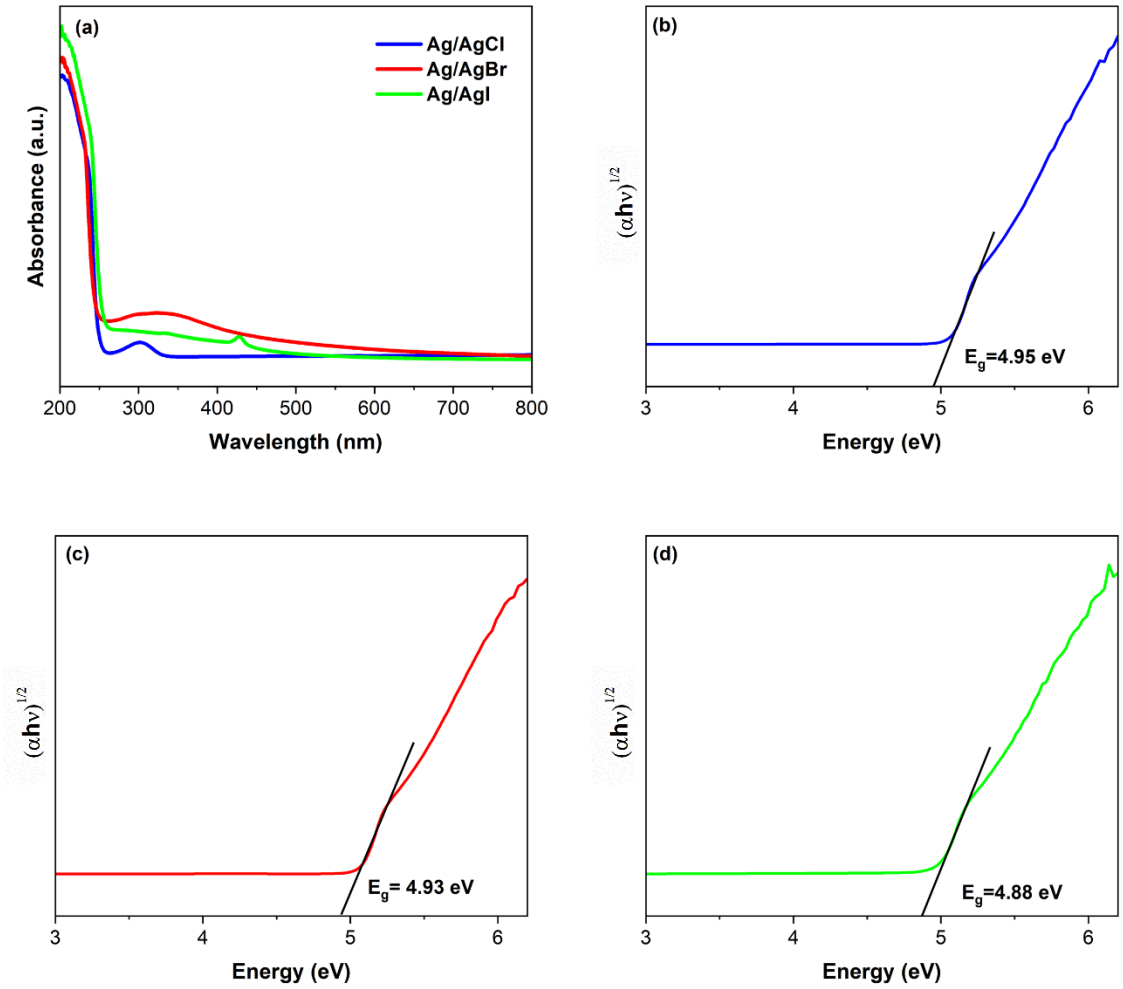

Figure 4-6. UV-visible diffuse reflectance spectra of the as prepared photocatalysts and band gap energy of (a) Ag/AgCl, (b) Ag/AgBr and (c) Ag/AgI

Moreover, the valance and conduction band edge potential for the synthesized Ag/AgX catalysts were calculated based on Mulliken Electronegativity Theory according to the empirical formula at the point of zero charge, which can be expressed as:

$$E_{VB} = \chi - E^C + 0.5E_g \quad (4\text{-}1)$$

$$E_{CB} = E_{VB} - E_g \quad (4\text{-}2)$$

© University of Pretoria

Where χ is the geometric average of the absolute electronegativity of each atom in AgX (X =Cl, Br, I); E^C is the potential of free electrons at a standard hydrogen scale (~ 4.5 eV); E_g is the band gap of the semiconductor; E_{CB} and E_{VB} are the band potential of the conduction band and valence band, respectively. The results are presented in Table 4-1.

Table 4-1. Band-gap (E_g), calculated valence band (E_{VB}) and conduction (E_{CB}) of the as prepared catalysts.

Semiconductor	χ /eV	E_{CB}/eV	E_{VB}/eV	E_g/eV
Ag/AgCl	6.07	-0.9	4.05	4.95
Ag/AgBr	5.81	-1.16	3.77	4.93
Ag/AgI	5.47	-1.47	3.41	4.88

Apart from the specific surface area of nanoparticles, the recombination rate of the photogenerated charge carriers and charge separation efficiency can affect photocatalytic activity. Due to the recombination of the free electron carriers, the photoluminescence (PL) emission spectra can be an effective approach to understanding the separation capacity of the photoinduced carriers (Cheng et al., 2010, Hou et al., 2013). Higher PL intensity indicate less efficient carrier participation in the photocatalytic procedure (Chen et al., 2018).

The photoluminescence of Ag/AgX (X=Cl, Br, I) nanoparticles, presented in Figure 4-7, was measured at an excitation wavelength of 360 nm. The PL spectra of Ag/AgCl and Ag/AgBr exhibited an emission peak centred at 411 nm which can be attributed to the recombination process of self-trapped exciton (Han et al., 2014, Wang, 2016). Moreover, Ag/AgI presents two peaks at around 411 and 602 nm which may be attributed to distant pair donor-acceptor (D-A) recombination mediated by the density of deep trap states involving exciton-phonon interactions or crystalline defects or impurities (Reddy et al., 2015). The high PL intensity of

© University of Pretoria

Ag/AgI at 602 nm demonstrated high recombination efficiency of the photogenerated electron-hole which will lower the photocatalytic activity of Ag/AgI.

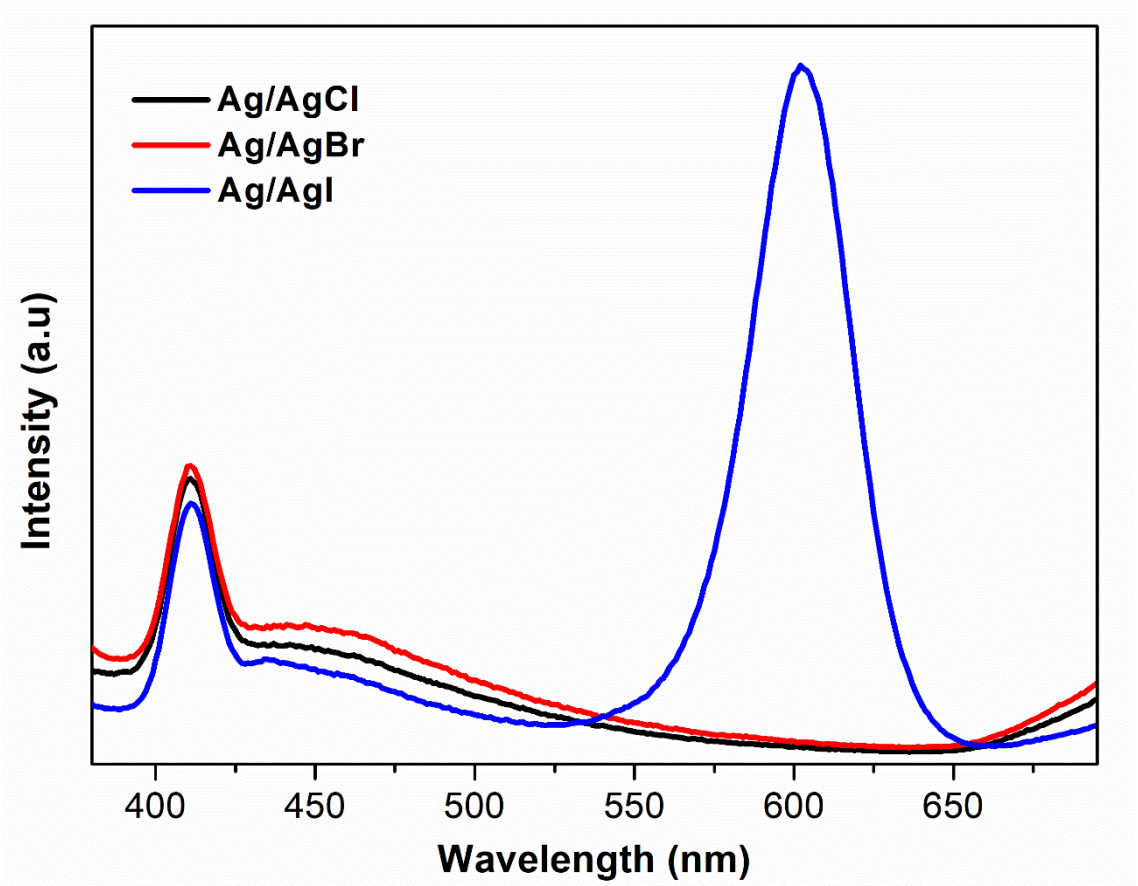

Figure 4-7. Photoluminescence spectra of the as-prepared photocatalysts.

© University of Pretoria

CHAPTER 5

5 Degradation studies

5.1 Photocatalytic degradation performance

The photocatalytic degradation potential of the as-prepared Ag/AgX nanoparticles were evaluated based on the degradation of 2,4-DCP under UV and visible-light irradiation. Figure 5-1a. and b show the temporal concentration changes of 2,4-DCP with different as-synthesized photocatalysts. As shown in Figure 5-1a. and b., 36.37 % and 30.97 % degradation of the pollutant in the blank experiment (photolysis process) was achieved with no photocatalysts added under UV and visible-light irradiation, respectively. The degradation of 2,4-DCP under UV and visible light photolysis could be attributed to the direct dichlorination of 2,4-DCP through a nucleophilic displacement of chlorine Kuo (1999). These results are lower than those reported by Kuo (1999) who reported a degradation 48.2 % under UV radiation after a 10 min reaction. Furthermore, the adsorption ability of the as-synthesized nanoparticles were investigated. As presented in Figure 5-1a. and b., Ag/AgCl exhibits an adsorption of 63.36 % after 300 min, which is slightly higher than Ag/AgBr (53.36 %) and Ag/AgI (55.11 %), this can be attributed to the catalysts surface polarity. The catalysts surface polarity played a critical role in adsorbing 2,4-DCP over the specific surface area (Sobiesiak, 2017). In the interaction between silver and halide atoms, the affinity is slightly negative, resulting in an overall negative charged surface. The interaction of Ag/AgX and 2,4-DCP would yield a high adsorption efficacy this is due to the attraction forces between the catalysts and absorbate. Figure 5-1a. and b., illustrate the photocatalytic degradation efficiencies of 2,4-DCP for Ag/AgCl, Ag/AgBr and Ag/AgI under UV and visible-light irradiation.

© University of Pretoria

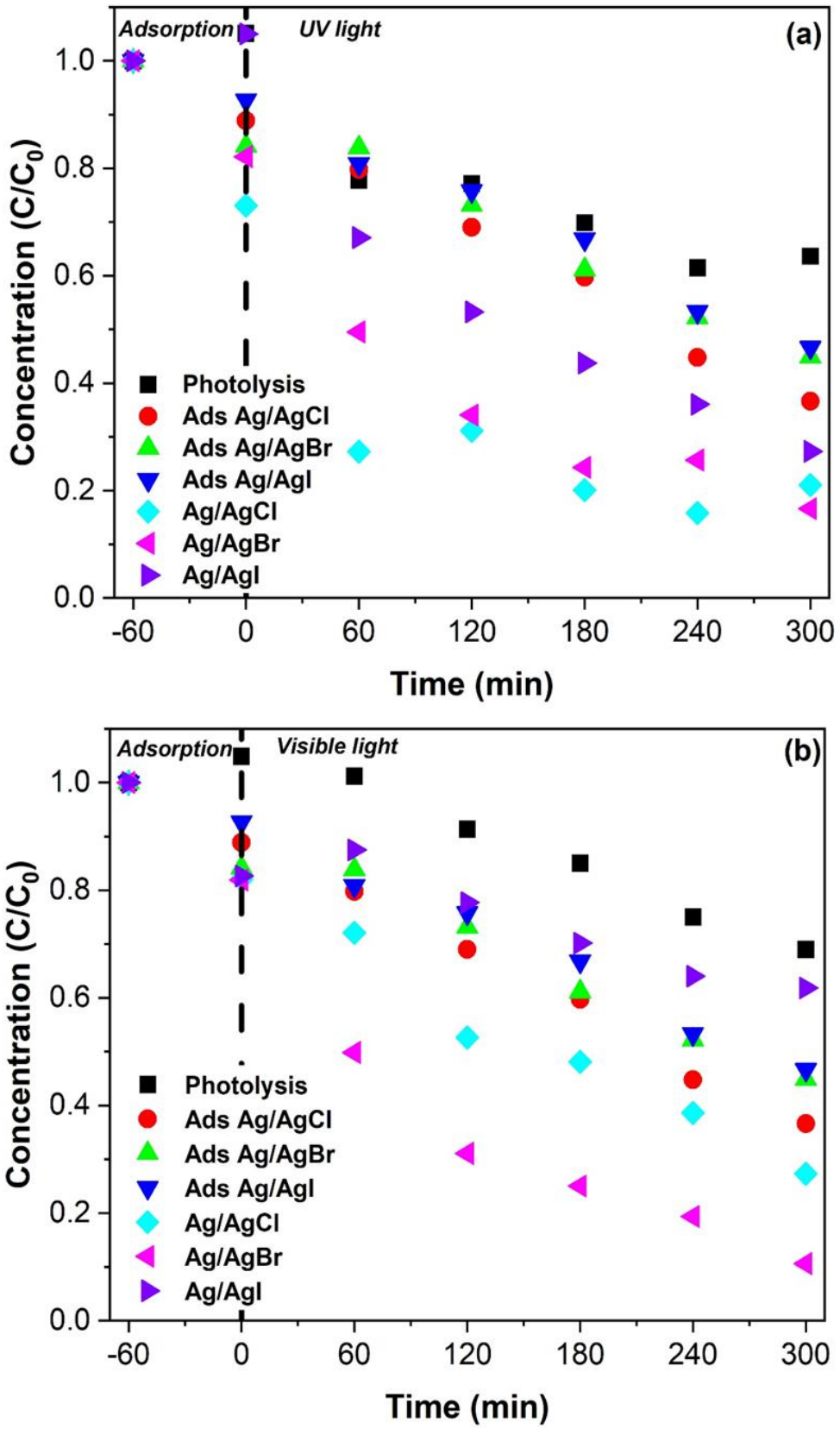

Figure 5-1. Photocatalytic degradation of 2,4-DCP with as-prepared catalysts Ag/AgX (X = Cl, Br, I) under (a) UV-light and (b) visible light irradiation.

© University of Pretoria

The Ag/AgBr photocatalyst exhibited the highest photodegradation efficiency under both UV and visible-light irradiation for 2,4-DCP removal, with a degradation of 83.37 % and 89.39 % respectively. Ag/AgI had the lowest efficiency under both lights with approximately 72.71 % removal under UV irradiation and 38.16 % under visible light after 300 min of irradiation. Ag/AgCl presented an efficiency of 78.96% and 72.70 % under UV and visible light, respectively. Tian (2012) has reported on the visible light response of Ag/AgX, stating that for Ag/AgCl photocatalyst the visible light photocatalytic activity is primarily related to the plasmonic adsorption of Ag, whereas in the case of Ag/AgBr and Ag/AgI both Ag and AgX respond to the visible-light irradiation producing more electrons and holes. Thus, Ag/AgBr usually presents higher photocatalytic activity than Ag/AgCl. This correlates with the results of this study wherein the Ag/AgBr photocatalyst exhibited the highest degradation under visible light irradiation. Ag/AgBr was chosen as the suitable photocatalyst for degrading 2,4-DCP under visible irradiation, thus the optimal amount of the photocatalyst was further investigated.

© University of Pretoria

5.2 Optimum operating conditions

The effect of operational parameters such as catalyst loading, pH as well as the initial concentration of 2,4-DCP were investigated utilising Ag/AgBr as the optimum photocatalyst.

5.2.1 Catalyst Loading

To determine the optimal amount of Ag/AgBr photocatalyst, the catalyst loading was investigated in the range of 0.25 to 2 g/L at 10 mg/L initial 2,4-DCP concentration and a pH of 5.8 (natural pH of 2,4-DCP). The effect of catalyst loading on the degradation efficiency is depicted in Figure 5-2. As can be observed, the optimum Ag/AgBr loading for degrading 2,4-DCP was 1.5 g/L. The optimum catalyst load obtained in this study is comparable to that reported for ZnO mediated degradation of 2,4-DCP (Gaya et al., 2010). It was observed that the degradation efficiency increases with an increase in the catalyst amount from 0.25 to 1.5 g/L which could be attributed to the increasing availability of photocatalytic sites (Gaya et al., 2010, Chen et al., 2015, Pinho and Mosquera, 2013, Guillard et al., 2005). Above the 1.5 g/L Ag/AgBr concentration, the degradation efficiency decreases, this may be attributed to the aggregation of AgBr nanoparticles at higher concentrations reducing the number of surface active sites and increasing the opacity and light scattering of AgBr nanoparticles and thus resulting in poor light utilization (Yu et al., 2000, Pinho and Mosquera, 2013, Pei and Leung, 2013).

© University of Pretoria

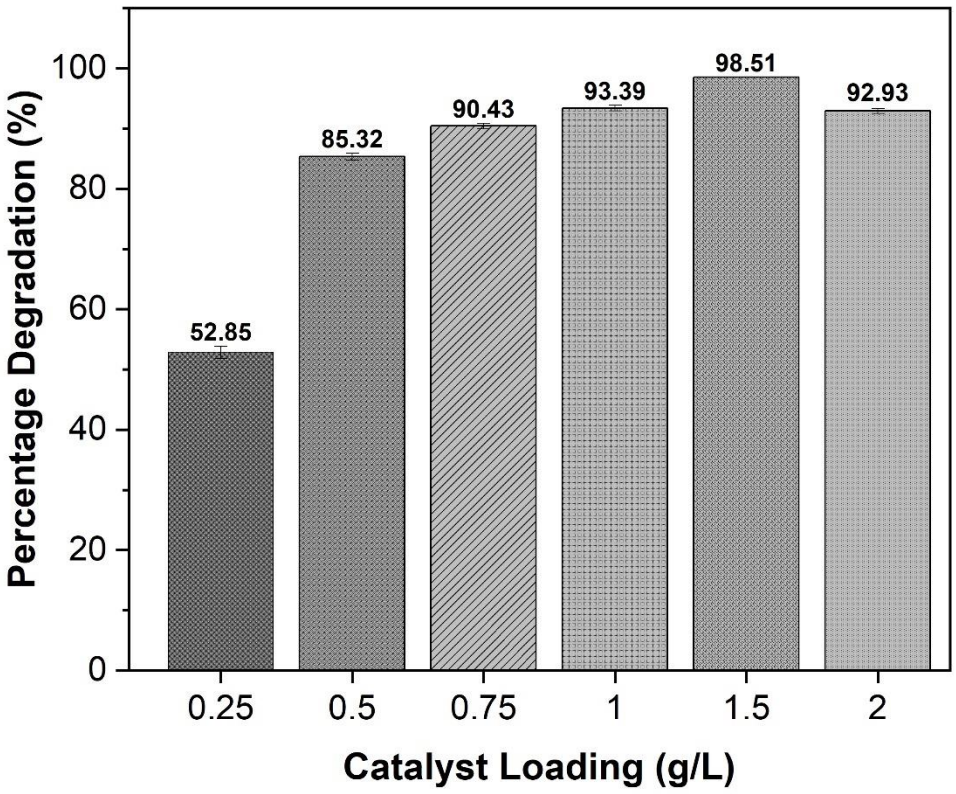

Figure 5-2. Effect of catalyst loading on the degradation of 2,4-DCP using Ag/AgBr under the following conditions: 2,4-DCP concentration; 10 mg/L; visible light illumination time: 300 min, pH 5.8.

5.2.2 pH effect

pH plays a critical role in influencing the degradation efficiency of pollutants in contaminated water. Effluents from industrial processes often have diverse pH values (Zhang et al., 2018), thus it is vital to investigate the degradation efficiency of 2,4-DCP at various pH values. The changes of the pH value and degradation of 2,4-DCP using Ag/AgBr (1.5 g/L; 10 mg/L) are presented in Figure 5-3. The degradation percentage was above 98 % for pH values from 3 to 9, with the highest degradation percentage observed at an initial pH of 7. When the pH value was increased to 11 the degradation percentage decreased slightly to 81.29 %. Thus Ag/AgBr

© University of Pretoria

may be applied over extensive pH values with weak acidic conditions being advantageous for the removal of contaminants (Lai et al., 2021). Hence pH 5 was considered as the optimum pH for this study.

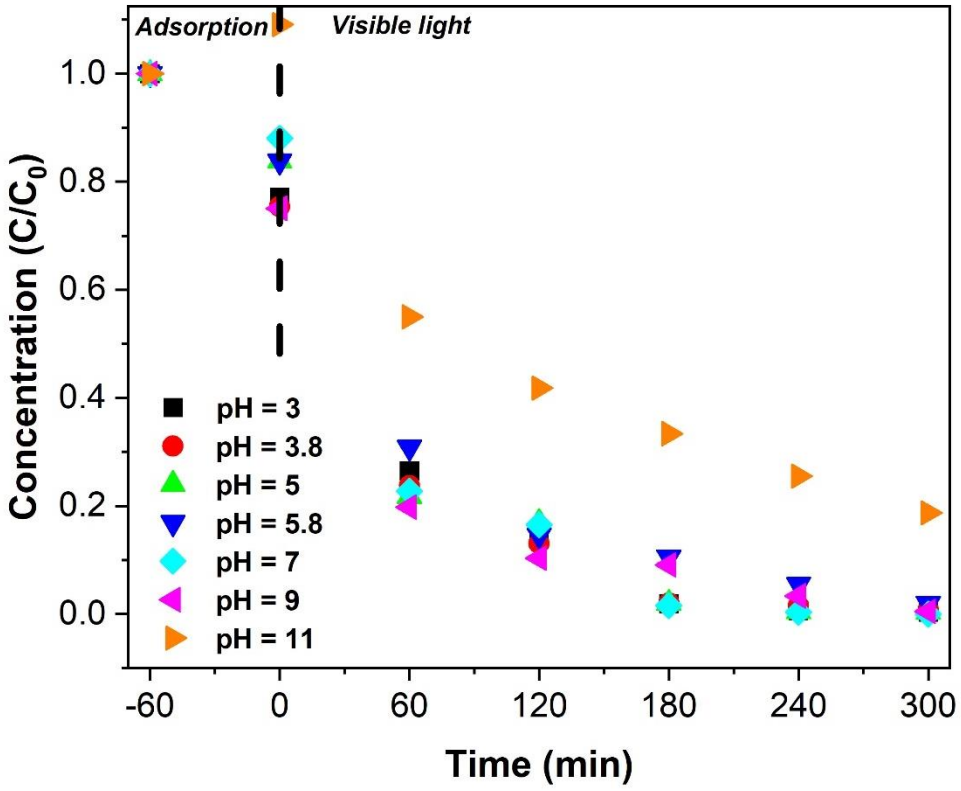

Figure 5-3. Effect of initial pH concentration on the photocatalytic degradation of 2,4-DCP in water using Ag/AgBr: 1.5 g/L; 2,4-DCP; 10 mg/L; illumination time: 300 min.

According to Zhang et al. (2018) the observed trend can be attributed to the increased generation of free radicals and oxidation potential of •OH radical under acidic conditions. Moreover, 2,4-DCP is easily destroyed/decomposed by •OH radical at lower pH as 2,4-DCP remains in its molecular state (pKa of 7.89) (Gaya et al., 2010). With an increase in pH value the concentration of the hydroxide ion will increase, consequently some hydroxyl radicals could combine with OH^- ions forming water and thus decreasing the degradation ratio; similar as in the case of pH 11 (Zhang et al., 2018).

© University of Pretoria

5.2.3 Effects of pollutant concentration

The concentration level is one of the significant factors for effective transformation of a pollutants (Gaya et al., 2010, Azubuike et al., 2016). The effect of the concentration was studied at 2.5 to 40 mg/L 2,4-DCP. Figure 5-4., displays the change of photocatalytic degradation efficiency over varied initial concentrations of 2,4-DCP. As shown in Figure 5-4., the initial concentration influences the degradation efficiency, the degradation rate increases with an increase in the initial concentration from 2.5 to 10 mg/L thereafter decreases over 10 mg/L. This observed trend may be attributed to two factors. Firstly, increasing the concentration of 2,4-DCP will result in an increase of absorbed 2,4-DCP molecules on the surface of Ag/AgBr, thus reducing active sites of the catalysts due to over saturation and consequently decreasing hydroxyl radical generation. Secondly, increasing the concentration of 2,4-DCP may cause a reduction in the photo-absorption capacity of Ag/AgBr particles, therefore reducing the photodegradation efficiency (Liang et al., 2019, Soltani and Lee, 2016).

© University of Pretoria

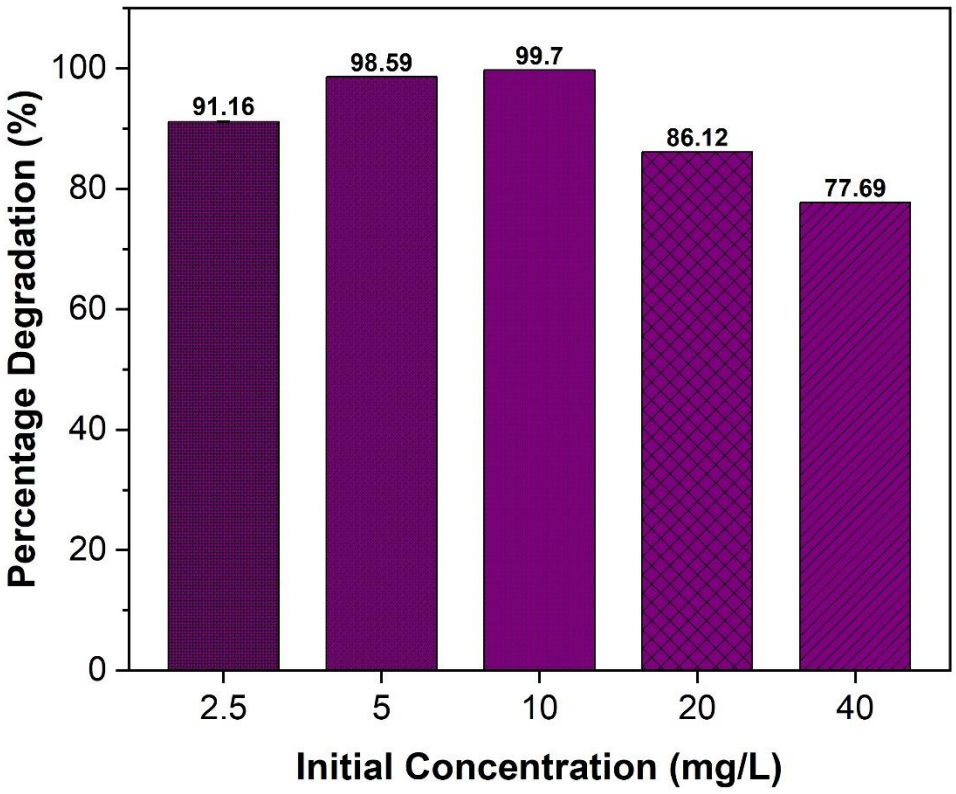

Figure 5-4. Effect of initial concentration on 2,4-DCP photodegradation at catalyst loading (Ag/AgBr) of 1.5 g/L and pH 5 after 300 min irradiation.

5.2.4 Kinetic Study

The reaction kinetics provide valuable information on the rate and mechanism of the reaction that indicates the degradation of pollutants (Ranjbar et al., 2019). Pollutant degradation kinetics in heterogeneous photocatalysis from the aqueous phase have commonly been analysed using the Langmuir-Hinshelwood model (Equation (5-1)) (Fan et al., 2018, Kumar et al., 2008, Melián et al., 2007):

$$r = -\frac{dC}{dt} = \frac{kKC}{1+KC} \qquad 5\text{-}1$$

Whereby:

- r - represents the initial rate of reaction (mg L^{-1} min^{-1})

© University of Pretoria

- t - is the reaction time (min)
- C - indicate the real-time concentration of pollutant (mg L^{-1})
- K - denotes the Langmuir adsorption equilibrium constant (L mg^{-1})
- k – expresses the Langmuir-Hinshelwood reaction rate constant (mg L^{-1} min^{-1})

For dilute concentration cases (KC<<1) of water pollutants, KC is negligible, thus a pseudo-first-order kinetics model can be deduced from Equation (5-1) through Equation (5-2) and (5-3):

$$r = -\frac{dC}{dt} = -kKC \quad (5\text{-}2)$$

$$ln\left(\frac{C}{C_0}\right) = -kKC = -k_{app}t \quad (5\text{-}3)$$

C_0 - represents the original concentration of water pollutants (mg L^{-1})

K_{app} – is the apparent rate constant (min^{-1})

During the study of the effect of the initial concentration on the efficiency of 2,4-DCP degradation, the normalised concentration of 2,4-DCP (ln (C_0/C)) indicate a linear relationship with irradiation time, thus proving that these degradations follow the first-order kinetics model (Equation (5-3)).

© University of Pretoria

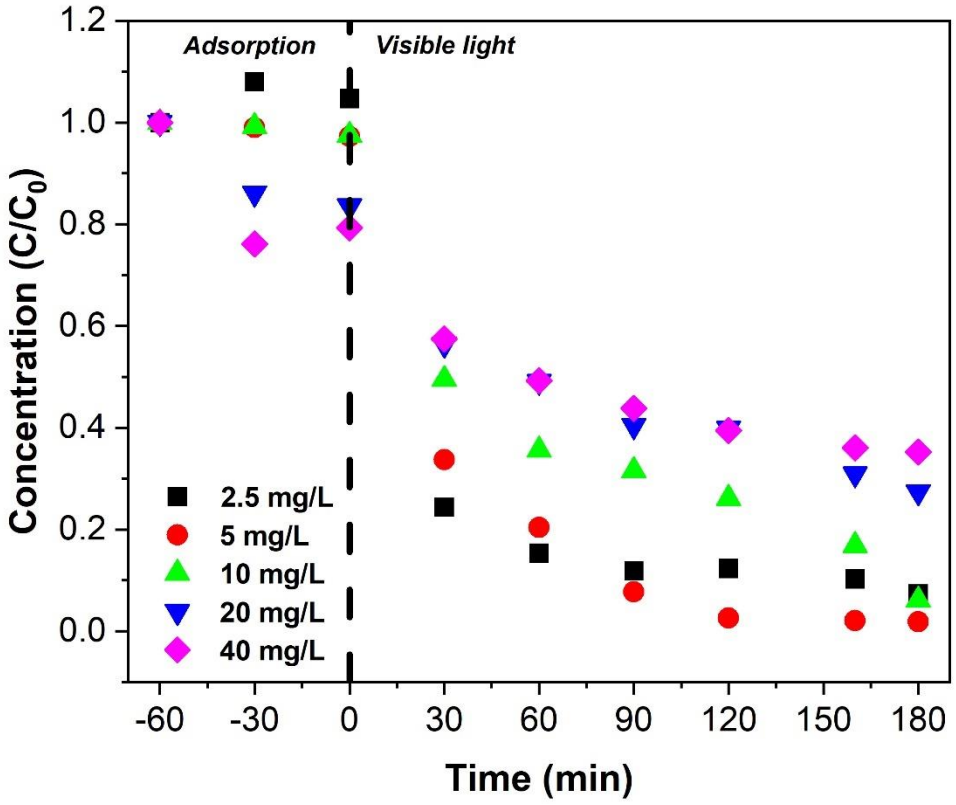

Figure 5-5. Photocatalytic degradation with different initial concentration of 2,4-DCP using Ag/AgBr under visible light irradiation.

Figure 5-5., show the photocatalytic degradation of 2,4-DCP over 180 min under visible light irradiation. Through pseudo first-order fitting between ln (C_0/C) and t (as presented in Figure 5-6) k_{app} can be determined from the linear slope and applied to evaluate the degradation rate among the different initial substrate concentrations in the same experiment. Approximately 98 % was removed in 180 min suggesting that at a concentration of 5 mg/L, Ag/AgBr is more photo-responsive for the removal of 2,4-DCP compared to other initial concentrations. The k_{app} for 2,4-DCP at an initial concentration of 5 mg/L was 0.01283 min^{-1}.

© University of Pretoria

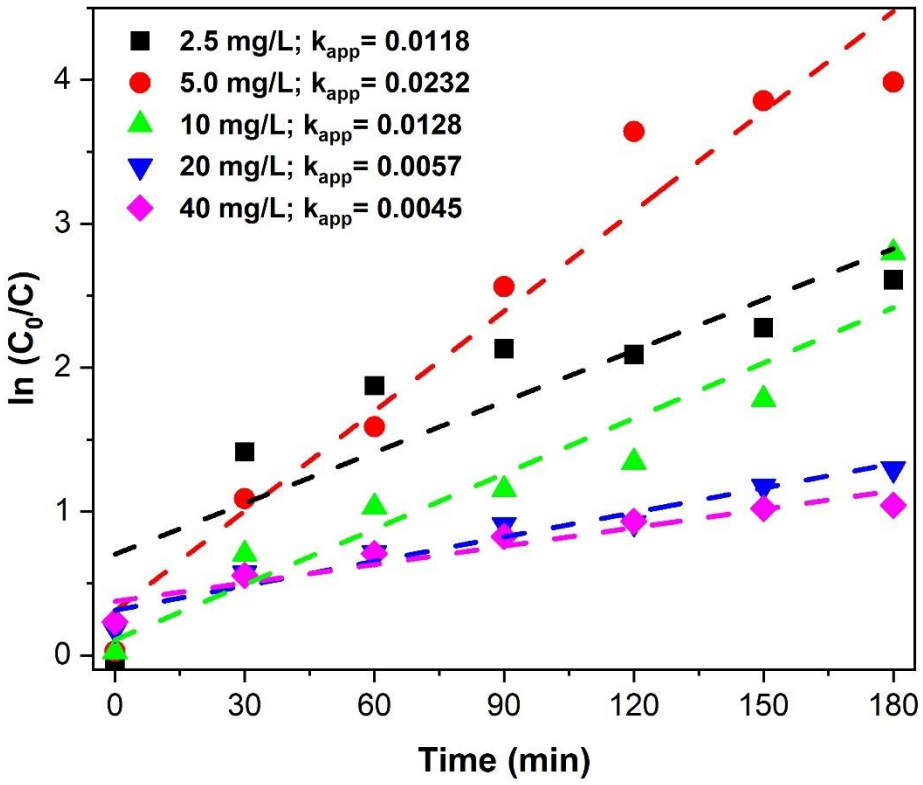

Figure 5-6. Pseudo first order reaction kinetics of 2,4-DCP at various initial 2,4-DCP concentration; catalyst loading 1.5 g/L; pH 5.

5.2.5 Total Organic Carbon Study

The decrease of total organic carbon (TOC) concentration was investigated to evaluate the extent of mineralisation of 2,4-DCP in the system. The TOC analysis was conducted under optimized conditions of 2,4-DCP concentration of 10 mg/L, pH of 5 and catalyst loading of 1.5 g/L under visible light irradiation. Figure 5-7, illustrates the final conversion of TOC compared to the extent of 2,4-DCP degradation after 300 min of radiation under visible light. From the TOC analysis, approximately 26.94 % of 2,4-DCP was mineralised, while 99.7 % degradation was achieved using Ag/AgBr. The low TOC removal was attributed to the possible formation of intermediate products during the breakdown of the primary 2,4-DCP molecule.

© University of Pretoria

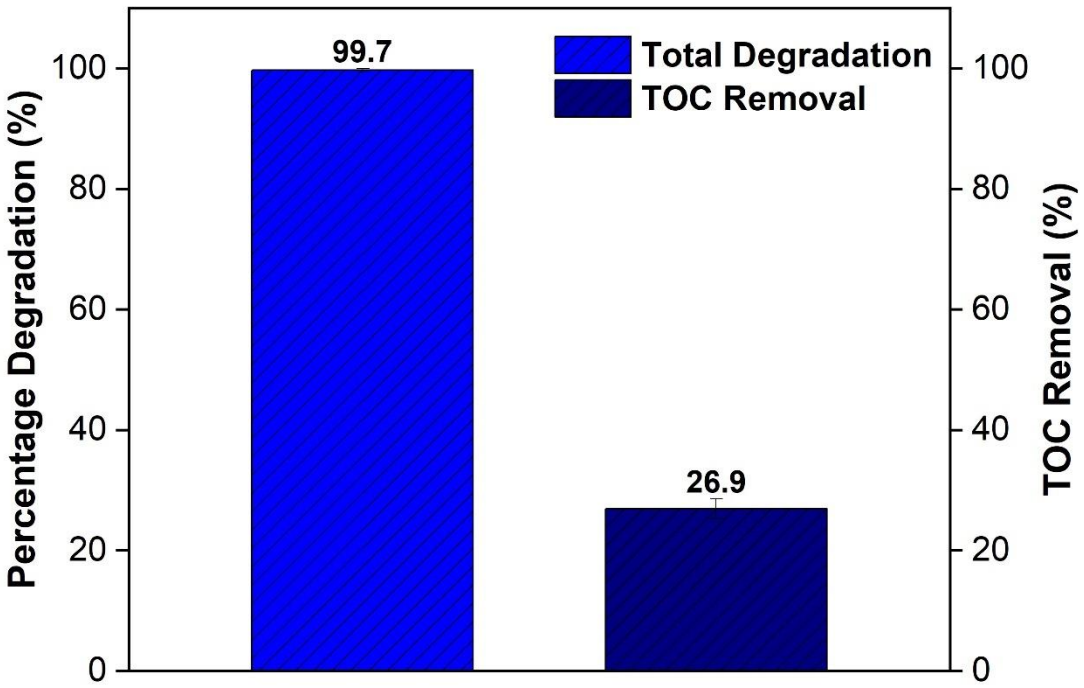

Figure 5-7. TOC removal during 2,4-DCP mineralisation (2.4-DCP: 10 mg/L; pH 5; Catalyst loading 1.5 g/L, visible light irradiation).

Based on literature (Zhang et al., 2018, Humayun et al., 2019a, Chen et al., 2017), a reaction pathway for the degradation of 2,4-DCP was proposed in Scheme 5-1. The pathway follows three routes wherein the first pathway of dechlorination proposes that the aromatic ring was attacked by hydroxyl radicals to form p-chlorophenol and o-chlorophenol (C_6H_5OCl, MW 128.00) dechlorination products (Zhang et al., 2018). In the second pathway, the dechlorination products were consistently attacked by hydroxyl radicals in the reaction solution(Tang and Huang, 1996). The hydroxyl radical was added onto the position of dechlorination reaction, forming dihydroxychlorobenzene and its isomers ($C_6H_5O_2Cl$, MW 144.00). In the third pathway, the aromatic hydroxylation involving generation of hydroxyl radical in solution is exposed to plasma oxidation(Constantin et al., 2018). Due to the electron-hole behaviour of the phenolic OH group and the electrophilic hydroxyl radical, the ($C_6H_5O_2Cl_2$, MW 177.96)

© University of Pretoria

(Deborde and Von Gunten, 2008). After dechlorination and hydroxylation of 2,4-DCP the intermediates were further oxidised and phenol (C_6H_6O, MW 94.04) (Tang and Huang, 1995) and 1,4-benzoquinone ($C_6H_4O_2$, MW 108.02) (Tang and Huang, 1996) were formed. Phenol could further be oxidised into cyclohexanone ($C_6H_{10}O$, MW 98.07) or 2,3-dihydroxybutanedioic acid ($C_4H_6O_6$, MW 150.02). Once the benzene rings were broken, the major products were organic acids such as oxalic acid, maleic acid and formic acid (Zazo et al., 2005); eventually all acids can be mineralised into CO_2 and H_2O.

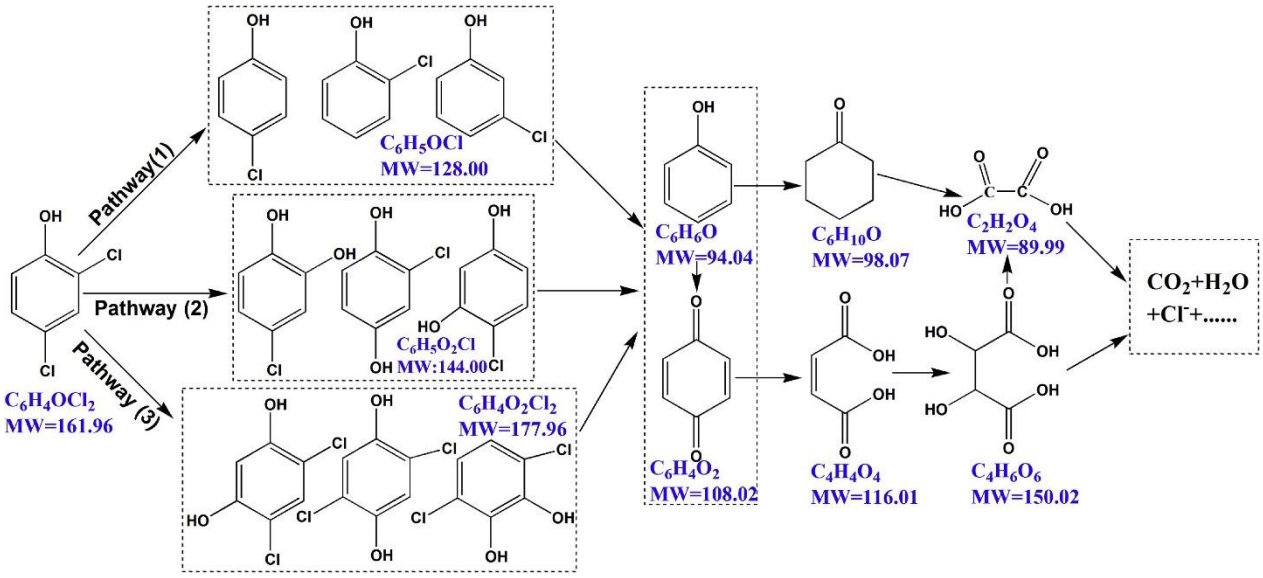

Scheme 5-1. Proposed 2,4-DCP degradation pathway (Zhang et al., 2018, Humayun et al., 2019a, Chen et al., 2017, Humayun et al., 2019b)

© University of Pretoria

5.3 Photochemical stability

The photocatalytic stability and reusability of the Ag/AgBr catalyst were evaluated. After every cycle the catalyst was collected and washed with ethanol and deionized water and thereafter dried overnight in an oven at 70 °C. As shown in Figure 5-8., after five (5) degradation cycles the photocatalytic capacity of Ag/AgBr had decreased by 50 % of the initial value. This decline of photocatalytic capacity can be attributed to the continuous generation of metallic Ag during the photocatalytic process (Duan et al., 2021). The continuous generation of Ag on the surface of AgBr creates a shielding effect, which reduces the light absorption ability of AgBr and thus greatly declines the photocatalytic capacity and stability of Ag/AgBr.

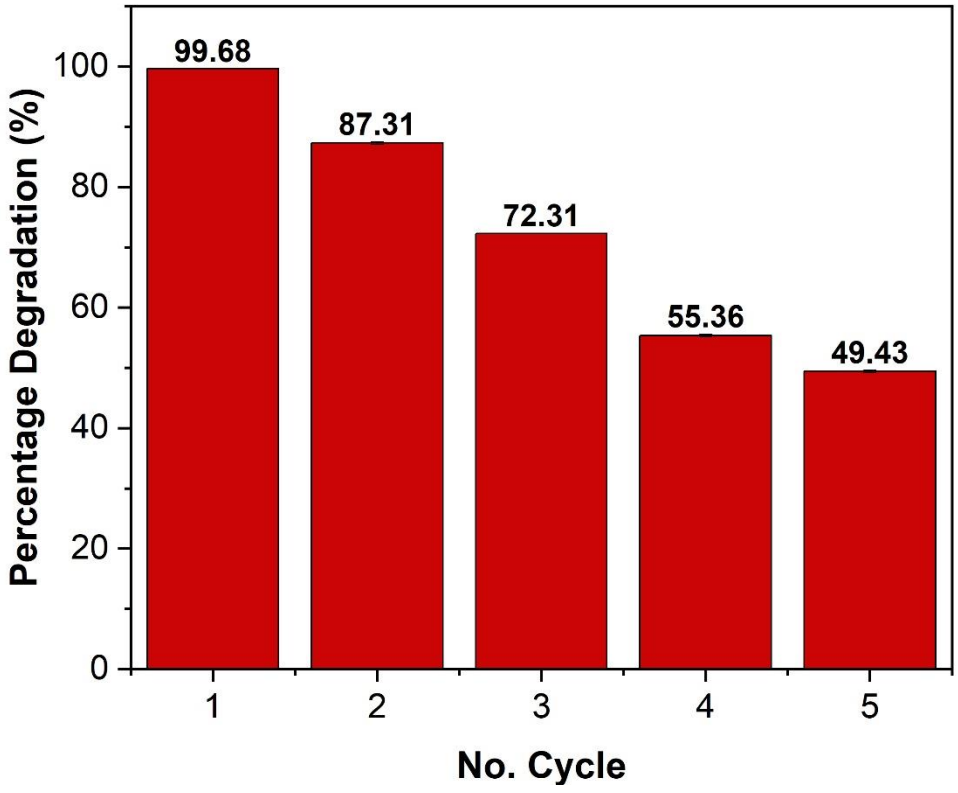

Figure 5-8. Photocatalytic reusability and stability of Ag/AgBr for the degradation of 2,4-DCP (10 mg/L); pH 5; catalyst loading: 1.5 g/L; under visible light irradiation.

The crystal phase, surface chemical composition and morphology of Ag/AgBr after 5 catalytic reactions were investigated. The XRD spectra of Ag/AgBr before and after photocatalytic

© University of Pretoria

reaction are presented in Figure 5-9. with Ag/AgBr after 5 cycles, exhibiting a distinct diffraction peak centred at 45° which is attributed to the cubic phase of Ag°. This further confirms the generation of metallic silver during the photodegradation process. In addition, according to the EDS data the atomic ratio of silver and bromide were 1:0.92 (Figure 4-2d) and 1:0.58 (Figure 5-10b.) respectively, before and after the photocatalytic reaction. This indicates a significant change of the content of Ag^0 or the surface chemical composition following the photocatalytic reaction. Figure 5-10c., shows the SEM image of the Ag/AgBr after 5 cycles whereby the spherical structure with silver nanoparticle deposited on the surface was eroded. This surface destruction creates a rough surface which cause a reduction in photocatalytic activity of Ag/AgBr due to less active sites, thus, reducing its stability and reusability.

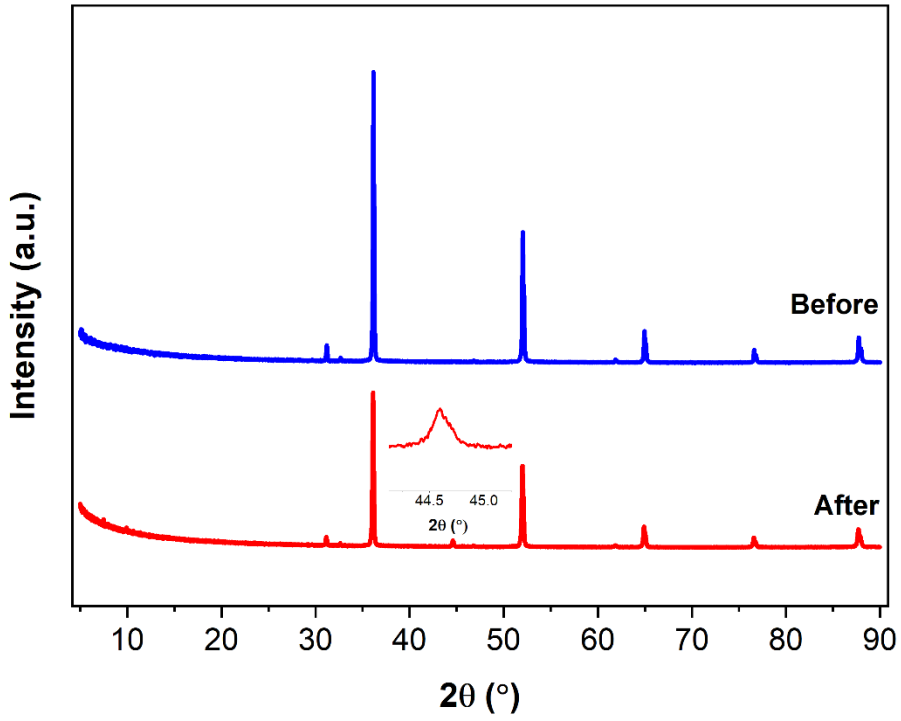

Figure 5-9. XRD spectra of Ag/AgBr before and after photostability and reusability evaluation.

© University of Pretoria

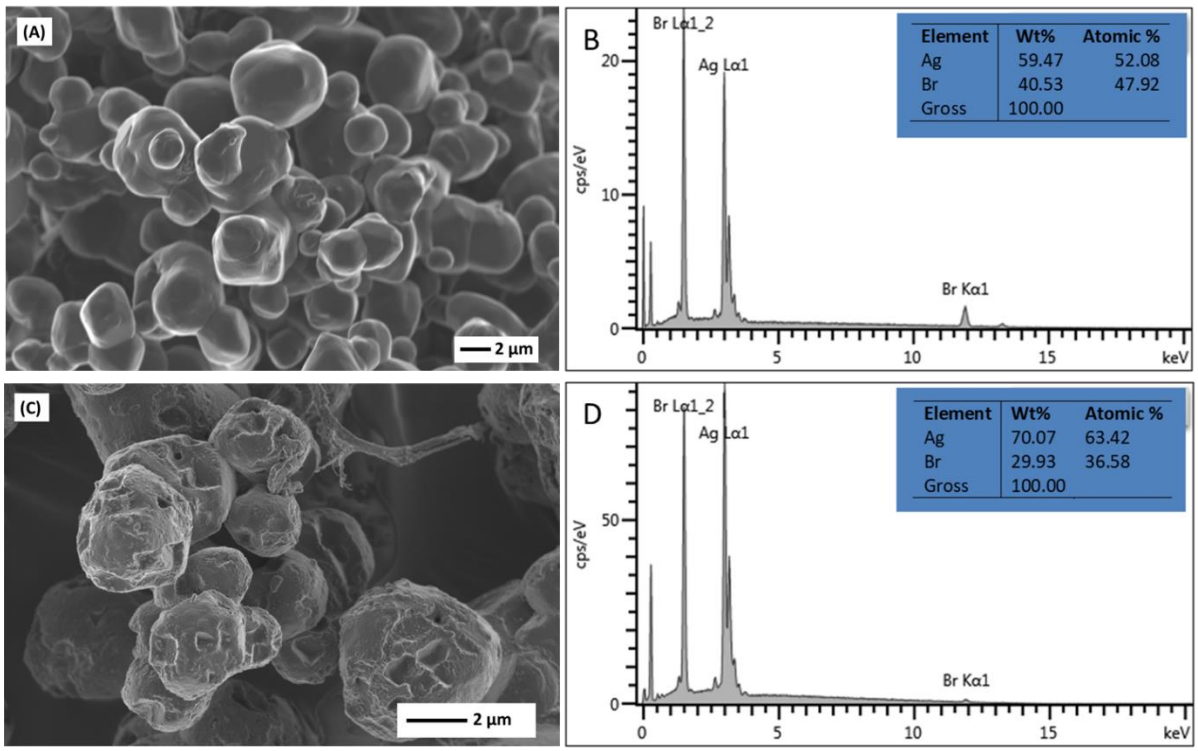

Figure 5-10. SEM images and EDS spectra of Ag/AgBr before and after photostability and reusability tests.

© University of Pretoria

5.4 Degradation mechanism

5.4.1 Effect of the presence of different Reactive Oxygen Species (ROS)

The photocatalytic activity of Ag/AgBr involves the generation of several reactive oxygen species (ROS) such as the hydroxyl radical ($^{\bullet}OH$), superoxide radical ($^{\bullet}O_2^-$) as well as trapped hole (h^+) and electrons (e^-) during the photodegradation process of organic pollutants. To investigate the fundamental mechanics behind the photocatalysis of Ag/AgBr a variety of radical scavengers were employed to evaluate the roles of different ROS during visible-light-activated photocatalysis in the degradation of 2,4-DCP. Benzoquinone (BQ) was utilized as the superoxide radical ($^{\bullet}O_2^-$) scavenger with the isopropanol as the hydroxyl radical ($^{\bullet}OH$) as well as triethanolamine and cupric nitrate as the holes (h^+) and electron (e^-) scavengers, respectively were all added to the 2,4-DCP solution before the adsorption process.

As presented in Figure 5-11., the 2,4-DCP degradation rate through the addition of BQ increased, suggesting the superoxide radical ($^{\bullet}O_2^-$) is not the main ROS in the degradation of 2,4-DCP but rather the presence of BQ enhanced the photocatalytic activity of Ag/AgBr. In the presence of isopropanol 2,4-DCP exhibited high degradation by Ag/AgBr within the first 60 min of visible light irradiation thereafter the degradation rate was greatly reduced. This may indicate that hydroxyl radicals could be a secondary species in the degradation of 2,4-DCP. With the addition of triethanolamine and cupric nitrate (copper nitrate) to the reaction system, there was a decrease in the degradation rate of 2,4-DCP.

The resulta demonstrate that the photogenerated holes (h^+) and electrons (e^-) are the dominate species in the degradation of 2,4-DCP. The adsorption of 2,4-DCP onto the Ag/AgBr catalyst increased in the presence of triethanolamine and cupric nitrate. This indicates that the major ROS in the degradation of 2,4-DCP through Ag/AgBr was the trapped electron (e^-) and hole (h^+) with the hydroxyl radical as the secondary species.

© University of Pretoria

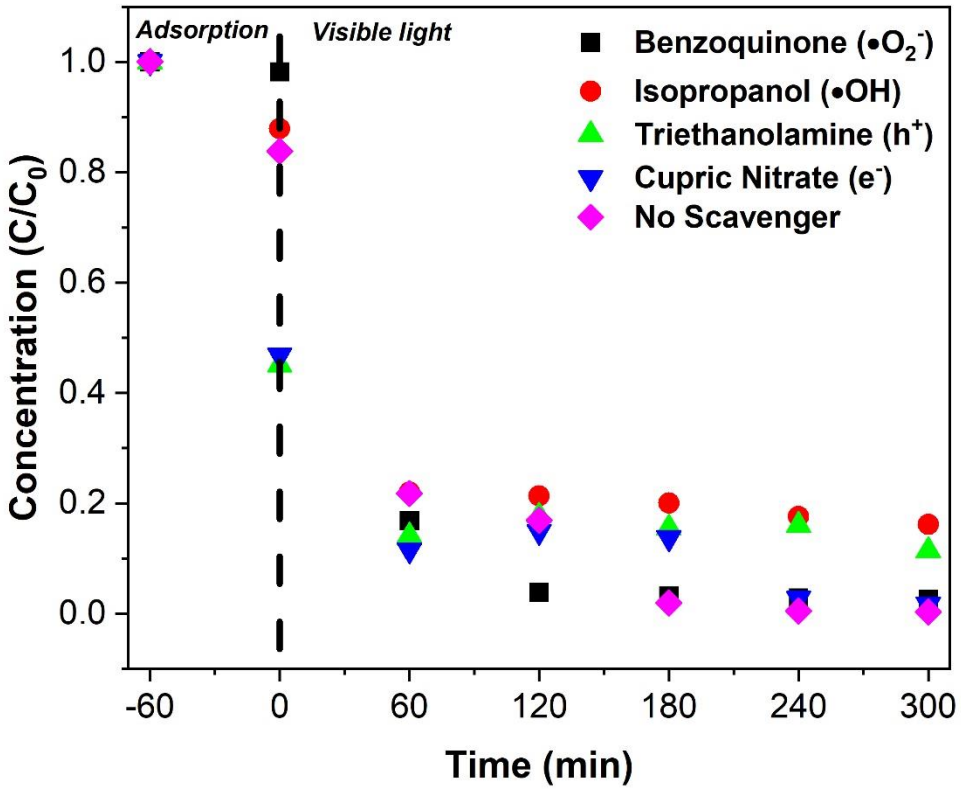

Figure 5-11. Effect of the radical scavengers on the removal of 2,4-DCP treated by Ag/AgBr under optimum conditions: 2,4-DCP concentration: 10 mg L^{-1}; catalyst loading: 1.5g L^{-1}; pH:5.

5.4.2 Photocatalytic decomposition mechanism of 2,4-DCP

The silver nanoparticles make a great contribution to the high visible light photocatalytic activity due to the SPR effect produced by the collective oscillations of surface electrons. Xiao et al. (2015) reported that the strong absorption of the visible light of Ag can be attributed to the SPR effect of the silver located at the visible light region. Moreover, the conductivity of silver nanoparticles can enhance the electron migration so as to enhance the interfacial charge transfer and inhibit the recombination of electron-hole pairs efficiently.

© University of Pretoria

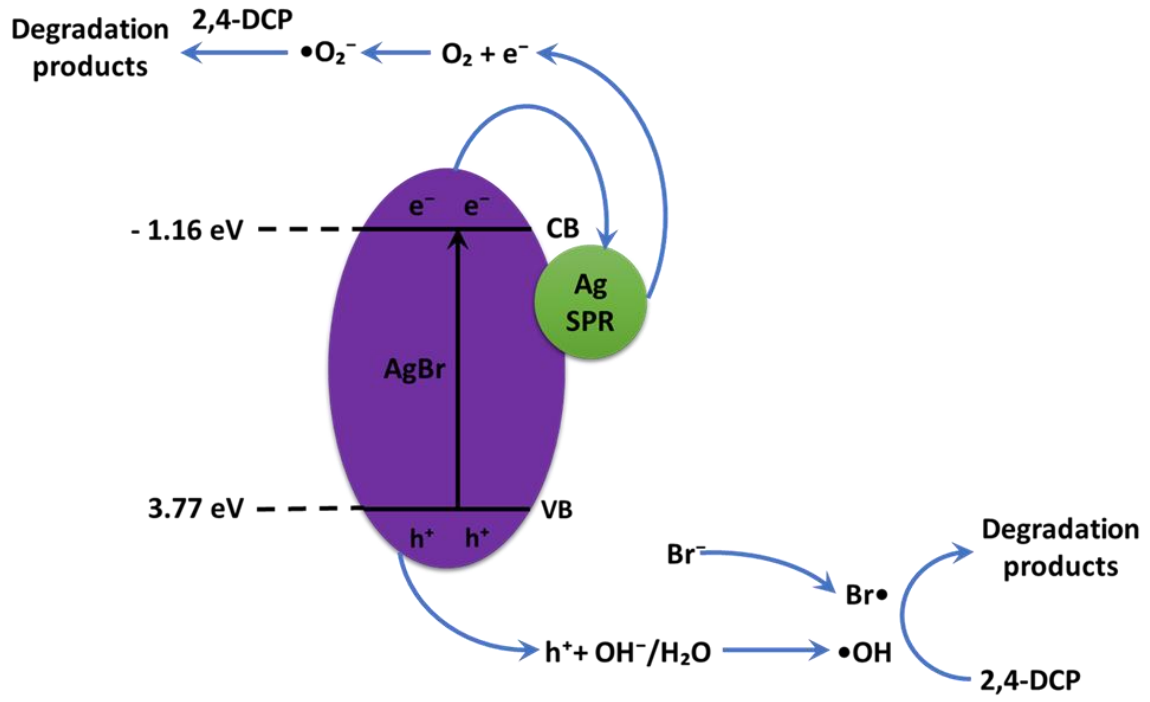

Scheme 5-2. Schematic representation of the proposed mechanism for photo-generated charge transfer in Ag/AgBr under visible light irradiation.

In the case of Ag/AgBr the visible light can be absorbed efficiently by both the Ag nanoparticles and AgBr semiconductor. Due to the SPR the induced local electromagnetic field, the separation efficiency of photogenerated charged carriers on Ag nanoparticles can be enhanced, leading to the generation of a large amount of electron-hole (e^-- h^+) pairs. The mechanism for the photocatalysis of Ag/AgBr is shown in Scheme 5-2. The photocatalytic process is generally governed by the oxidation potential of photogenerated holes, band gap and separation capability of photoinduced carriers in the Ag/AgBr nanoparticles that may be governed by Mulliken Electronegativity Relation presented in Table 4-1.The valence band and conduction band potential of AgBr was calculated to be 3.77 eV and -1.16 eV, respectively. When Ag/AgBr nanoparticles are irradiated under visible light, AgBr generate electron-hole

© University of Pretoria

pairs by formulating electrons and holes in the conduction band (CB) and valence band (VB), respectively. The electron from CB band of AgBr quickly gets migrated to the Ag nanoparticles because the CB potential of AgBr is negative relative the Fermi level of Ag (0.4 eV) (Tun et al., 2019).

The SPR effects of Ag nanoparticles have high reduction capability which combines with oxygen molecule and leads to the formation of $^{\bullet}O_2^-$ radical. This results in the delay of the recombination reaction between holes and electrons. Moreover, the photoinduced hole in the valence band of AgBr (+3.77 eV) were involved in the oxidising reaction of H_2O/OH^- in solution to generate $^{\bullet}OH$ radical as the potential of h^+ in the valence band is higher than $^{\bullet}OH$ (+1.99 eV vs SHE). The formed radical is a powerful oxidising agent to degrade 2,4-DCP directly. Furthermore, AgBr is highly sensitive to light and may undergo dissociation into silver and bromine atoms during the reaction.

Then, the photogenerated electron reduces the Ag^+ ions produced by AgBr into metallic Ag by preventing further photocorrosion of AgBr. Simultaneously, some holes may combine with Br^- and oxidizes to Br^0 atom, a strong oxidant in degrading organic pollutants (Sanni et al., 2019). Furthermore, the photogenerated electrons in the reaction system could be trapped by O_2 molecules to form $^{\bullet}O_2^-$ radical and holes (h^+) through H_2O to generate $^{\bullet}OH$ radical which both have strong oxidability for the degradation of organic pollutants.

© University of Pretoria

CHAPTER 6

6 CONCLUSION AND RECOMMENDATIONS

In this study, visible light responsive photocatalysts Ag/AgX (X=Cl, Br, I) were successfully synthesized using a hydrothermal method. The efficiency of the synthesized method was confirmed through different characterization strategies to determine the crystallinity, purity, morphology as well as the chemical states and composition of the synthesized photocatalysts. The Ag/AgBr and Ag/AgBr presented cubic phases while the Ag/AgI presented two phases namely the hexagonal β-AgI and cubic γ-AgI. All diffraction peaks presented high degree of crystallinity of the synthesised nanoparticles. Ag/AgCl, Ag/AgBr and Ag/AgI displayed near-spherical, irregular sphere-like and polygonal plate morphologies, respectively.

The photodegradation efficiency of the prepared photocatalysts were evaluated under both UV and visible-light irradiation in the degrading 2,4-DCP. The batch experiment was designed to study individual effects of factors such as light, catalyst loading, pH, as well as the concentration of pollutants. The results depicts that all synthesized materials are activated under both UV and visible-light irradiation with Ag/AgBr exhibiting the highest overall efficiency of approximately 89.39 % (under initial conditions) photodegradation under visible-light irradiation. pH 3 to 9 were more favourable in degrading 2,4-DCP than pH 11. Under optimised catalyst loading, pH and initial concentration of 2,4-DCP, the photocatalytic reaction efficiently removed 2,4-DCP while observing a low TOC reduction. The possible photocatalytic mechanism was evaluated using an active species trapping experiment which verified that electrons and holes play the primary role in the process of degrading 2,4-DCP. This study indicates the potential use of silver halides (AgX), particularly Ag/AgBr under visible-light irradiation for the remediation of 2,4-DCP in the environment.

© University of Pretoria

The following are some recommendations for future studies:

The improvement of the synthesis method should be investigated to attain controlled morphology of the photocatalysts. This will assist to increase the surface area of the photocatalysts thus enhancing its photocatalytic performance.

Furthermore, investigation of the effectiveness of the synthesized Ag/AgBr under natural sunlight. The stability and reusability of Ag/AgBr under natural sunlight should be evaluated.

The recommendation a comprehensive study of the degradation pathway of 2,4-DCP and its toxicity throughout the study. This study would assist in determining the toxicity of the intermediates.

© University of Pretoria

REFERENCES

Abou Asi, M., Zhu, L., He, C., Sharma, V. K., Shu, D., Li, S., Yang, J. & Xiong, Y. 2013. Visible-light-harvesting reduction of CO2 to chemical fuels with plasmonic Ag@ AgBr/CNT nanocomposites. *Catalysis today*, 216**,** 268-275.

Abulizi, A., Kadeer, K., Maimaitizi, H., Tursun, Y. & Talifu, D. 2020. In situ ultrasound-assisted ion exchange synthesis of sphere-like AgCl x Br 1-x composites with enhanced photocatalytic activity and stability. *Environmental Science and Pollution Research*, 27**,** 43615-43624.

Adenuga, D., Skosana, S., Tichapondwa, S. & Chirwa, E. 2021. Synthesis of a plasmonic AgCl and oxygen-rich Bi 24 O 31 Cl 10 composite heterogeneous catalyst for enhanced degradation of tetracycline and 2, 4-dichlorophenoxy acetic acid. *RSC Advances*, 11**,** 36760-36768.

Adenuga, D., Tichapondwa, S. & Chirwa, E. 2019. Synthesis and Characterization of Potential Visible-light Photocatalyst and Its Photocatalytic Activity in the Decomposition of Phenol. *Chemical Engineering Transactions*, 74**,** 1087-1092.

Adenuga, D. O., Tichapondwa, S. M. & Chirwa, E. M. 2020. Facile synthesis of a Ag/AgCl/BiOCl composite photocatalyst for visible–light–driven pollutant removal. *Journal of Photochemistry and Photobiology A: Chemistry*, 401**,** 112747.

Adeola, A. 2018. Fate and toxicity of chlorinated phenols of environmental implications: a review. *Medicinal and Analytical Chemistry International Journal*, 2**,** 000126.

Ai, L., Zhang, C. & Jiang, J. 2013. Hierarchical porous AgCl@ Ag hollow architectures: self-templating synthesis and highly enhanced visible light photocatalytic activity. *Applied Catalysis B: Environmental*, 142**,** 744-751.

An, C., Liu, J., Wang, S., Zhang, J., Wang, Z., Long, R. & Sun, Y. 2014a. Concaving AgI sub-microparticles for enhanced photocatalysis. *Nano Energy*, 9**,** 204-211.

© University of Pretoria

An, C., Peng, S. & Sun, Y. 2010. Facile synthesis of sunlight-driven AgCl: Ag plasmonic nanophotocatalyst. *Advanced Materials,* 22**,** 2570-2574.

An, C., Wang, J., Jiang, W., Zhang, M., Ming, X., Wang, S. & Zhang, Q. 2012a. Strongly visible-light responsive plasmonic shaped AgX: Ag (X= Cl, Br) nanoparticles for reduction of CO 2 to methanol. *Nanoscale,* 4**,** 5646-5650.

An, C., Wang, J., Liu, J., Wang, S. & Zhang, Q.-H. 2014b. Plasmonic enhancement of photocatalysis over Ag incorporated AgI hollow nanostructures. *RSC advances,* 4**,** 2409-2413.

An, C., Wang, J., Qin, C., Jiang, W., Wang, S., Li, Y. & Zhang, Q. 2012b. Synthesis of Ag@ AgBr/AgCl heterostructured nanocashews with enhanced photocatalytic performance via anion exchange. *Journal of Materials Chemistry,* 22**,** 13153-13158.

An, C., Wang, S., Sun, Y., Zhang, Q., Zhang, J., Wang, C. & Fang, J. 2016. Plasmonic silver incorporated silver halides for efficient photocatalysis. *Journal of Materials Chemistry A,* 4**,** 4336-4352.

Andreozzi, R., Caprio, V., Insola, A. & Marotta, R. 1999. Advanced oxidation processes (AOP) for water purification and recovery. *Catalysis today,* 53**,** 51-59.

Anku, W. W., Mamo, M. A. & Govender, P. P. 2017. Phenolic compounds in water: sources, reactivity, toxicity and treatment methods. *Phenolic compounds-natural sources, importance and applications***,** 419-443.

Assis, M., Groppo Filho, F. C., Pimentel, D. S., Robeldo, T., Gouveia, A. F., Castro, T. F., Fukushima, H. C., de Foggi, C. C., da Costa, J. P. & Borra, R. C. 2020. Ag Nanoparticles/AgX (X= Cl, Br and I) Composites with Enhanced Photocatalytic Activity and Low Toxicological Effects. *ChemistrySelect,* 5**,** 4655-4673.

Aziz, K. H. H., Miessner, H., Mueller, S., Mahyar, A., Kalass, D., Moeller, D., Khorshid, I. & Rashid, M. A. M. 2018. Comparative study on 2, 4-dichlorophenoxyacetic acid and 2, 4-

© University of Pretoria

dichlorophenol removal from aqueous solutions via ozonation, photocatalysis and non-thermal plasma using a planar falling film reactor. *Journal of hazardous materials,* 343**,** 107-115.

Azubuike, C. C., Chikere, C. B. & Okpokwasili, G. C. 2016. Bioremediation techniques–classification based on site of application: principles, advantages, limitations and prospects. *World Journal of Microbiology and Biotechnology,* 32**,** 1-18.

Bai, C., Bi, J., Wu, J., Xu, Y., Wohlrab, S., Han, Y. & Zhang, X. 2019. In-situ solid-phase fabrication of Ag/AgX (X= Cl, Br, I)/g-C3N4 composites for enhanced visible-light hydrogen evolution. *International Journal of Hydrogen Energy,* 44**,** 21397-21405.

Bai, S., Li, X., Kong, Q., Long, R., Wang, C., Jiang, J. & Xiong, Y. 2015. Toward enhanced photocatalytic oxygen evolution: synergetic utilization of plasmonic effect and schottky junction via interfacing facet selection. *Advanced Materials,* 27**,** 3444-3452.

Bel Hadjltaief, H., Sdiri, A., Gálvez, M. E., Zidi, H., Da Costa, P. & Ben Zina, M. 2018. Natural Hematite and Siderite as Heterogeneous Catalysts for an Effective Degradation of 4-Chlorophenol via Photo-Fenton Process. *ChemEngineering,* 2**,** 29.

Benitez, F., Acero, J., Real, F., Rubio, F. & Leal, A. 2001. The role of hydroxyl radicals for the decomposition of p-hydroxy phenylacetic acid in aqueous solutions. *Water Research,* 35**,** 1338-1343.

Benitez, F. J., Acero, J. L., Real, F. J. & Roman, S. 2004. Oxidation of MCPA and 2, 4-D by UV radiation, ozone, and the combinations UV/H2O2 and O3/H2O2. *Journal of Environmental Science and Health, Part B,* 39**,** 393-409.

Bhatt, D. K. & Patel, U. D. 2019. Mechanism underlying visible-light photocatalytic activity of Ag/AgBr: Experimental and theoretical approaches. *Journal of Physics and Chemistry of Solids,* 135**,** 109118.

© University of Pretoria

Bi, Y. & Ye, J. 2010. Direct conversion of commercial silver foils into high aspect ratio AgBr nanowires with enhanced photocatalytic properties. *Chemistry–A European Journal,* 16**,** 10327-10331.

Bissey, L. L., Smith, J. L. & Watts, R. J. 2006. Soil organic matter–hydrogen peroxide dynamics in the treatment of contaminated soils and groundwater using catalyzed H2O2 propagations (modified Fenton's reagent). *Water research,* 40**,** 2477-2484.

Brandão, Y. B., OLIVEIRA, J. & Benachour, M. 2017. Phenolic Wastewaters: Definition, Sources and Treatment Processes. *Phenolic compounds: natural sources, importance and applications,* 1**,** 323-342.

Butt, A. L., Mpinga, J. K. & Tichapondwa, S. M. 2021. Photo-Fenton Oxidation of Methyl Orange Dye Using South African Ilmenite Sands as a Catalyst. *Catalysts,* 11**,** 1452.

Cai, B., Wang, J., Gan, S., Han, D., Wu, Z. & Niu, L. 2014. A distinctive red Ag/AgCl photocatalyst with efficient photocatalytic oxidative and reductive activities. *Journal of Materials Chemistry A,* 2**,** 5280-5286.

Cai, B., Wang, J., Han, D., Gan, S., Zhang, Q., Wu, Z. & Niu, L. 2013. Ternary alloyed AgCl x Br 1− x nanocrystals: facile modulation of electronic structures toward advanced photocatalytic performance. *Nanoscale,* 5**,** 10989-10995.

Canfield, D. E., Glazer, A. N. & Falkowski, P. G. 2010. The evolution and future of Earth's nitrogen cycle. *science,* 330**,** 192-196.

Cao, J., Luo, B., Lin, H. & Chen, S. 2011. Photocatalytic activity of novel AgBr/WO3 composite photocatalyst under visible light irradiation for methyl orange degradation. *Journal of hazardous materials,* 190**,** 700-706.

Chang, X., Sun, S., Dong, L. & Yin, Y. 2012. Efficient synthesis of Ag/AgCl/W18O49 nanorods and their antibacterial activities. *Materials Letters,* 83**,** 133-135.

© University of Pretoria

Chaplin, B. P. 2018. Advantages, disadvantages, and future challenges of the use of electrochemical technologies for water and wastewater treatment. *Electrochemical Water and Wastewater Treatment.* Elsevier.

Chen, C., Ma, W. & Zhao, J. 2010. Semiconductor-mediated photodegradation of pollutants under visible-light irradiation. *Chemical Society Reviews,* 39**,** 4206-4219.

Chen, H. M., Chen, C. K., Tseng, M. L., Wu, P. C., Chang, C. M., Cheng, L. C., Huang, H. W., Chan, T. S., Huang, D. W. & Liu, R. S. 2013. Plasmonic ZnO/Ag embedded structures as collecting layers for photogenerating electrons in solar hydrogen generation photoelectrodes. *Small,* 9**,** 2926-2936.

Chen, J., Xiao, X., Wang, Y. & Xiao, Y. 2020. AgI nanoparticles decorated Bi3O4Cl microspheres: An efficient Z-scheme heterojunction photocatalyst for the degradation of rhodamine B and tetracycline. *Solid State Sciences,* 107**,** 106357.

Chen, S., Yan, R., Zhang, X., Hu, K., Li, Z., Humayun, M., Qu, Y. & Jing, L. 2017. Photogenerated electron modulation to dominantly induce efficient 2, 4-dichlorophenol degradation on BiOBr nanoplates with different phosphate modification. *Applied Catalysis B: Environmental,* 209**,** 320-328.

Chen, W.-F., Koshy, P. & Sorrell, C. C. 2015. Effect of intervalence charge transfer on photocatalytic performance of cobalt-and vanadium-codoped TiO2 thin films. *International Journal of Hydrogen Energy,* 40**,** 16215-16229.

Chen, X.-J., Cabello, G., Wu, D.-Y. & Tian, Z.-Q. 2014. Surface-enhanced Raman spectroscopy toward application in plasmonic photocatalysis on metal nanostructures. *Journal of Photochemistry and Photobiology C: Photochemistry Reviews,* 21**,** 54-80.

Chen, X., Zhu, H. Y., Zhao, J. C., Zheng, Z. F. & Gao, X. P. 2008. Visible-light-driven oxidation of organic contaminants in air with gold nanoparticle catalysts on oxide supports. *Angewandte Chemie,* 120**,** 5433-5436.

© University of Pretoria

Chen, Z., Fan, T.-T., Yu, X., Wu, Q.-L., Zhu, Q.-H., Zhang, L.-Z., Li, J.-H., Fang, W.-P. & Yi, X.-D. 2018. Gradual carbon doping of graphitic carbon nitride towards metal-free visible light photocatalytic hydrogen evolution. *Journal of Materials Chemistry A,* 6**,** 15310-15319.

Cheng, H., Huang, B., Dai, Y., Qin, X. & Zhang, X. 2010. One-step synthesis of the nanostructured AgI/BiOI composites with highly enhanced visible-light photocatalytic performances. *Langmuir,* 26**,** 6618-6624.

Cheng, H., Huang, B., Wang, P., Wang, Z., Lou, Z., Wang, J., Qin, X., Zhang, X. & Dai, Y. 2011. In situ ion exchange synthesis of the novel Ag/AgBr/BiOBr hybrid with highly efficient decontamination of pollutants. *Chemical Communications,* 47**,** 7054-7056.

Cheng, Z., Dong, Q., Chen, S., Zhao, W., Chu, X., Zhong, H., Zhao, P., Zhang, L., Xu, J. & Guo, X. 2021. Novel AgClxBr1− x solid solutions photocatalyst with enhanced photocatalytic activity for reduction of Cr6+ and oxidation of Bisphenol A under simulated sunlight. *Materials Research Bulletin,* 139**,** 111257.

Chindo, I. Y., Karu, E., Ziyok, I. & Amanki, E. D. 2013. Physicochemical Analysis of Groundwater of Selected Areas of Dass and Ganjuwa local Government Areas, Bauchi State Nigeria. *World Journal of Analytical Chemistry,* 1**,** 73-79.

Choi, S. M., Yoo, S. D. & Lee, B. M. 2004. Toxicological characteristics of endocrine-disrupting chemicals: developmental toxicity, carcinogenicity, and mutagenicity. *Journal of Toxicology and Environmental Health, Part B,* 7**,** 1-23.

Chowdhury, P., Nag, S. & Ray, A. K. 2017. Degradation of phenolic compounds through UV and visible-light-driven photocatalysis: technical and economic aspects. *Phenolic Compounds-Natural Sources, Importance and Applications,* 16**,** 395-417.

Clark, N. J., Clough, R., Boyle, D. & Handy, R. D. 2021. Quantification of particulate Ag in rainbow trout organs following dietary exposure to silver nitrate, or two forms of engineered silver nanoparticles. *Environmental Science: Nano,* 8**,** 1642-1653.

© University of Pretoria

Constantin, L. A., Nitoi, I., Cristea, N. I. & Constantin, M. A. 2018. Possible degradation pathways of triclosan from aqueous systems via TiO2 assisted photocatalyis. *Journal of Industrial and Engineering Chemistry,* 58**,** 155-162.

Cui, L., Jiao, T., Zhang, Q., Zhou, J. & Peng, Q. 2015. Facile preparation of silver halide nanoparticles as visible light photocatalysts. *Nanomaterials and Nanotechnology*, 5**,** 20.

Deborde, M. & Von Gunten, U. 2008. Reactions of chlorine with inorganic and organic compounds during water treatment—kinetics and mechanisms: a critical review. *Water research,* 42**,** 13-51.

Deng, J., Xue, R., Huang, C., Yang, J., Li, L., Yang, L. & Fan, X. 2021. Preparation of Z-scheme Ag/AgBr/BiOBr composite photocatalyst for effective removal of organic pollutants. *Chemical Physics,* 548**,** 111228.

Di, J., Xia, J., Li, H., Guo, S. & Dai, S. 2017. Bismuth oxyhalide layered materials for energy and environmental applications. *Nano Energy*, 41**,** 172-192.

Ding, T., Xiao, X., Wang, Y. & Lu, M. 2020. AgI Nanoparticles Decorated Bi 24 O 31 Br 10 Nanosheets: An Efficient 0D/2D Z-Scheme Heterojunction Photocatalyst for the Degradation of Rhodamine B. *Journal of Inorganic and Organometallic Polymers and Materials*, 30**,** 4954-4968.

Dixit, A., Tirpude, A. J., Mungray, A. & Chakraborty, M. 2011. Degradation of 2, 4 DCP by sequential biological–advanced oxidation process using UASB and UV/TiO2/H2O2. *Desalination,* 272**,** 265-269.

Dong, Q., Wu, M., Mei, D., Shao, Y., Wang, Y., Liu, J., Li, H. & Hong, L. 2018. Multifunctional Pd-Sn electrocatalysts enabled by in situ formed SnOx and TiC triple junctions. *Nano Energy,* 53**,** 940-948.

© University of Pretoria

Dong, R., Tian, B., Zeng, C., Li, T., Wang, T. & Zhang, J. 2013. Ecofriendly synthesis and photocatalytic activity of uniform cubic Ag@ AgCl plasmonic photocatalyst. *The Journal of Physical Chemistry C,* 117**,** 213-220.

Duan, Y., Chen, X., Zhang, X., Xiang, W. & Wu, C. 2018. Influence of carbon source on the anatase and brookite mixed phase of the C-doped TiO2 nanoparticles and their photocatalytic activity. *Solid state sciences,* 86**,** 12-18.

Duan, Y., Zhu, X., Luo, Q., Wang, L., Li, Z. & Wang, D. 2021. Improvement in photocatalytic stability of AgBr under visible light through melt processing. *Journal of Catalysis,* 400**,** 160-165.

Esplugas, S., Gimenez, J., Contreras, S., Pascual, E. & Rodríguez, M. 2002. Comparison of different advanced oxidation processes for phenol degradation. *Water research,* 36**,** 1034-1042.

Fan, W. & Leung, M. K. 2016. Recent development of plasmonic resonance-based photocatalysis and photovoltaics for solar utilization. *Molecules,* 21**,** 180.

Fan, Y., Han, D., Song, Z., Sun, Z., Dong, X. & Niu, L. 2018. Regulations of silver halide nanostructure and composites on photocatalysis. *Advanced Composites and Hybrid Materials,* 1**,** 269-299.

Fan, Y., Ma, W., Han, D., Gan, S., Dong, X. & Niu, L. 2015. Convenient recycling of 3D AgX/graphene aerogels (X= Br, Cl) for efficient photocatalytic degradation of water pollutants. *Advanced materials,* 27**,** 3767-3773.

Fechete, I., Wang, Y. & Védrine, J. C. 2012. The past, present and future of heterogeneous catalysis. *Catalysis Today,* 189**,** 2-27.

Feng, W., Wang, B., Zheng, Z., Fang, Z., Wang, Z., Zhang, S., Li, Y. & Liu, P. 2016. Predictive model for optimizing the near-field electromagnetic energy transfer in plasmonic nanostructure-involved photocatalysts. *Applied Catalysis B: Environmental,* 186**,** 143-150.

© University of Pretoria

Gangu, K. K., Maddila, S. & Jonnalagadda, S. B. 2019. A review on novel composites of MWCNTs mediated semiconducting materials as photocatalysts in water treatment. *Science of the Total Environment,* 646**,** 1398-1412.

Gao, W., Ran, C., Wang, M., Li, L., Sun, Z. & Yao, X. 2016. The role of reduction extent of graphene oxide in the photocatalytic performance of Ag/AgX (X= Cl, Br)/rGO composites and the pseudo-second-order kinetics reaction nature of the Ag/AgBr system. *Physical Chemistry Chemical Physics,* 18**,** 18219-18226.

Gao, X., Shang, Y., Liu, L. & Fu, F. 2019. Chemisorption-enhanced photocatalytic nitrogen fixation via 2D ultrathin p–n heterojunction AgCl/δ-Bi2O3 nanosheets. *Journal of Catalysis,* 371**,** 71-80.

Gaya, U. I., Abdullah, A. H., Zainal, Z. & Hussein, M. Z. 2010. Photocatalytic degradation of 2, 4-dichlorophenol in irradiated aqueous ZnO suspension. *International Journal of Chemistry,* 2**,** 180.

Ge, M., Liu, W., Hu, X.-R. & Li, Z.-L. 2017. Magnetically separable Ag/AgBr/NiFe2O4 composite as a highly efficient visible light plasmonic photocatalyst. *Journal of Physics and Chemistry of Solids,* 109**,** 1-8.

Geng, Y., Lei, G., Liao, Y., Jiang, H.-Y., Xie, G. & Chen, S. 2017. Rapid organic degradation and bacteria destruction under visible light by ternary photocatalysts of Ag/AgX/TiO2. *Journal of Environmental Chemical Engineering,* 5**,** 5566-5572.

Giulivo, M., de Alda, M. L., Capri, E. & Barceló, D. 2016. Human exposure to endocrine disrupting compounds: Their role in reproductive systems, metabolic syndrome and breast cancer. A review. *Environmental research,* 151**,** 251-264.

Grabowska, E., Zaleska, A., Sorgues, S., Kunst, M., Etcheberry, A., Colbeau-Justin, C. & Remita, H. 2013. Modification of titanium (IV) dioxide with small silver nanoparticles: application in photocatalysis. *The Journal of Physical Chemistry C,* 117**,** 1955-1962.

© University of Pretoria

Grebel, J. E., Pignatello, J. J. & Mitch, W. A. 2010. Effect of halide ions and carbonates on organic contaminant degradation by hydroxyl radical-based advanced oxidation processes in saline waters. *Environmental science & technology,* 44**,** 6822-6828.

Gu, X., Li, C., Yuan, S., Ma, M., Qiang, Y. & Zhu, J. 2016. ZnO based heterojunctions and their application in environmental photocatalysis. *Nanotechnology,* 27**,** 402001.

Guillard, C., Puzenat, E., Lachheb, H., Houas, A. & Herrmann, J.-M. 2005. Why inorganic salts decrease the TiO2 photocatalytic efficiency. *International Journal of Photoenergy,* 7**,** 1-9.

Guo, X., Mahmud, S., Zhang, X., Yu, N. & Faridul Hasan, K. 2021. One-pot green synthesis of Ag@ AgCl nanoparticles with excellent photocatalytic performance. *Surface Innovations,* 9**,** 277-284.

Gupta, V. K. & Saleh, T. A. 2013. Sorption of pollutants by porous carbon, carbon nanotubes and fullerene-an overview. *Environmental science and pollution research,* 20**,** 2828-2843.

Habibi-Yangjeh, A., Asadzadeh-Khaneghah, S. & Ghosh, S. 2020. Anchoring Bi4O5I2 and AgI nanoparticles over g-C3N4 nanosheets: Impressive visible-light-induced photocatalysts in elimination of hazardous contaminates by a cascade mechanism. *Advanced Powder Technology,* 31**,** 2618-2628.

Han, C., Ge, L., Chen, C., Li, Y., Zhao, Z., Xiao, X., Li, Z. & Zhang, J. 2014. Site-selected synthesis of novel Ag@ AgCl nanoframes with efficient visible light induced photocatalytic activity. *Journal of Materials Chemistry A,* 2**,** 12594-12600.

Han, L., Wang, P., Zhu, C., Zhai, Y. & Dong, S. 2011. Facile solvothermal synthesis of cube-like Ag@ AgCl: a highly efficient visible light photocatalyst. *Nanoscale,* 3**,** 2931-2935.

Hanchang, S. 2009. Industrial wastewater-types, amounts and effects. *Point sources of pollution: Local effects and their control,* 2**,** 191.

© University of Pretoria

Hao, C., Liao, Y., Wu, Y., An, Y., Lin, J., Gu, Z., Jiang, M., Hu, S. & Wang, X. 2020. RuO2-loaded TiO2–MXene as a high performance photocatalyst for nitrogen fixation. *Journal of Physics and Chemistry of Solids,* 136**,** 109141.

Hasija, V., Raizada, P., Sudhaik, A., Singh, P., Thakur, V. K. & Khan, A. A. P. 2020. Fabrication of Ag/AgI/WO3 heterojunction anchored P and S co-doped graphitic carbon nitride as a dual Z scheme photocatalyst for efficient dye degradation. *Solid State Sciences,* 100**,** 106095.

Hassan, H., Jin, B., Donner, E., Vasileiadis, S., Saint, C. & Dai, S. 2018. Microbial community and bioelectrochemical activities in MFC for degrading phenol and producing electricity: microbial consortia could make differences. *Chemical Engineering Journal,* 332**,** 647-657.

Hoang, S. & Gao, P. X. 2016. Nanowire array structures for photocatalytic energy conversion and utilization: a review of design concepts, assembly and integration, and function enabling. *Advanced Energy Materials,* 6**,** 1600683.

Hoigné, J. & Bader, H. 1994. Kinetics of reactions of chlorine dioxide (OClO) in water—I. Rate constants for inorganic and organic compounds. *Water Research,* 28**,** 45-55.

Hong, L. 2020. Surface plasmon resonance enhanced hydrogen evolution from water with graphitic carbon nitride photocatalyst.

Hosseini-Sarvari, M. & Dehghani, A. 2020. Visible-light-driven photochemical activity of ternary Ag/AgBr/TiO 2 nanotubes for oxidation C (sp 3)–H and C (sp 2)–H bonds. *New Journal of Chemistry,* 44**,** 16776-16785.

Hou, D., Hu, X., Hu, P., Zhang, W., Zhang, M. & Huang, Y. 2013. Bi 4 Ti 3 O 12 nanofibers–BiOI nanosheets p–n junction: facile synthesis and enhanced visible-light photocatalytic activity. *Nanoscale,* 5**,** 9764-9772.

© University of Pretoria

Hou, Y., Zuo, F., Ma, Q., Wang, C., Bartels, L. & Feng, P. 2012. Ag3PO4 oxygen evolution photocatalyst employing synergistic action of Ag/AgBr nanoparticles and graphene sheets. *The Journal of Physical Chemistry C,* 116**,** 20132-20139.

Hu, C., Peng, T., Hu, X., Nie, Y., Zhou, X., Qu, J. & He, H. 2010. Plasmon-induced photodegradation of toxic pollutants with Ag− AgI/Al2O3 under visible-light irradiation. *Journal of the American Chemical Society,* 132**,** 857-862.

Hu, X., Yong, Y., Xu, Y., Hong, X., Weng, Y., Wang, X. & Yao, X. 2020. Enhanced photocatalytic nitrogen fixation of AgI modified g-C3N4 with nitrogen vacancy synthesized by an in-situ decomposition-thermal polymerization method. *Applied Surface Science,* 531**,** 147348.

Huang, D., Li, J., Zeng, G., Xue, W., Chen, S., Li, Z., Deng, R., Yang, Y. & Cheng, M. 2019. Facile construction of hierarchical flower-like Z-scheme AgBr/Bi2WO6 photocatalysts for effective removal of tetracycline: Degradation pathways and mechanism. *Chemical Engineering Journal,* 375**,** 121991.

Humayun, M., Hu, Z., Khan, A., Cheng, W., Yuan, Y., Zheng, Z., Fu, Q. & Luo, W. 2019a. Highly efficient degradation of 2, 4-dichlorophenol over CeO2/g-C3N4 composites under visible-light irradiation: detailed reaction pathway and mechanism. *Journal of hazardous materials,* 364**,** 635-644.

Humayun, M., Zheng, Z., Fu, Q. & Luo, W. 2019b. Photodegradation of 2, 4-dichlorophenol and rhodamine B over n-type ZnO/p-type BiFeO3 heterojunctions: detailed reaction pathway and mechanism. *Environmental Science and Pollution Research,* 26**,** 17696-17706.

Igbinosa, E. O., Odjadjare, E. E., Chigor, V. N., Igbinosa, I. H., Emoghene, A. O., Ekhaise, F. O., Igiehon, N. O. & Idemudia, O. G. 2013. Toxicological profile of chlorophenols and their derivatives in the environment: the public health perspective. *The Scientific World Journal,* 2013.

© University of Pretoria

Intaphong, P., Phuruangrat, A., Akhbari, K., Sakhon, T., Thongtem, T. & Thongtem, S. 2021. Hierarchical ZnO nanostructure flowers loaded with AgI nanoparticles for photodegradation of methylene blue under UV visible radiation. *Inorganic and Nano-Metal Chemistry***,** 1-8.

Islam, M. J., Reddy, D. A., Han, N. S., Choi, J., Song, J. K. & Kim, T. K. 2016. An oxygen-vacancy rich 3D novel hierarchical MoS 2/BiOI/AgI ternary nanocomposite: enhanced photocatalytic activity through photogenerated electron shuttling in a Z-scheme manner. *Physical Chemistry Chemical Physics,* 18**,** 24984-24993.

Ismael, M. 2021. Ferrites as solar photocatalytic materials and their activities in solar energy conversion and environmental protection: a review. *Solar Energy Materials and Solar Cells,* 219**,** 110786.

Jayaraj, R., Megha, P. & Sreedev, P. 2016. Organochlorine pesticides, their toxic effects on living organisms and their fate in the environment. *Interdisciplinary toxicology,* 9**,** 90.

Ji, P., Takeuchi, M., Cuong, T.-M., Zhang, J., Matsuoka, M. & Anpo, M. 2010. Recent advances in visible light-responsive titanium oxide-based photocatalysts. *Research on Chemical Intermediates,* 36**,** 327-347.

Jia, T., Fu, F., Li, J., Wang, W. & Hu, X. 2019. Constructing a novel Zn2SnO4/C/AgBr nanocomposite with extended spectral response and improved photocatalytic performance. *Journal of Alloys and Compounds,* 783**,** 687-696.

Jiang, J., Li, H. & Zhang, L. 2012. New insight into daylight photocatalysis of AgBr@ Ag: synergistic effect between semiconductor photocatalysis and plasmonic photocatalysis. *Chemistry–A European Journal,* 18**,** 6360-6369.

Jiang, W., An, C., Liu, J., Wang, S., Zhao, L., Guo, W. & Liu, J. 2014. Facile aqueous synthesis of β-AgI nanoplates as efficient visible-light-responsive photocatalyst. *Dalton Transactions,* 43**,** 300-305.

© University of Pretoria

Jin, X., Ye, L., Xie, H. & Chen, G. 2017. Bismuth-rich bismuth oxyhalides for environmental and energy photocatalysis. *Coordination Chemistry Reviews,* 349**,** 84-101.

Jones, R. J., Muller, J., Haynes, D. & Schreiber, U. 2003. Effects of herbicides diuron and atrazine on corals of the Great Barrier Reef, Australia. *Marine Ecology Progress Series,* 251**,** 153-167.

Kakuta, N., Goto, N., Ohkita, H. & Mizushima, T. 1999. Silver bromide as a photocatalyst for hydrogen generation from CH3OH/H2O solution. *The Journal of Physical Chemistry B,* 103**,** 5917-5919.

Kaneco, S., Katsumata, H., Suzuki, T. & Ohta, K. 2006. Titanium dioxide mediated photocatalytic degradation of dibutyl phthalate in aqueous solution—kinetics, mineralization and reaction mechanism. *Chemical Engineering Journal,* 125**,** 59-66.

Khan, M. M., Pradhan, D. & Sohn, Y. 2017. *Nanocomposites for visible light-induced photocatalysis,* Springer.

Kuai, L., Geng, B., Chen, X., Zhao, Y. & Luo, Y. 2010. Facile subsequently light-induced route to highly efficient and stable sunlight-driven Ag− AgBr plasmonic photocatalyst. *Langmuir,* 26**,** 18723-18727.

Kuang, Q., Zheng, X. & Yang, S. 2014. AgI microplate monocrystals with polar {0001} facets: spontaneous photocarrier separation and enhanced photocatalytic activity. *Chemistry–A European Journal,* 20**,** 2637-2645.

Kumar, A., Choudhary, P., Kumar, A., Camargo, P. H. & Krishnan, V. 2022. Recent advances in plasmonic photocatalysis based on TiO2 and noble metal nanoparticles for energy conversion, environmental remediation, and organic synthesis. *Small,* 18**,** 2101638.

Kumar, K. V., Porkodi, K. & Rocha, F. 2008. Langmuir–Hinshelwood kinetics–a theoretical study. *Catalysis Communications,* 9**,** 82-84.

© University of Pretoria

Kumar, S. & Chakarvarti, S. 2012. Chemical synthesis of AgCl microstructures using etched ion track polycarbonate membranes. *Synthesis and Reactivity in Inorganic, Metal-Organic, and Nano-Metal Chemistry*, 42**,** 1242-1245.

Kumar, S., Kumar, A., Kumar, A. & Krishnan, V. 2020. Nanoscale zinc oxide based heterojunctions as visible light active photocatalysts for hydrogen energy and environmental remediation. *Catalysis Reviews*, 62**,** 346-405.

Kuo, W. 1999. Synergistic effects of combination of photolysis and ozonation on destruction of chlorophenols in water. *Chemosphere*, 39**,** 1853-1860.

Kurniawan, T. A., Sillanpää, M. E. & Sillanpää, M. 2012. Nanoadsorbents for remediation of aquatic environment: local and practical solutions for global water pollution problems. *Critical reviews in environmental science and technology*, 42**,** 1233-1295.

Lai, C., Shi, X., Li, L., Cheng, M., Liu, X., Liu, S., Li, B., Yi, H., Qin, L. & Zhang, M. 2021. Enhancing iron redox cycling for promoting heterogeneous Fenton performance: A review. *Science of the Total Environment*, 775**,** 145850.

Lelieveld, J., Dentener, F., Peters, W. & Krol, M. 2004. On the role of hydroxyl radicals in the self-cleansing capacity of the troposphere. *Atmospheric Chemistry and Physics*, 4**,** 2337-2344.

Leontopoulos, S., Skenderidis, P. & Vagelas, I. 2020. Potential Use of Polyphenolic Compounds Obtained from Olive Mill Waste Waters on Plant Pathogens and Plant Parasitic Nematodes. *Plant Defence: Biological Control*, 22**,** 137.

Li, B., Wang, H., Zhang, B., Hu, P., Chen, C. & Guo, L. 2013a. Facile synthesis of one dimensional AgBr@ Ag nanostructures and their visible light photocatalytic properties. *ACS applied materials & interfaces*, 5**,** 12283-12287.

Li, H., Wu, T., Cai, B., Ma, W., Sun, Y., Gan, S., Han, D. & Niu, L. 2015. Efficiently photocatalytic reduction of carcinogenic contaminant Cr (VI) upon robust AgCl: Ag hollow nanocrystals. *Applied Catalysis B: Environmental*, 164**,** 344-351.

© University of Pretoria

Li, J., Yang, W., Ning, J., Zhong, Y. & Hu, Y. 2014. Rapid formation of AgnX (X= S, Cl, PO4, C2O4) nanotubes via an acid-etching anion exchange reaction. *Nanoscale,* 6**,** 5612-5615.

Li, Q., Chang, S., Wu, D., Bao, S., Zeng, C., Nasir, M., Tian, B. & Zhang, J. 2018. Synthesis of cubic Ag@ AgCl and Ag@ AgBr plasmonic photocatalysts and comparison of their photocatalytic activity for degradation of methyl orange and 2, 4-dichlorophenol. *Research on Chemical Intermediates,* 44**,** 4651-4661.

Li, Q., Wang, K., Lu, X., Luo, R., Zhang, M., Cui, C. & Zhu, G. 2020. In situ synthesis of AgI/SnS2 heterojunction photocatalysts with superior photocatalytic activity. *Int. J. Electrochem. Sci,* 15**,** 9256-9270.

Li, T., Luo, S. & Yang, L. 2013b. Three-dimensional hierarchical Ag/AgI/BiOI microspheres with high visible-light photocatalytic activity. *Materials Letters,* 109**,** 247-252.

Li, W., Ma, Q., Wang, X., He, S.-a., Li, M. & Ren, L. 2019a. Hydrogen evolution by catalyzing water splitting on two-dimensional g-C3N4-Ag/AgBr heterostructure. *Applied Surface Science,* 494**,** 275-284.

Li, Y., Hou, X., Wang, J., Feng, X., Cheng, L., Zhang, H. & Han, S. 2019b. Co-Mo nanoparticles loaded on three–dimensional graphene oxide as efficient catalysts for hydrogen generation from catalytic hydrolysis of sodium borohydride. *International Journal of Hydrogen Energy,* 44**,** 29075-29082.

Liang, C., Niu, C.-G., Zhang, L., Wen, X.-J., Yang, S.-F., Guo, H. & Zeng, G.-M. 2019. Construction of 2D heterojunction system with enhanced photocatalytic performance: Plasmonic Bi and reduced graphene oxide co-modified Bi5O7I with high-speed charge transfer channels. *Journal of hazardous materials,* 361**,** 245-258.

Liang, C., Niu, H.-Y., Guo, H., Niu, C.-G., Huang, D.-W., Yang, Y.-Y., Liu, H.-Y., Shao, B.-B. & Feng, H.-P. 2020. Insight into photocatalytic nitrogen fixation on graphitic carbon nitride:

© University of Pretoria

Defect-dopant strategy of nitrogen defect and boron dopant. *Chemical Engineering Journal,* 396**,** 125395.

Liang, H., Li, C., Bai, J., Wang, J., Shan, A., Guo, L. & Yu, D. 2015. Fabrication of visible-light-responsed calcium metasilicate-supported Ag–AgX/TiO2 (X= Cl, Br, I) composites and their photocatalytic properties. *Advanced Powder Technology,* 26**,** 1005-1012.

Lin, H., Cao, J., Luo, B., Xu, B. & Chen, S. 2012. Synthesis of novel Z-scheme AgI/Ag/AgBr composite with enhanced visible light photocatalytic activity. *Catalysis Communications,* 21**,** 91-95.

Linic, S., Christopher, P. & Ingram, D. B. 2011. Plasmonic-metal nanostructures for efficient conversion of solar to chemical energy. *Nature materials,* 10**,** 911-921.

Litter, M. I. 2005. Introduction to photochemical advanced oxidation processes for water treatment. *Environmental photochemistry part II***,** 325-366.

Liu, C., Wu, K., Meng, G., Wu, J., Peng, B., Hou, J., Liu, Z. & Guo, X. 2017a. Explore the properties and photocatalytic performance of iron-doped g-C3N4 nanosheets decorated with Ni2P. *Molecular Catalysis,* 437**,** 80-88.

Liu, H., Cao, W., Su, Y., Wang, Y. & Wang, X. 2012. Synthesis, characterization and photocatalytic performance of novel visible-light-induced Ag/BiOI. *Applied Catalysis B: Environmental,* 111**,** 271-279.

Liu, J., Chen, J., Wu, Z., Zhu, K., Wang, J., Li, Z., Tai, G., Liu, X. & Lu, S. 2021. Enhanced visible-light photocatalytic performances of ZnO through loading AgI and coupling piezo-photocatalysis. *Journal of Alloys and Compounds,* 852**,** 156848.

Liu, L., Deng, J., Niu, T., Zheng, G., Zhang, P., Jin, Y., Jiao, Z. & Sun, X. 2017b. One-step synthesis of Ag/AgCl/GO composite: a photocatalyst of extraordinary photoactivity and stability. *Journal of colloid and interface science,* 493**,** 281-287.

© University of Pretoria

Liu, Y., Yan, Z., Chen, R., Yu, Y., Chen, X., Zheng, X. & Huang, X. 2019. 2, 4-Dichlorophenol removal from water using an electrochemical method improved by a composite molecularly imprinted membrane/bipolar membrane. *Journal of hazardous materials,* 377**,** 259-266.

Loka, C. & Lee, K.-S. 2021. Dewetted Silver Nanoparticle-Dispersed WO 3 Heterojunction Nanostructures on Glass Fibers for Efficient Visible-Light-Active Photocatalysis by Magnetron Sputtering. *ACS omega,* 7**,** 1483-1493.

Long, M. & Cai, W. 2014. Advanced nanoarchitectures of silver/silver compound composites for photochemical reactions. *Nanoscale,* 6**,** 7730-7742.

Lou, S., Chen, Q., Wang, W., Wang, Y. & Zhou, S. 2021. Template-assisted synthesis of Ag/AgCl hollow microcubes and their composition-dependent photocatalytic activity for the degradation of phenol. *RSC Advances,* 11**,** 26311-26318.

Lou, S., Jia, X., Wang, Y. & Zhou, S. 2015. Template-assisted in-situ synthesis of porous AgBr/Ag composite microspheres as highly efficient visible-light photocatalyst. *Applied Catalysis B: Environmental,* 176**,** 586-593.

Lou, Z., Huang, B., Ma, X., Zhang, X., Qin, X., Wang, Z., Dai, Y. & Liu, Y. 2012a. A 3D AgCl hierarchical superstructure synthesized by a wet chemical oxidation method. *Chemistry–A European Journal,* 18**,** 16090-16096.

Lou, Z., Huang, B., Qin, X., Zhang, X., Cheng, H., Liu, Y., Wang, S., Wang, J. & Dai, Y. 2012b. One-step synthesis of AgCl concave cubes by preferential overgrowth along< 111> and< 110> directions. *Chemical Communications,* 48**,** 3488-3490.

Lou, Z., Huang, B., Qin, X., Zhang, X., Wang, Z., Zheng, Z., Cheng, H., Wang, P. & Dai, Y. 2011a. One-step synthesis of AgBr microcrystals with different morphologies by ILs-assisted hydrothermal method. *CrystEngComm,* 13**,** 1789-1793.

© University of Pretoria

Lou, Z., Huang, B., Wang, P., Wang, Z., Qin, X., Zhang, X., Cheng, H., Zheng, Z. & Dai, Y. 2011b. The synthesis of the near-spherical AgCl crystal for visible light photocatalytic applications. *Dalton Transactions*, 40**,** 4104-4110.

Lu, J., Wang, H., Dong, Y., Wang, F. & Dong, S. 2014. Plasmonic AgX nanoparticles-modified ZnO nanorod arrays and their visible-light-driven photocatalytic activity. *Chinese Journal of Catalysis*, 35**,** 1113-1125.

Lv, J., Hu, Q., Cao, C. & Zhao, Y. 2018. Modulation of valence band maximum edge and photocatalytic activity of BiOX by incorporation of halides. *Chemosphere*, 191**,** 427-437.

M'arimi, M., Mecha, C., Kiprop, A. K. & Ramkat, R. 2020. Recent trends in applications of advanced oxidation processes (AOPs) in bioenergy production. *Renewable and Sustainable Energy Reviews*, 121**,** 109669.

Ma, B., Guo, J., Dai, W.-L. & Fan, K. 2013. Highly stable and efficient Ag/AgCl core–shell sphere: controllable synthesis, characterization, and photocatalytic application. *Applied Catalysis B: Environmental*, 130**,** 257-263.

Ma, L., Islam, S. M., Liu, H., Zhao, J., Sun, G., Li, H., Ma, S. & Kanatzidis, M. G. 2017. Selective and efficient removal of toxic oxoanions of As (III), As (V), and Cr (VI) by layered double hydroxide intercalated with MoS42–. *Chemistry of Materials*, 29**,** 3274-3284.

Ma, X., Dai, Y., Guo, M. & Huang, B. 2012. The role of effective mass of carrier in the photocatalytic behavior of silver halide-based Ag@ AgX (X= Cl, Br, I): A theoretical study. *ChemPhysChem*, 13**,** 2304-2309.

Mao, S., Bao, R., Fang, D. & Yi, J. 2018. Facile synthesis of Ag/AgX (X= Cl, Br) with enhanced visible-light-induced photocatalytic activity by ultrasonic spray pyrolysis method. *Advanced Powder Technology*, 29**,** 2670-2677.

Marty, M. S., Borgert, C., Coady, K., Green, R., Levine, S. L., Mihaich, E., Ortego, L., Wheeler, J. R., Yi, K. D. & Zorrilla, L. M. 2018. Distinguishing between endocrine disruption

© University of Pretoria

and non-specific effects on endocrine systems. *Regulatory Toxicology and Pharmacology*, 99**,** 142-158.

Melián, E. P., Díaz, O. G., Arana, J., Rodríguez, J. D., Rendón, E. T. & Melián, J. H. 2007. Kinetics and adsorption comparative study on the photocatalytic degradation of o-, m-and p-cresol. *Catalysis Today,* 129**,** 256-262.

Melián, E. P., Díaz, O. G., Rodríguez, J. D., Araña, J. & Peña, J. P. 2013. Adsorption and photocatalytic degradation of 2, 4-dichlorophenol in TiO2 suspensions. Effect of hydrogen peroxide, sodium peroxodisulphate and ozone. *Applied Catalysis A: General,* 455**,** 227-233.

Mena, E., Rey, A., Acedo, B., Beltrán, F. & Malato, S. 2012. On ozone-photocatalysis synergism in black-light induced reactions: Oxidizing species production in photocatalytic ozonation versus heterogeneous photocatalysis. *Chemical engineering journal,* 204**,** 131-140.

Meng, X.-h., Shao, X., Li, H.-y., Yin, J., Wang, J., Liu, F.-z., Liu, X.-h., Wang, M. & Zhong, H.-l. 2013. Ag/AgBr/rGO nanocomposite: Synthesis and its application in photocatalysis. *Materials Letters,* 105**,** 162-165.

Meng, X. & Zhang, Z. 2016. Bismuth-based photocatalytic semiconductors: introduction, challenges and possible approaches. *Journal of Molecular Catalysis A: Chemical,* 423**,** 533-549.

Michalowicz, J. & Duda, W. 2007. Phenols-sources and toxicity. *Polish Journal of Environmental Studies,* 3**,** 347-362.

Moja, M., Chirwa, E. M. & Tichapondwa, S. 2021. Visible Light Activated Photocatalytic Degradation of 2, 4-dichlorophenol Using Silver Halide Photocatalysts. *Chemical Engineering Transactions,* 86**,** 1411-1416.

Murali, A., Sarswat, P. K., Perez, J. P. L. & Free, M. L. 2020. Synergetic effect of surface plasmon resonance and schottky junction in Ag-AgX-ZnO-rGO (X= Cl & Br) nanocomposite

© University of Pretoria

for enhanced visible-light driven photocatalysis. *Colloids and Surfaces A: Physicochemical and Engineering Aspects,* 595**,** 124684.

Naya, S.-i. & Tada, H. 2020. Au–Ag alloy nanoparticle-incorporated AgBr plasmonic photocatalyst. *Scientific reports,* 10**,** 1-7.

Organization, W. H. 2003. Lead in drinking-water: background document for development of WHO guidelines for drinking-water quality. World Health Organization.

Organization, W. H. 2021. Manganese in drinking water: background document for development of WHO Guidelines for drinking-water quality. World Health Organization.

Pan, J., Cao, J., Mei, J., Zhang, X., Wang, S., Zheng, Y., Cui, C. & Li, C. 2016. The preparation of Ag@ AgCl modified K2Ta2O6 and its natural light photocatalysis. *Materials Letters,* 184**,** 52-56.

Parida, V. K., Saidulu, D., Majumder, A., Srivastava, A., Gupta, B. & Gupta, A. K. 2021. Emerging contaminants in wastewater: A critical review on occurrence, existing legislations, risk assessment, and sustainable treatment alternatives. *Journal of Environmental Chemical Engineering,* 9**,** 105966.

Pei, C. C. & Leung, W. W.-F. 2013. Photocatalytic degradation of Rhodamine B by TiO2/ZnO nanofibers under visible-light irradiation. *Separation and purification technology,* 114**,** 108-116.

Phongarthit, K., Amornpitoksuk, P. & Suwanboon, S. 2020. Photocatalytic degradation of rhodamine B, reactive orange, and bisphenol A under visible light irradiation over AgX/ZnO (X= Cl, Br, I) prepared from green approach. *Optik,* 204**,** 164224.

Pinho, L. & Mosquera, M. J. 2013. Photocatalytic activity of TiO2–SiO2 nanocomposites applied to buildings: influence of particle size and loading. *Applied Catalysis B: Environmental,* 134**,** 205-221.

© University of Pretoria

Postigo, C. & Barceló, D. 2015. Synthetic organic compounds and their transformation products in groundwater: occurrence, fate and mitigation. *Science of the Total Environment,* 503**,** 32-47.

Pourshirband, N., Nezamzadeh-Ejhieh, A. & Mirsattari, S. N. 2020. The coupled AgI/BiOI catalyst: synthesis, brief characterization, and study of the kinetic of the EBT photodegradation. *Chemical Physics Letters,* 761**,** 138090.

Prado, C., Murcott, G. G., Marken, F., Foord, J. S. & Compton, R. G. 2002. Detection of Chlorophenols in Aqueous Solution via Hydrodynamic Channel Flow Cell Voltammetry Using a Boron-Doped Diamond Electrode. *Electroanalysis: An International Journal Devoted to Fundamental and Practical Aspects of Electroanalysis,* 14**,** 975-979.

Prieto, G., Tüysüz, H., Duyckaerts, N., Knossalla, J., Wang, G.-H. & Schüth, F. 2016. Hollow nano-and microstructures as catalysts. *Chemical reviews,* 116**,** 14056-14119.

Quan, X., Shi, H., Liu, H., Lv, P. & Qian, Y. 2004. Enhancement of 2, 4-dichlorophenol degradation in conventional activated sludge systems bioaugmented with mixed special culture. *Water research,* 38**,** 245-253.

Radha, R., Kulangara, R. V., Elaiyappillai, E., Sridevi, J. & Balakumar, S. 2019. Modulation in the band dispersion of Bi2WO6 nanocrsytals using the electronegativity of transition elements for enhanced visible light Photocatalysis. *Crystal Growth & Design,* 19**,** 6224-6238.

Rahman, M. S., Islam, S. M., Haque, A. & Shahjahan, M. 2020. Toxicity of the organophosphate insecticide sumithion to embryo and larvae of zebrafish. *Toxicology reports,* 7**,** 317-323.

Ramírez-García, R., Gohil, N. & Singh, V. 2019. Recent advances, challenges, and opportunities in bioremediation of hazardous materials. *Phytomanagement of Polluted Sites.* Elsevier.

© University of Pretoria

Rani, L., Thapa, K., Kanojia, N., Sharma, N., Singh, S., Grewal, A. S., Srivastav, A. L. & Kaushal, J. 2021. An extensive review on the consequences of chemical pesticides on human health and environment. *Journal of Cleaner Production,* 283**,** 124657.

Ranjbar, P. Z., Ayati, B. & Ganjidoust, H. 2019. Kinetic study on photocatalytic degradation of Acid Orange 52 in a baffled reactor using TiO2 nanoparticles. *Journal of Environmental Sciences,* 79**,** 213-224.

Rasdi, F. L. M., Mohamad, S., Manan, N. S. A. & Nodeh, H. R. 2016. Electrochemical determination of 2, 4-dichlorophenol at β-cyclodextrin functionalized ionic liquid modified chemical sensor: voltammetric and amperometric studies. *RSC advances,* 6**,** 100186-100194.

Reddy, A. V. B., Yusop, Z., Jaafar, J., Reddy, Y. V. M., Aris, A. B., Majid, Z. A., Talib, J. & Madhavi, G. 2016. Recent progress on Fe-based nanoparticles: synthesis, properties, characterization and environmental applications. *Journal of environmental chemical engineering,* 4**,** 3537-3553.

Reddy, C. V., Reddy, K. R., Harish, V. a., Shim, J., Shankar, M., Shetti, N. P. & Aminabhavi, T. M. 2020. Metal-organic frameworks (MOFs)-based efficient heterogeneous photocatalysts: synthesis, properties and its applications in photocatalytic hydrogen generation, CO2 reduction and photodegradation of organic dyes. *International Journal of Hydrogen Energy,* 45**,** 7656-7679.

Reddy, D. A., Choi, J., Lee, S., Ma, R. & Kim, T. K. 2015. Green synthesis of AgI nanoparticle-functionalized reduced graphene oxide aerogels with enhanced catalytic performance and facile recycling. *RSC advances,* 5**,** 67394-67404.

Rehan, M., Khattab, T. A., Barohum, A., Gätjen, L. & Wilken, R. 2018. Development of Ag/AgX (X= Cl, I) nanoparticles toward antimicrobial, UV-protected and self-cleanable viscose fibers. *Carbohydrate polymers,* 197**,** 227-236.

© University of Pretoria

Ren, Y., Dong, T., Ding, S., Liu, X., Zheng, H., Gao, L. & Hu, J. 2021. AgBr Nanoparticles Anchored on CdS Nanorods as Photocatalysts for H2 Evolution. *ACS Applied Nano Materials*.

Rodriguez-Proteau, R. & Grant, R. L. 2005. Toxicity Evaluation and Human Health Risk Assessment of Surface and Ground Water Contaminated by Recycled Hazardous Waste Materials. *Water Pollution,* 2**,** 133.

Sanni, S., Viljoen, E. & Ofomaja, A. 2019. Accelerated electron transport and improved photocatalytic activity of Ag/AgBr under visible light irradiation based on conductive carbon derived biomass. *Catalysis Letters,* 149**,** 3027-3040.

Saravanan, A., Kumar, P. S., Jeevanantham, S., Karishma, S., Tajsabreen, B., Yaashikaa, P. & Reshma, B. 2021. Effective water/wastewater treatment methodologies for toxic pollutants removal: Processes and applications towards sustainable development. *Chemosphere,* 280**,** 130595.

Saravanan, R., Gracia, F. & Stephen, A. 2017. Basic principles, mechanism, and challenges of photocatalysis. *Nanocomposites for visible light-induced photocatalysis.* Springer.

Schwarzenbach, R. P., Egli, T., Hofstetter, T. B., Von Gunten, U. & Wehrli, B. 2010. Global water pollution and human health. *Annual review of environment and resources,* 35**,** 109-136.

Senthil, R. A., Osman, S., Pan, J., Sun, M., Khan, A., Yang, V. & Sun, Y. 2019. A facile single-pot synthesis of WO3/AgCl composite with enhanced photocatalytic and photoelectrochemical performance under visible-light irradiation. *Colloids and Surfaces A: Physicochemical and Engineering Aspects,* 567**,** 171-183.

Shi, H., Chen, J., Li, G., Nie, X., Zhao, H., Wong, P.-K. & An, T. 2013. Synthesis and characterization of novel plasmonic Ag/AgX-CNTs (X= Cl, Br, I) nanocomposite photocatalysts and synergetic degradation of organic pollutant under visible light. *ACS applied materials & interfaces,* 5**,** 6959-6967.

© University of Pretoria

Shi, L., Liang, L., Ma, J., Meng, Y., Zhong, S., Wang, F. & Sun, J. 2014. Highly efficient visible light-driven Ag/AgBr/ZnO composite photocatalyst for degrading Rhodamine B. *Ceramics International,* 40**,** 3495-3502.

Shi, R., Zhao, Y., Waterhouse, G. I., Zhang, S. & Zhang, T. 2019. Defect engineering in photocatalytic nitrogen fixation. *ACS Catalysis,* 9**,** 9739-9750.

Sobiesiak, M. 2017. *Chemical structure of phenols and its consequence for sorption processes,* IntechOpen.

Solá-Gutiérrez, C., Schröder, S., San Román, M. F. & Ortiz, I. 2019. PCDD/Fs traceability during triclosan electrochemical oxidation. *Journal of hazardous materials,* 369**,** 584-592.

Soltani, T. & Lee, B.-K. 2016. Sono-synthesis of nanocrystallized BiFeO3/reduced graphene oxide composites for visible photocatalytic degradation improvement of bisphenol A. *Chemical Engineering Journal,* 306**,** 204-213.

Song, B., Tang, Q., Wu, W., Shao, T., Li, Q., Cao, J. & Ma, M. 2017. A novel in-situ synthesis and enhanced photocatalytic performance of Ag/AgBr/Ag2O/sulfonated polystyrene sphere heterostructure photocatalyst. *Materials Letters,* 208**,** 92-94.

Song, J., Lee, I., Roh, J. & Jang, J. 2014. Fabrication of Ag-coated AgBr nanoparticles and their plasmonic photocatalytic applications. *RSC Advances,* 4**,** 4558-4563.

Sridharan, K., Shenoy, S., Kumar, S. G., Terashima, C., Fujishima, A. & Pitchaimuthu, S. 2021. Advanced two-dimensional heterojunction photocatalysts of stoichiometric and non-stoichiometric bismuth oxyhalides with graphitic carbon nitride for sustainable energy and environmental applications. *Catalysts,* 11**,** 426.

Srinivasan, K. R. & Fogler, H. S. 1990. Use of inorgano-organo-clays in the removal of priority pollutants from industrial wastewaters: adsorption of benzo (a) pyrene and chlorophenols from aqueous solutions. *Clays and Clay Minerals,* 38**,** 287-293.

© University of Pretoria

Strade, E. & Kalnina, D. 2019. Cost Effective Method for toxicity screening of pharmaceutical wastewater containing inorganic salts and harmful organic compounds. *Environmental and Climate Technologies,* 23**,** 52-63.

Sun, J., Li, X., Zhao, Q., Tadé, M. O. & Liu, S. 2015. Quantum-sized BiVO 4 modified TiO 2 microflower composite heterostructures: efficient production of hydroxyl radicals towards visible light-driven degradation of gaseous toluene. *Journal of Materials Chemistry A,* 3**,** 21655-21663.

Svoboda, L., Bednář, J., Dvorský, R., Rybková, Z., Malachová, K., Henych, J., Matýsek, D. & Němečková, Z. 2020. Novel synthesis of Ag@ AgCl/ZnO by different radiation sources including radioactive isotope 60Co: Physicochemical and antimicrobial study. *Applied Surface Science,* 529**,** 147098.

Tang, W. i. & Huang, C. 1996. 2, 4-dichlorophenol oxidation kinetics by Fenton's reagent. *Environmental technology,* 17**,** 1371-1378.

Tang, W. Z. & Huang, C. 1995. The effect of chlorine position of chlorinated phenols on their dechlorination kinetics by Fenton's reagent. *Waste Management,* 15**,** 615-622.

Tang, Y., Jiang, Z., Xing, G., Li, A., Kanhere, P. D., Zhang, Y., Sum, T. C., Li, S., Chen, X. & Dong, Z. 2013. Efficient Ag@ AgCl cubic cage photocatalysts profit from ultrafast plasmon-induced electron transfer processes. *Advanced Functional Materials,* 23**,** 2932-2940.

Tang, Y., Subramaniam, V. P., Lau, T. H., Lai, Y., Gong, D., Kanhere, P. D., Cheng, Y. H., Chen, Z. & Dong, Z. 2011. In situ formation of large-scale Ag/AgCl nanoparticles on layered titanate honeycomb by gas phase reaction for visible light degradation of phenol solution. *Applied Catalysis B: Environmental,* 106**,** 577-585.

Tang, Y., Wang, W., Wang, B., Sun, X., Guo, C. & Xu, J. 2021. A novel AgCl-based visible-light photocatalyst through in-situ assembly of carbon dots for efficient dye degradation and hydrogen evolution. *Sustainable Materials and Technologies,* 27**,** e00242.

© University of Pretoria

Thakur, P., Raizada, P., Singh, P., Kumar, A., Khan, A. A. P. & Asiri, A. M. 2020. Exploring recent advances in silver halides and graphitic carbon nitride-based photocatalyst for energy and environmental applications. *Arabian Journal of Chemistry,* 13**,** 8271-8300.

Tian, B., Dong, R., Zhang, J., Bao, S., Yang, F. & Zhang, J. 2014. Sandwich-structured AgCl@ Ag@ TiO2 with excellent visible-light photocatalytic activity for organic pollutant degradation and E. coli K12 inactivation. *Applied Catalysis B: Environmental,* 158**,** 76-84.

Tian, B. & Zhang, J. 2012. Morphology-controlled synthesis and applications of silver halide photocatalytic materials. *Catalysis Surveys from Asia,* 16**,** 210-230.

Tian, D., Zhou, H., Zhang, H., Zhou, P., You, J., Yao, G., Pan, Z., Liu, Y. & Lai, B. 2022. Heterogeneous photocatalyst-driven persulfate activation process under visible light irradiation: From basic catalyst design principles to novel enhancement strategies. *Chemical Engineering Journal,* 428**,** 131166.

Torres, J. A., Nogueira, A. E., da Silva, G. T., Lopes, O. F., Wang, Y., He, T. & Ribeiro, C. 2020. Enhancing TiO2 activity for CO2 photoreduction through MgO decoration. *Journal of CO2 utilization,* 35**,** 106-114.

Tun, P., Wang, K., Naing, H., Wang, J. & Zhang, G. 2019. Facile preparation of visible-light-responsive kaolin-supported Ag@ AgBr composites and their enhanced photocatalytic properties. *Applied Clay Science,* 175**,** 76-85.

Ullah, Z., Khan, H., Waseem, A., Mahmood, Q. & Farooq, U. 2013. Water quality assessment of the River Kabul at Peshawar, Pakistan: industrial and urban wastewater impacts. *Journal of Water Chemistry and Technology,* 35**,** 170-176.

Ustaoğlu, F. & Tepe, Y. 2019. Water quality and sediment contamination assessment of Pazarsuyu Stream, Turkey using multivariate statistical methods and pollution indicators. *International Soil and Water Conservation Research,* 7**,** 47-56.

© University of Pretoria

Venkataswamy, P., Sunku, M., Gundeboina, R., Velchuri, R. & Vithal, M. 2019. Fabrication of Novel Ag/AgBr/Cs 2 Nb 4 O 11 Ternary Composite for Visible-Light Driven Photocatalysis. *Catalysis Letters,* 149**,** 2332-2346.

Verma, R. & Dwivedi, P. 2013. Heavy metal water pollution-A case study. *Recent Research in Science and Technology,* 5.

Vesali-Kermani, E., Habibi-Yangjeh, A. & Ghosh, S. 2020. Efficiently enhanced nitrogen fixation performance of g-C3N4 nanosheets by decorating Ni3V2O8 nanoparticles under visible-light irradiation. *Ceramics International,* 46**,** 24472-24482.

Victora, R. 1997. Calculated electronic structure of silver halide crystals. *Physical Review B,* 56**,** 4417.

Walling, C. & Goosen, A. 1973. Mechanism of the ferric ion catalyzed decomposition of hydrogen peroxide. Effect of organic substrates. *Journal of the American Chemical Society,* 95**,** 2987-2991.

Wang, D., Duan, Y., Luo, Q., Li, X. & Bao, L. 2011. Visible light photocatalytic activities of plasmonic Ag/AgBr particles synthesized by a double jet method. *Desalination,* 270**,** 174-180.

Wang, G., Mitomo, H., Matsuo, Y., Shimamoto, N., Niikura, K. & Ijiro, K. 2013a. DNA-templated plasmonic Ag/AgCl nanostructures for molecular selective photocatalysis and photocatalytic inactivation of cancer cells. *Journal of Materials Chemistry B,* 1**,** 5899-5907.

Wang, H., Gao, J., Guo, T., Wang, R., Guo, L., Liu, Y. & Li, J. 2012a. Facile synthesis of AgBr nanoplates with exposed {111} facets and enhanced photocatalytic properties. *Chemical Communications,* 48**,** 275-277.

Wang, H., Lang, X., Gao, J., Liu, W., Wu, D., Wu, Y., Guo, L. & Li, J. 2012b. Polyhedral AgBr Microcrystals with an Increased Percentage of Exposed {111} Facets as a Highly Efficient Visible-Light Photocatalyst. *Chemistry–A European Journal,* 18**,** 4620-4626.

© University of Pretoria

Wang, J., An, C., Liu, J., Xi, G., Jiang, W., Wang, S. & Zhang, Q.-H. 2013b. Graphene oxide coupled AgBr nanosheets: an efficient dual-functional visible-light-responsive nanophotocatalyst with enhanced performance. *Journal of Materials Chemistry A,* 1**,** 2827-2832.

Wang, J., An, C., Zhang, M., Qin, C., Ming, X. & Zhang, Q. 2012c. Photochemical conversion of AgCl nanocubes to hybrid AgCl–Ag nanoparticles with high activity and long-term stability towards photocatalytic degradation of organic dyes. *Canadian Journal of Chemistry*, 90**,** 858-864.

Wang, P., Huang, B., Dai, Y. & Whangbo, M.-H. 2012d. Plasmonic photocatalysts: harvesting visible light with noble metal nanoparticles. *Physical Chemistry Chemical Physics*, 14**,** 9813-9825.

Wang, P., Huang, B., Lou, Z., Zhang, X., Qin, X., Dai, Y., Zheng, Z. & Wang, X. 2010a. Synthesis of highly efficient Ag@ AgCl plasmonic photocatalysts with various structures. *Chemistry–A European Journal*, 16**,** 538-544.

Wang, P., Huang, B., Qin, X., Zhang, X., Dai, Y., Wei, J. & Whangbo, M. H. 2008. Ag@ AgCl: a highly efficient and stable photocatalyst active under visible light. *Angewandte Chemie International Edition,* 47**,** 7931-7933.

Wang, P., Huang, B., Zhang, Q., Zhang, X., Qin, X., Dai, Y., Zhan, J., Yu, J., Liu, H. & Lou, Z. 2010b. Highly efficient visible light plasmonic photocatalyst Ag@ Ag (Br, I). *Chemistry–A European Journal,* 16**,** 10042-10047.

Wang, P., Huang, B., Zhang, X., Qin, X., Jin, H., Dai, Y., Wang, Z., Wei, J., Zhan, J. & Wang, S. 2009. Highly efficient visible-light plasmonic photocatalyst Ag@ AgBr. *Chemistry–A European Journal,* 15**,** 1821-1824.

© University of Pretoria

Wang, S.-G., Liu, X.-W., Zhang, H.-Y., Gong, W.-X., Sun, X.-F. & Gao, B.-Y. 2007. Aerobic granulation for 2, 4-dichlorophenol biodegradation in a sequencing batch reactor. *Chemosphere,* 69**,** 769-775.

Wang, W.-S., Du, H., Wang, R.-X., Wen, T. & Xu, A.-W. 2013c. Heterostructured Ag 3 PO 4/AgBr/Ag plasmonic photocatalyst with enhanced photocatalytic activity and stability under visible light. *Nanoscale,* 5**,** 3315-3321.

Wang, W., Zhao, L. & Cao, X. 2020a. The microorganism and biochar-augmented bioreactive top-layer soil for degradation removal of 2, 4-dichlorophenol from surface runoff. *Science of The Total Environment,* 733**,** 139244.

Wang, X., Sui, Y., Jian, J., Yuan, Z., Zeng, J., Zhang, L., Wang, T. & Zhou, H. 2020b. Ag@ AgCl nanoparticles in-situ deposited cellulose acetate/silk fibroin composite film for photocatalytic and antibacterial applications. *Cellulose,* 27**,** 7721-7737.

Wang, Y. 2016. Synthesis of plasmonic Ag@ AgBr nanowires as highly efficient sunlight photocatalyst. *Journal of Materials Science: Materials in Electronics,* 27**,** 10122-10127.

Wang, Y., Sun, L. & Fugetsu, B. 2013d. Morphology-controlled synthesis of sunlight-driven plasmonic photocatalysts Ag@ AgX (X= Cl, Br) with graphene oxide template. *Journal of Materials Chemistry A,* 1**,** 12536-12544.

Wang, Z., Liu, J. & Chen, W. 2012e. Plasmonic Ag/AgBr nanohybrid: synergistic effect of SPR with photographic sensitivity for enhanced photocatalytic activity and stability. *Dalton Transactions,* 41**,** 4866-4870.

Webb, H. K., Arnott, J., Crawford, R. J. & Ivanova, E. P. 2013. Plastic degradation and its environmental implications with special reference to poly (ethylene terephthalate). *Polymers,* 5**,** 1-18.

© University of Pretoria

Xia, C., Wang, H., Kim, J. K. & Wang, J. 2021. Rational Design of Metal Oxide-Based Heterostructure for Efficient Photocatalytic and Photoelectrochemical Systems. *Advanced Functional Materials,* 31**,** 2008247.

Xiao, C., Zhang, L., Wang, K., Wang, H., Zhou, Y. & Wang, W. 2018. A new approach to enhance photocatalytic nitrogen fixation performance via phosphate-bridge: a case study of SiW12/K-C3N4. *Applied Catalysis B: Environmental,* 239**,** 260-267.

Xiao, X., Ge, L., Han, C., Li, Y., Zhao, Z., Xin, Y., Fang, S., Wu, L. & Qiu, P. 2015. A facile way to synthesize Ag@ AgBr cubic cages with efficient visible-light-induced photocatalytic activity. *Applied Catalysis B: Environmental,* 163**,** 564-572.

Xiong, W., Zhao, Q., Li, X. & Zhang, D. 2011. One-step synthesis of flower-like Ag/AgCl/BiOCl composite with enhanced visible-light photocatalytic activity. *Catalysis Communications,* 16**,** 229-233.

Xu, B., Li, Y., Gao, Y., Liu, S., Lv, D., Zhao, S., Gao, H., Yang, G., Li, N. & Ge, L. 2019. Ag-AgI/Bi3O4Cl for efficient visible light photocatalytic degradation of methyl orange: the surface plasmon resonance effect of Ag and mechanism insight. *Applied Catalysis B: Environmental,* 246**,** 140-148.

Xu, H., Li, H., Xia, J., Yin, S., Luo, Z., Liu, L. & Xu, L. 2011. One-pot synthesis of visible-light-driven plasmonic photocatalyst Ag/AgCl in ionic liquid. *ACS applied materials & interfaces,* 3**,** 22-29.

Xu, Q., Zhang, L., Yu, J., Wageh, S., Al-Ghamdi, A. A. & Jaroniec, M. 2018. Direct Z-scheme photocatalysts: Principles, synthesis, and applications. *Materials Today,* 21**,** 1042-1063.

Xu, Y., Xu, H., Li, H., Yan, J., Xia, J., Yin, S. & Zhang, Q. 2013. Ionic liquid oxidation synthesis of Ag@ AgCl core–shell structure for photocatalytic application under visible-light irradiation. *Colloids and Surfaces A: Physicochemical and Engineering Aspects,* 416**,** 80-85.

© University of Pretoria

Yamashita, Y., Aoyama, N., Takezawa, N. & Yoshida, K. 1999. Photocatalytic conversion of NOx on AgCl/Al2O3 catalyst. *Journal of Molecular Catalysis A: Chemical,* 150**,** 233-239.

Yan, Q., Fu, Y., Zhang, Y., Wang, H., Wang, S. & Cui, W. 2021. Ag/γ-AgI/Bi2O2CO3/Bi S-scheme heterojunction with enhanced photocatalyst performance. *Separation and Purification Technology,* 263**,** 118389.

Yan, T., Zhang, H., Luo, Q., Ma, Y., Lin, H. & You, J. 2013. Controllable synthesis of plasmonic Ag/AgBr photocatalysts by a facile one-pot solvothermal route. *Chemical engineering journal,* 232**,** 564-572.

Yang, M. & Zhou, K. 2011. Synthesis and characterizations of spherical hollow composed of AgI nanoparticle using AgBr as the precursor. *Applied Surface Science,* 257**,** 2503-2507.

Yao, S., Xue, S., Zhang, J. & Shen, X. 2016. Characterization and mechanism analysis of AgBr mixed cuboid WO 3 rods with enhanced photocatalytic activity. *RSC advances,* 6**,** 93436-93444.

Ye, L., Liu, J., Gong, C., Tian, L., Peng, T. & Zan, L. 2012. Two different roles of metallic Ag on Ag/AgX/BiOX (X= Cl, Br) visible light photocatalysts: surface plasmon resonance and Z-scheme bridge. *Acs Catalysis,* 2**,** 1677-1683.

Ye, L., Su, Y., Jin, X., Xie, H. & Zhang, C. 2014. Recent advances in BiOX (X= Cl, Br and I) photocatalysts: synthesis, modification, facet effects and mechanisms. *Environmental Science: Nano,* 1**,** 90-112.

Yentür, G. & Dükkancı, M. 2020. Fabrication of magnetically separable plasmonic composite photocatalyst of Ag/AgBr/ZnFe2O4 for visible light photocatalytic oxidation of carbamazepine. *Applied Surface Science,* 510**,** 145374.

Ying, Z., Chen, S., Zhang, S., Peng, T. & Li, R. 2019. Efficiently enhanced N2 photofixation performance of sea-urchin-like W18O49 microspheres with Mn-doping. *Applied Catalysis B: Environmental,* 254**,** 351-359.

© University of Pretoria

Youssef, N. A., Shaban, S. A., Ibrahim, F. A. & Mahmoud, A. S. 2016. Degradation of methyl orange using Fenton catalytic reaction. *Egyptian Journal of Petroleum,* 25**,** 317-321.

Yu, D., Bai, J., Liang, H., Wang, J. & Li, C. 2015. A new fabrication of AgX (X= Br, I)–TiO 2 nanoparticles immobilized on polyacrylonitrile (PAN) nanofibers with high photocatalytic activity and renewable property. *RSC advances,* 5**,** 91457-91465.

Yu, H., Liu, L., Wang, X., Wang, P., Yu, J. & Wang, Y. 2012. The dependence of photocatalytic activity and photoinduced self-stability of photosensitive AgI nanoparticles. *Dalton Transactions,* 41**,** 10405-10411.

Yu, J., Zhao, X. & Zhao, Q. 2000. Effect of surface structure on photocatalytic activity of TiO2 thin films prepared by sol-gel method. *Thin solid films,* 379**,** 7-14.

Zai, J., Fu, Y., Zai, X., Ji, H., Liu, A. & Chai, F. 2017. Fabrication of novel Ag/AgCl electrode pair on the template of carbon foam as marine electric field sensor and its electrochemical performances. *Ionics,* 23**,** 2213-2219.

Zanjanchi, M., Ebrahimian, A. & Arvand, M. 2010. Sulphonated cobalt phthalocyanine–MCM-41: an active photocatalyst for degradation of 2, 4-dichlorophenol. *Journal of hazardous materials,* 175**,** 992-1000.

Zazo, J., Casas, J., Mohedano, A., Gilarranz, M. & Rodriguez, J. 2005. Chemical pathway and kinetics of phenol oxidation by Fenton's reagent. *Environmental science & technology,* 39**,** 9295-9302.

Zhang, H., Lu, Y., Liu, H. & Fang, J. 2015. One-pot synthesis of high-index faceted AgCl nanocrystals with trapezohedral, concave hexoctahedral structures and their photocatalytic activity. *Nanoscale,* 7**,** 11591-11601.

Zhang, H., Shen, Y., Liu, W., He, Z., Fu, J., Cai, Z. & Jiang, G. 2019. A review of sources, environmental occurrences and human exposure risks of hexachlorobutadiene and its association with some other chlorinated organics. *Environmental Pollution,* 253**,** 831-840.

© University of Pretoria

Zhang, H., Zhang, Q., Miao, C. & Huang, Q. 2018. Degradation of 2, 4-dichlorophenol in aqueous solution by dielectric barrier discharge: effects of plasma-working gases, degradation pathways and toxicity assessment. *Chemosphere,* 204**,** 351-358.

Zhang, Q., Gangadharan, D. T., Liu, Y., Xu, Z., Chaker, M. & Ma, D. 2017. Recent advancements in plasmon-enhanced visible light-driven water splitting. *Journal of Materiomics,* 3**,** 33-50.

Zhang, S., Li, J., Wang, X., Huang, Y., Zeng, M. & Xu, J. 2014. In situ ion exchange synthesis of strongly coupled Ag@ AgCl/g-C3N4 porous nanosheets as plasmonic photocatalyst for highly efficient visible-light photocatalysis. *ACS applied materials & interfaces,* 6**,** 22116-22125.

Zhang, X., Ren, B., Li, X., Xu, Y., Liu, B., Yu, P., Sun, Y. & Mei, D. 2021a. Efficiently enhanced visible-light photocatalytic activity by in situ deposition of Ag@ AgBr on g-C3N4/Fe3O4 magnetic heterogeneous materials. *Separation and Purification Technology,* 254**,** 117596.

Zhang, Y., Guo, Z., Yu, M., Xu, Z., Liu, Y., Li, F. & Wang, L. 2021b. Preparation of enhanced AgI@ MnO2 heterojunction photocatalysts for rapid sterilization under visible light. *Journal of Alloys and Compounds,* 887**,** 161431.

Zhang, Y., Ma, Z., Fang, Z., Qian, Y., Zhong, P. & Yan, J. 2020. Review of harmless treatment of municipal solid waste incineration fly ash. *Waste Disposal & Sustainable Energy,* 2**,** 1-25.

Zhi, L., Zhang, S., Xu, Y., Tu, J., Li, M., Hu, D. & Liu, J. 2020. Controlled growth of AgI nanoparticles on hollow WO3 hierarchical structures to act as Z-scheme photocatalyst for visible-light photocatalysis. *Journal of Colloid and Interface Science,* 579**,** 754-765.

Zhong, D., Liu, W., Tan, P., Zhu, A., Liu, Y., Xiong, X. & Pan, J. 2018. Insights into the synergy effect of anisotropic {001} and {230} facets of BaTiO3 nanocubes sensitized with

© University of Pretoria

CdSe quantum dots for photocatalytic water reduction. *Applied Catalysis B: Environmental,* 227**,** 1-12.

Zhou, X., Hu, C., Hu, X., Peng, T. & Qu, J. 2010. Plasmon-assisted degradation of toxic pollutants with Ag− AgBr/Al2O3 under visible-light irradiation. *The Journal of Physical Chemistry C,* 114**,** 2746-2750.

Zhu, M., Chen, P. & Liu, M. 2011a. Graphene oxide enwrapped Ag/AgX (X= Br, Cl) nanocomposite as a highly efficient visible-light plasmonic photocatalyst. *ACS nano,* 5**,** 4529-4536.

Zhu, M., Chen, P. & Liu, M. 2011b. Sunlight-driven plasmonic photocatalysts based on Ag/AgCl nanostructures synthesized via an oil-in-water medium: enhanced catalytic performance by morphology selection. *Journal of Materials Chemistry,* 21**,** 16413-16419.

© University of Pretoria

APPENDIX A

Table A - 1. XRF elemental analysis of the synthesized photocatalysts Ag/AgX (X = Cl, Br, I).

	Ag/ AgCl		Ag/ AgBr		Ag/ AgI
Ba	0,10	**Al**	1,60	**Sn**	0,38
Pu	0,04	**As**	0,11	**Ti**	0,30
Fe	0,04	**Mo**	0,08	**Mo**	0,10
Br	0,03	**Mg**	0,08	**Rh**	0,07
Th	0,02	**Pu**	0,05	**Pu**	0,06
Sr	0,01	**Ru**	0,05	**Cd**	0,05
Al	0,01	**Ba**	0,04	**Ru**	0,05
Y	0,01	**Pd**	0,03	**Te**	0,04
Ti	0,00	**Th**	0,02	**Sb**	0,04
%AgCl	99,66	**Cd**	0,02	**Br**	0,03
	99,92	**Sr**	0,02	**Sr**	0,02
		Rh	0,02	**Th**	0,02
		Fe	0,01	**Al**	0,01
		Hf	0,01	**Hf**	0,01
		Yb	0,01	**Yb**	0,01
		Y	0,01	**Y**	0,01
		%AgBr	97,67	**%AgI**	98,91
		Total	**99,80**		**100,10**

© University of Pretoria

APPENDIX B

Table B - 1. Copyright permission of Figure 2-4.

ELSEVIER LICENSE
TERMS AND CONDITIONS
Apr 28, 2022

This Agreement between University of Pretoria -- Mahlako Moja ("You") and Elsevier ("Elsevier") consists of your license details and the terms and conditions provided by Elsevier and Copyright Clearance Center.

License Number	5297700781575
License date	Apr 28, 2022
Licensed Content Publisher	Elsevier
Licensed Content Publication	Materials Research Bulletin
Licensed Content Title	Novel AgClxBr1−x solid solutions photocatalyst with enhanced photocatalytic activity for reduction of Cr6+ and oxidation of Bisphenol A under simulated sunlight
Licensed Content Author	Zhipeng Cheng,Qian Dong,Shu Chen,Wei Zhao,Xiaozhong Chu,Hui Zhong,Pusu Zhao,Lili Zhang,Jiming Xu,Xujing Guo,Feng Liang,Fengling Yang
Licensed Content Date	Jul 1, 2021
Licensed Content Volume	139
Licensed Content Issue	n/a
Licensed Content Pages	1
Start Page	111257
End Page	0
Type of Use	reuse in a thesis/dissertation

© University of Pretoria

Table B - 2. Copyright permission of Figure 2-7.

ELSEVIER LICENSE
TERMS AND CONDITIONS
Apr 28, 2022

This Agreement between University of Pretoria -- Mahlako Moja ("You") and Elsevier ("Elsevier") consists of your license details and the terms and conditions provided by Elsevier and Copyright Clearance Center.

License Number		5297710527207
License date		Apr 28, 2022
Licensed Content Publisher		Elsevier
Licensed Content Publication		International Journal of Hydrogen Energy
Licensed Content Title		In- situ solid-phase fabrication of Ag/AgX (X=Cl, Br, I)/g-C3N4 composites for enhanced visible-light hydrogen evolution
Licensed Content Author		Chunpeng Bai,Jingce Bi,Junbiao Wu,Yan Xu,Sebastian Wohlrab,Yide Han,Xia Zhang
Licensed Content Date		Aug 13, 2019
Licensed Content Volume		44
Licensed Content Issue		39
Licensed Content Pages		9
Start Page		21397
End Page		21405
Type of Use		reuse in a thesis/dissertation

© University of Pretoria

Table B - 3. Copyright permission of Scheme 5-1.

Apr 27, 2022

This Agreement between University of Pretoria -- Mahlako Moja ("You") and Elsevier ("Elsevier") consists of your license details and the terms and conditions provided by Elsevier and Copyright Clearance Center.

License Number	5297311141599
License date	Apr 27, 2022
Licensed Content Publisher	Elsevier
Licensed Content Publication	Chemosphere
Licensed Content Title	Degradation of 2, 4-dichlorophenol in aqueous solution by dielectric barrier discharge: Effects of plasma-working gases, degradation pathways and toxicity assessment
Licensed Content Author	Hong Zhang,Qifu Zhang,Chunguang Miao,Qing Huang
Licensed Content Date	Aug 1, 2018
Licensed Content Volume	204
Licensed Content Issue	n/a
Licensed Content Pages	8
Start Page	351
End Page	358

© University of Pretoria

UNIVERSITEIT VAN PRETORIA
UNIVERSITY OF PRETORIA
YUNIBESITHI YA PRETORIA

ACS Publications
Most Trusted. Most Cited. Most Read.

Facile Subsequently Light-Induced Route to Highly Efficient and Stable Sunlight-Driven Ag−AgBr Plasmonic Photocatalyst

Author:

Long Kuai, Baoyou Geng, Xiaoting Chen, et al

Publication:

Langmuir

Publisher:

American Chemical Society

Date:

Dec 1, 2010

Copyright © 2010, American Chemical Society

PERMISSION/LICENSE IS GRANTED FOR YOUR ORDER AT NO CHARGE

This type of permission/license, instead of the standard Terms and Conditions, is sent to you because no fee is being charged for your order. Please note the following:

- Permission is granted for your request in both print and electronic formats, and translations.
- If figures and/or tables were requested, they may be adapted or used in part.
- Please print this page for your records and send a copy of it to your publisher/graduate school.
- One-time permission is granted only for the use specified in your RightsLink request. No additional uses are granted (such as derivative works or other editions). For any uses, please submit a new request.

© University of Pretoria

UNIVERSITEIT VAN PRETORIA
UNIVERSITY OF PRETORIA
YUNIBESITHI YA PRETORIA

ACS Publications
Most Trusted. Most Cited. Most Read.

Ecofriendly Synthesis and Photocatalytic Activity of Uniform Cubic Ag@AgCl Plasmonic Photocatalyst

Author:

Rongfang Dong, Baozhu Tian, Cuiyun Zeng, et al

Publication:

The Journal of Physical Chemistry C

Publisher:

American Chemical Society

Date:

Jan 1, 2013

Copyright © 2013, American Chemical Society

PERMISSION/LICENSE IS GRANTED FOR YOUR ORDER AT NO CHARGE

This type of permission/license, instead of the standard Terms and Conditions, is sent to you because no fee is being charged for your order. Please note the following:

- Permission is granted for your request in both print and electronic formats, and translations.
- If figures and/or tables were requested, they may be adapted or used in part.
- Please print this page for your records and send a copy of it to your publisher/graduate school.
- One-time permission is granted only for the use specified in your RightsLink request. No additional uses are granted (such as derivative works or other editions). For any uses, please submit a new request.

© University of Pretoria